

Surrogate based Multidisciplinary Design Optimization of a VTOL aircraft

Catarina João Fonseca Ribeiro

Thesis to obtain the Master of Science Degree in

Aerospace Engineering

Supervisors: Prof. Afzal Suleman
Prof. Frederico José Prata Rente Reis Afonso

Examination Committee

Chairperson: Prof. Fernando José Parracho Lau
Supervisor: Prof. Frederico José Prata Rente Reis Afonso
Member of the Committee: Prof. Pedro Vieira Gamboa

May 2021

To my mom...

Acknowledgments

First I would like to express my deepest appreciation to Professor Frederico Afonso for all the support, patience and constant helpful advice given throughout this project.

I would also like to show my sincere gratitude to Professor Afzal Suleman who gave me the opportunity to develop this work, and was always available to help me during the process and was always making sure everyone was integrated on the group of researchers.

I extend my appreciation to Martin Sohst, for all the advice given and the extreme flexibility and availability to help.

I could not forget to thank all my closest friends, who gave me immense support during these five years, and with whom I shared lots of experiences, good moments but also some all nighters and stressful situations that we overcame together.

To my family and Filipe, I could not thank enough for all the time spent to support me and for all the sacrifices made so that I could grow and be who I am today.

Lastly, to my mom, wherever you are, I hope I am making you proud.

Resumo

Esta tese apresenta uma comparação entre uma otimização multidisciplinar (MDO), baseada em modelos de aproximação, e MDO usando funções reais de uma aeronave de asa fixa com capacidade de decolagem e aterragem vertical (VTOL) para Mobilidade Aérea Urbana (UAM). Durante a fase conceptual de projeto aeronáutico, é importante ter uma vasta exploração do espaço de projeto, usando modelos de várias disciplinas que precisam ser considerados para satisfazer os requisitos da missão. Modelos de aproximação são uma abordagem com potencial para explorar rapidamente o espaço de projeto. Desta maneira, nesta tese, é realizada uma comparação entre os resultados de uma MDO usando funções reais e os modelos aproximados dessas funções.

Três abordagens principais para a otimização são realizadas: uma otimização usando as funções analíticas reais e as suas derivadas com o método *adjoint*; uma otimização baseada em modelos aproximados para a função objetivo e constrangimentos, usando a Surrogate Modeling Toolbox (SMT); e uma otimização baseada em amostragem adaptativa e critérios de preenchimento, como o critério de Watson e Barnes (WB2).

Para comparar estas estratégias de otimização multidisciplinar, resolvidas com recurso à ferramenta OpenMDAO, um problema com o objectivo de minimizar a energia é definido para a aeronave VTOL, sendo as disciplinas de aerodinâmica e estruturas modeladas com recurso aos modelos de baixa fidelidade implementados no OpenAeroStruct (OAS). Inicialmente, apenas duas variáveis de projeto são utilizadas. São depois adicionadas mais variáveis ao problema, aumentando assim a complexidade do problema de otimização.

Palavras-chave: Otimização multidisciplinar, modelos aproximados, amostragem adaptativa, projeto aeronáutico, aeroestrutural

Abstract

This thesis aims at evaluating surrogate based Multidisciplinary Design Optimization (MDO) strategies for designing an Urban Air Mobility (UAM) Vertical Take-Off and Landing (VTOL) aircraft. During the conceptual stages, it is important to have a vast exploration of the design space, using models for several disciplines that need to be considered regarding the mission requirements. Surrogate models are a potentially good approach to rapidly explore the design space. Therefore, in this work, a comparison between the results of a MDO using real functions and the surrogate models of these functions is provided.

Three major strategies for the aircraft optimization are carried out: an optimization using the real, analytical functions and their derivatives with the adjoint method; a surrogate-based optimization where surrogate models for both the objective function and constraints are built, using the Surrogate Modeling Toolbox (SMT); and an optimization based on adaptive sampling and infill criteria such as the Watson and Barnes criterion (WB2).

To compare these MDO strategies, an energy minimization problem is established for the VTOL aircraft as a case study in OpenMDAO, where aerodynamics and structures are modeled using the low-fidelity models provided in the OpenAeroStruct (OAS) framework. Initially, only two design variables are considered. Then, more design variables are added to the problem, and therefore increasing the complexity of the optimization problem.

Keywords: Multidisciplinary design optimization, surrogate models, adaptive sampling, aircraft design, aerostructural

Contents

Acknowledgments	v
Resumo	vii
Abstract	ix
List of Tables	xv
List of Figures	xvii
Nomenclature	xix
Acronyms	xxv
1 Introduction	1
1.1 Motivation	1
1.2 Project Overview	1
1.3 State of the art	2
1.3.1 Urban Air Mobility	2
1.3.2 Aircraft Design	3
1.3.3 Multidisciplinary Optimization	3
1.3.4 Multidisciplinary analysis	3
1.3.5 Framework architectures	4
1.3.6 Surrogate models	4
1.3.7 Design of Experiments	4
1.4 Objectives	5
1.5 Thesis Outline	5
2 Theoretical Overview	7
2.1 Multidisciplinary Analysis	7
2.1.1 Structural Analysis	7
2.1.1.1 Spatial Beam Element	7
2.1.1.2 Global Stiffness Matrix	8
2.1.1.3 Failure criterion	8
2.1.2 Aerodynamic Analysis	9
2.1.2.1 Vortex Flow Element	9
2.1.2.2 Lifting Line Theory	10

2.1.2.3	Vortex Lattice Method	11
2.1.2.4	Compressible Correction	13
2.1.2.5	Viscous empirical corrections	14
2.1.3	Fluid Structure Interaction	15
2.2	Multidisciplinary Optimization	15
2.2.1	Basic Concepts	15
2.2.2	MDO architectures	16
2.2.2.1	Multi Discipline Feasible	16
2.3	Surrogate Models	16
2.3.1	Sampling Techniques	17
2.3.1.1	Classical Design of Experiments	18
2.3.1.2	Modern Design of Experiments	19
2.3.1.3	Hybrid Designs	20
2.3.1.4	Adaptive sampling	20
2.3.2	Surrogate Modelling Techniques	20
2.3.2.1	Kriging	21
2.3.2.2	Radial Basis Function	23
2.3.3	Error metrics	24
2.4	Surrogate Search	24
2.4.1	Expected Improvement	24
2.4.2	Watson and Barnes	25
2.5	Optimization Algorithms	26
2.5.1	Deterministic Algorithms	26
2.5.1.1	Gradient-free	26
2.5.1.2	Gradient-based	26
2.5.2	Heuristic Algorithms	28
2.5.3	Sensitivity Analysis	28
3	Implementation	30
3.1	Conceptual Design	30
3.1.1	Analytical Hierarchy Process	31
3.1.2	Design Point	33
3.1.3	Weight and Balance Estimations	37
3.1.4	Wing Design	37
3.1.5	Propulsive System Architecture	39
3.2	Optimization Problem Formulation	39
3.2.1	Mission Requirements	39
3.2.2	Objective Function	40
3.2.3	Design Variables	41

3.2.4	Constraints	41
3.2.5	Optimization Problem Statement	41
3.3	MDA implementation	42
3.3.1	Discipline coupling	42
3.3.2	Aerodynamic analysis	43
3.3.3	Structural analysis	44
3.3.4	Mesh convergence	44
3.4	MDO methodology	45
3.4.1	Test functions studies	46
3.4.2	Optimization cycle	48
4	Results	50
4.1	Baseline	50
4.2	Case studies conditions	51
4.3	Cases with 2 design variables	51
4.3.1	Surrogate models' accuracy	51
4.3.1.1	Case 2.1	51
4.3.1.2	Case 2.2	52
4.3.1.3	Case 2.3	53
4.3.2	Optimization results	55
4.3.2.1	Case 2.1	55
4.3.2.2	Case 2.2	57
4.3.2.3	Case 2.3	59
4.4	Case 4	61
4.4.1	Surrogate models' quality	61
4.4.2	Optimization results	62
4.5	Case 8	65
4.5.1	Surrogate model's quality	65
4.5.2	Optimization results	66
4.6	Optimal solution	68
5	Conclusions	70
5.1	Achievements	70
5.2	General conclusions	71
5.3	Future Work	71
	Bibliography	71
A	Aerodynamics	81
A.1	Fundamentals	81

B Surrogate models **85**
B.1 Test functions studies for surrogate models and sampling plans 85
B.2 Optimization using the real functions 87

C Conceptual design **89**
C.1 Analytical Hierarchy Process 89
C.2 Weight and position Estimations 90

List of Tables

3.1	Scale of relative importance [100]	32
3.2	Pairwise comparison between the different criteria	32
3.3	Global comparison of the concepts	33
3.4	Initial sizing based on the design point considerations	36
3.5	Initial sizing based on the design point considerations	37
3.6	Total mass and CG position	37
3.7	Wing dimensions	38
3.8	Horizontal stabilizer dimensions	38
3.9	Constraints' minimum and maximum allowable values	42
3.10	Design variables bounds	42
3.11	Average relative error obtained with the different surrogate models representing the Branin function	47
4.1	Baseline geometric parameters	50
4.2	Baseline performance	51
4.3	Results of the different solutions of case 2.1	57
4.4	Computational cost of the four methods for case 2.1	57
4.5	Results of the different solutions of Case 2.2	59
4.6	Computational cost of the different approaches for Case 2.2	59
4.7	Results of the different solutions of Case 2.3	61
4.8	Computational cost of the three methods for case 2.3	61
4.9	Results of the different solutions obtained in Case study 4	64
4.10	Computational cost of the different optimization approaches for case 4	64
4.11	Number of starting sample points according to the function	66
4.12	Design variables values of the different solutions obtained in case study 8	68
4.13	Performance parameters of the different solutions obtained in case study 8	68
4.14	Computational cost of the different optimization approaches for Case 8	68
B.1	Average relative error obtained with the different surrogate models representing the Rosenbrock function with two design variables, when using LHS plan	86

B.2	Average relative error obtained with the different surrogate models representing the Rosenbrock function with four design variables	87
C.1	Aerodynamics comparison of all the concepts	89
C.2	Structures and Weight comparison of all the concepts	89
C.3	Propulsion comparison of all the concepts	89
C.4	Manufacturing and Maintenance comparison of all the concepts	90
C.5	Stability and Control comparison of all the concepts	90
C.6	Take-off and Landing comparison of all the concepts	90
C.7	Noise comparison of all the concepts	90
C.8	Structural components' weight estimation and position	91
C.9	Propulsion components' weight estimation and position	91
C.10	Equipment components' weight estimation and position	91
C.11	Other components. (Note: * are estimated with design point expressions and transition study)	92

List of Figures

1.1	Mission profile	2
2.1	Spatial beam representation [22]	8
2.2	Global matrix representation	9
2.3	Vortex flow element [78]	9
2.4	Vortex filament of strength Γ [78]	10
2.5	Single horseshoe vortex modelling [78]	11
2.6	Superimposition of horseshoe vortices along the lifting line [78]	11
2.7	Lifting panel schematic with one horseshoe vortex [78]	12
2.8	Influence of the vortex Γ_n on point B [78]	12
2.9	2^3 Full-factorial design geometrical view [73]	18
3.1	Implementation process flowchart	30
3.2	Flexcraft configuration [99]	31
3.3	Configurations analysed during the conceptual design phase. The rotors with a solid colour have tilting capability.	33
3.4	Design space for forward flight	35
3.5	Design space for vertical flight	36
3.6	Schematics of the aircraft and the referential used	37
3.7	Static margin variation with respect to the wing sweep angle	38
3.8	High-level representation of the propulsive system	39
3.9	eXtended Design Structure Matrix (XDSM) diagram [108] for aerostructural optimization using a Gauss-Seidel approach. The x vectors are design variables and the y vectors are states, where * represents the values at the design optimum. Figure from [22].	43
3.10	Wingbox representation [23]	44
3.11	Aerodynamic and structural discretization [23]	44
3.12	Critical stress combinations [23]	45
3.13	Mesh convergence study	46
3.14	Average relative error with the different sampling plans using a Kriging surrogate model to represent the Branin function and the Rosenbrock function with 2 design variables	47

3.15 Training time to build the different surrogate models represent the Branin function and the Rosenbrock function with 2 design variables	48
3.16 Optimization cycle with the surrogate models functions	49
3.17 Optimization cycle with the surrogate models functions using an adaptive sampling plan	49
4.1 Average relative error of different functions vs number of sample points used for case 2.1	52
4.2 Behaviour of the real functions varying with the two design variables used in case 2.1	52
4.3 Average relative error of different functions vs number of sample points used for case 2.2	53
4.4 Behaviour of the real functions varying with the two design variables used in case 2.2	53
4.5 Average relative error of different functions vs number of sample points used for case 2.3	54
4.6 Behaviour of the real functions varying with the two design variables used in case 2.3	54
4.7 Optimization history of the objective function in case 2.1 (when using the real functions)	55
4.8 Optimization history of the total energy in Case 2.1 using the adaptive sampling approach	56
4.9 Optimization history of the objective function in case 2.2 (when using the real functions)	57
4.10 Optimization history of the total energy in Case 2.2 when using the adaptive sampling approach	58
4.11 Optimization history of the total energy in Case 2.3 (when using the real functions)	59
4.12 Optimization history of the total energy in case 2.3 using the adaptive sampling plan	60
4.13 Average relative error of different functions vs number of sample points used for case 4	62
4.14 Optimization history of the total energy in case 4 (when using the real functions)	63
4.15 Optimization history of the total energy in Case 4	63
4.16 Average relative error of different functions vs number of sample points used for case 8	65
4.17 Optimization history of the total energy in Case 8 (when using the real functions)	66
4.18 Optimization history of the total energy in Case 8	67
4.19 Baseline and optimal solution general configurations	69
A.1 Airfoil in the physical space [78]	83
B.1 Average relative error with the different sampling plans to represent the Branin function	85
B.2 Average relative error with the different sampling plans to represent the Rosenbrock function with 2 design variables	86
B.3 Optimization history in Case 2.1 (when using the real functions)	87
B.4 Optimization history in Case 2.2 (when using the real functions)	87
B.5 Optimization history of Case 2.3 (when using the real function)	88
B.6 Optimization history of Case 4 (when using the real function)	88
B.7 Optimization history of Case 8 (when using the real function)	88

Nomenclature

Greek symbols

α	Angle of attack	◦
α_{pull}	Angle of attack during pull up	◦
α_{vc}	Angle of attack during vertical climb	◦
χ	Design space	
Γ	Circulation	
γ	Heat capacity ratio	—
Γ_d	Dihedral angle	◦
γ_{ca}	Climb angle	◦
Λ	Sweep angle	◦
λ	Lagrange multipliers vector	
μ	Advance ratio	
μ_m	Mean of the response at a sampled design point	
ϕ	Velocity potencial	
$\Phi(\cdot)$	Cumulative distribution function of the standart normal distribution	
$\phi(\cdot)$	Probability density function of the standart normal distribution	
ϕ_{bf}	Basis function	
$\phi_{xx}, \phi_{yy}, \phi_{zz}$	Velocity potencial's second derivatives	
Ψ	Correlation matrix	
ψ	Vector of correlation with the new prediction	
ρ	Density	kg m ⁻³
σ^2	Gaussian process variance	

σ_r	Solidity ratio of the rotors	
$\sigma_{11}, \sigma_{22}, \sigma_{33}$	Direct stresses	N m^{-2}
$\sigma_{12}, \sigma_{23}, \sigma_{31}$	Shear stresses	N m^{-2}
σ_{VM}	Equivalent Von Mises stress	N m^{-2}
θ	Hyperparameters	
θ_{tilt}	Rotors' tilt angle measured clock-wise from horizontal axes	$^\circ$
ξ, η	Coordinates of the reference frame for compressible flow	

Roman symbols

A	Cross-sectional area	m^2
a	Speed of sound	m s^{-1}
A_R	Rotor area	m^2
$A_{i,j}$	Aerodynamic influence coefficient matrix	
AR	Aspect ratio	—
b	Span	m
b_f	Regression gradient	
b_i	Vector describing the bound vortex for the panel i	
\bar{c}	Mean aerodynamic chord	m
C_L	Lift coefficient	—
C_M	Pitch moment coefficient	—
C_p	Pressure coefficient	—
C_{D_0}	Zero-lift drag coefficient	—
$C_{L_{max}}$	Maximum lift coefficient	—
c_{root}	Root chord	m
c_{tip}	Tip chord	m
$cov(\cdot, \cdot)$	Covariance	
D	Drag	N
$d(\cdot, \cdot)$	Distance between two points	
$d\vec{l}$	Finite element size	m

E	Energy	MJ
e	Oswald's efficiency factor	—
$E[\cdot]$	Expected value	
E_y	Young's modulus	Pa
E_{spec}	Specific energy density	MJ kg ⁻¹
\vec{f}	Force per mass unit	N kg ⁻¹
\vec{F}_i	Aerodynamic load vector applied on panel i	N
$\{F\}$	Load vector	N
$f(\cdot)$	Regression model	
G	Shear modulus	Pa
g	Acceleration of gravity	m s ⁻²
$g(\cdot)$	Inequality constraints	
H	Hessian matrix	
$h(\cdot)$	Equality constraints	
$I(\cdot)$	Improvement	
I_y, I_z	Second moments of inertia about y -axes and z -axes	m ⁴
J	Polar moment of inertia	m ⁴
jb	Jacobian vector of the Lagrangian	
$[k]$	Stiffness matrix	N m ⁻¹
$[k_a]$	Truss element stiffness matrix	N m ⁻¹
$[k_b]$	Plane beam element stiffness matrix	N m ⁻¹
$[k_t]$	Torsional bar element stiffness matrix	N m ⁻¹
k	Induced drag factor	—
k_i	Induced power factor	—
K_n	Static margin	—
L	Lift	N
L_b	Beam's length	m
L_p	Flat-plate length	m

Lh	Likelihood function	
M	Mach number	—
m	Mass	kg
m_{fuel}	Fuel mass	kg
\vec{n}	Normal to the surface	
n	Load factor	—
n_x	Number of chordwise divisions	—
n_y	Number of spanwise divisions	—
P	Power	W
p	Pressure	Pa
$P[\cdot]$	Probability	
P_{hover}	Hover required power	W
P_{vc}	Vertical climb required power	W
q	Dynamic pressure	Pa
Q_i	Equality constraints gradients	
Re	Reynold's number	—
\vec{r}	Position vector	m
R	Range	km
r	Radius	m
$R[\cdot, \cdot]$	Correlation	
S	Finite volume's surface	m ²
S	Wing area	m ²
s^2	Kriging model variance estimate	
st	Finite difference step-size	
t	Time, thickness	s, m
t/c	Thickness-to-chord ratio	—
t_{skin}	Skin thickness	m
t_{spar}	Spar thickness	m

$\hat{u}, \hat{v}, \hat{w}$	Perturbation velocity cartesian components	m s^{-1}
$\{u\}$	Displacement vector	m
$\{u_a\}$	Truss element displacement vector	m
$\{u_b\}$	Plane beam element displacement vector	m
$\{u_t\}$	Torsional bat element displacement vector	m
u, v, w	Velocity cartesian components	m s^{-1}
u_1, u_2	Axial displacements of nodes 1 and 2, in the x -axes direction	m
u_n	Induced flow velocity component	m s^{-1}
\vec{V}	Flow's velocity vector	m s^{-1}
\vec{V}_∞	Undisturbed flow's velocity, vector	m s^{-1}
\vec{v}_i	Induced velocity by the vortices in panel i	m s^{-1}
V	Flow's velocity, scalar	m s^{-1}
v_1, v_2	Normal displacements of nodes 1 and 2, in the y -axes direction	m
V_∞	Undisturbed flow's velocity, scalar	m s^{-1}
V_θ	Flow's velocity tangential component	m s^{-1}
V_h	Horizontal component of the forward flight speed	m s^{-1}
V_r	Flow's velocity radial component	m s^{-1}
V_x, V_y, V_z	Flow's velocity cartesian components	m s^{-1}
V_{ca}	Climb speed	m s^{-1}
V_{cr}	Cruise speed	m s^{-1}
V_{stall}	Stall speed	m s^{-1}
V_{tip}	Rotor's tip speed	m s^{-1}
V_{vc}	Vertical climb speed	m s^{-1}
w_1, w_2	Normal displacements of nodes 1 and 2, in the z -axes direction	m
W	Aircraft's weight	N
WL	Wing Loading	N m^{-2}
x_N	Chordwise position of the neutral point	m
x_{CG}	Chordwise position of the center of gravity	m

$Y(\cdot)$ Stochastic process
 $y(\cdot)$ Deterministic response
 $Z(\cdot)$ Random process

Subscripts

0 Property of the incompressible flow
1,2 Nodes indices
 ∞ Free-stream condition
 ca Climb angle condition
 cr Cruise condition
 ff Forward flight
 $fuel$ Property of the fuel
 $hover$ Hover condition
 i, j, k Computational indices
 lam Laminar condition
 max Maximum value
 min Minimum value
 n Normal component
 $range$ Range condition
 $root$ Property at the lifting surfaces' root position
 $skin$ Property of the lifting surfaces' skin
 $spar$ Property of the lifting surfaces' spar
 $stall$ Stall condition
 $tail$ Property of the horizontal stabilizer
 $test$ Test point
 tip Property at the lifting surfaces' tip position
 tr Transition condition
 $turb$ Turbulent condition
 vc Vertical climb condition

vf Vertical flight

$wing$ Property of the wing

x, y, z Cartesian components

Superscripts

— Reference frame property, mean

→ Vector

* Optimal solution

^ Perturbation, prediction

T Transpose

Acronyms

AC	Alternating Current
AHP	Analytical Hierarchy Process
BFGS	Broyden-Fletcher-Goldfarb-Shanno
CG	Center of Gravity
DC	Direct Current
DFP	Davidon-Fletcher-Powel
DL	Disc Loading
DOE	Design Of Experiments
DV	Design Variable
DoF	Degrees of Freedom
EI	Expected Improvement
FEA	Finite Element Analysis
FEM	Finite Element Method
FF	Full Factorial
FSI	Fluid Structure Interaction
GA	Genetic Algorithm
GEK	Gradient-enhanced Kriging
HF	High-Fidelity
ICE	Internal Combustion Engine
IDF	Individual Discipline Feasible
KKT	Karush-Kuhn-Tucker
LF	Low-Fidelity
LHS	Latin Hypercube Sampling
MAUD	Modular Analysis and Unified Derivatives
MDAO	Multidisciplinary Design Analysis and Optimization
MDA	Multidisciplinary Design Analysis
MDF	Multiple Discipline Feasible
MDO	Multidisciplinary Design Optimization
MF	Multi-Fidelity

MLE	Maximum Likelihood Estimate
MTOM	Maximum Take-Off Mass
NLBGS	Non-Linear Block Gauss-Seidel
NRMSE	Normalized Root Mean Squared Error
OAS	OpenAeroStruct
PLS	Partial Least-Squares
PL	Power Loading
RBF	Radial Basis Function
RMSE	Root Mean Squared Error
SFC	Specific Fuel Consumption
SLSQP	Sequential Least-Square Quadratic Programming
SMT	Surrogate Modeling Toolbox
SQP	Sequential Quadratic Programming
UAM	Urban Air Mobility
VLM	Vortex Lattice Method
VTOL	Vertical Take-Off and Landing
WB2	Watson and Barnes criterion
WL	Wing Loading
XDSM	eXtended Design Structure Matrix

Chapter 1

Introduction

1.1 Motivation

Over the last years, there has been a significant increase in the research of Urban Air Mobility (UAM), with the number of applications also growing.

This new concept of using aircraft in an urban scenario to transport people or cargo raises a series of new problems to be solved as the society also demands a cleaner and more sustainable aviation. Also, to have practical solutions to be used inside cities, more and more solutions are using vertical take-off and landing (VTOL) procedures so that the aircraft can land and take-off virtually at any place inside an urban context.

As these demands grow, the necessity for developing tools that consider different requirements from different disciplines also increases. Hence, Multidisciplinary Analysis and Optimization (MDAO) is a tool that can be very useful in early stages of designing a new aircraft, where usually there is a great exploration of possible concepts.

Using MDAO allows a designer to integrate multiple disciplines, for example aerodynamics, structures, propulsion, emissions, performance, among others, with the objective of considering the influence of a discipline on the others, so that in the end, the obtained solution is one that satisfies a compromise between all the disciplines taken into account.

As the complexity of the problem increases, by the increment in disciplines considered, or the higher fidelity models used, the computational burden of this optimization can become too demanding. To solve this problem, surrogate models can be used to simplify this complexity by approximating the real models.

1.2 Project Overview

The work developed during this thesis intends to find a solution for an aircraft design problem using multidisciplinary optimization. The problem includes aerodynamics, structures, and longitudinal static stability. The optimization was performed using both the real and surrogate models, and the two were compared.

The aircraft is a VTOL Unmanned Aerial Vehicle (UAV) which is an adaptation of the Flexcraft solution, which was presented at the 2019 Paris Air Show. This previous solution consists in an innovative modular aircraft concept to be used for several purposes, including passenger transportation, logistics, civil protection scenarios and air ambulance. The work developed uses this concept as a base to be changed so that the new aircraft has VTOL capability. This way the mission profile is updated, as shown in Figure 1.1.

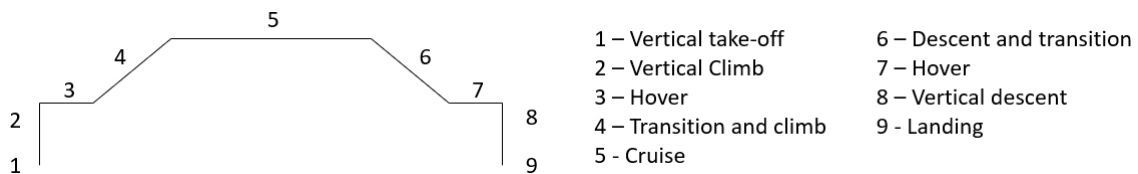


Figure 1.1: Mission profile

The new mission consists in a vertical take-off and climb to 50 ft above ground, a transition to forward flight and climb to the cruise altitude (4000 ft) which is followed by a cruise segment of up to 800 km. After, the aircraft will descend and start the transition to vertical flight again, followed by a vertical descent and landing. As mentioned above, this design is a change of the Flexcraft concept [1] and therefore some aspects of its design were maintained:

- Vertical tail dimensions
- Fuselage shape and weight
- Booms' design
- Lifting surfaces' airfoils

1.3 State of the art

In this section a brief literature review on the topic is provided. First an overview on the work that is being developed on UAM is given. After this, some simplifications commonly used in aircraft design, and the disciplines usually used in a conceptual/preliminary phase are reviewed. Then, a review on Multidisciplinary Design Optimization (MDO) and its uses is shown, followed by a revision on some optimization framework architectures. Finally, a summary on surrogate models and sampling plans is provided.

1.3.1 Urban Air Mobility

In the last decade, the number of companies investing in UAM solutions is increasing significantly with the market expected to reach a 9.1 billion US dollars value by 2030 [2], and at the moment the concept is close to become a reality. The number of recent studies [3–6] on the matter is very significant, with increasing efforts for building a faster and more flexible means of transport in urban centres. Some

concepts that are already at advanced stages of design are for example the CityAirbus [7], Lilium Jet [8], or the Joby S4 [9, 10]. A survey on recent developments on the field can be found in [11, 12].

Different configurations are being proposed, with diverse solutions so that the aircraft can take-off vertically [13]. The solution may be to use a Lift+Cruise configuration, where there are some designated fixed motors for the take-off and others, also fixed, for the cruise phase. On the other hand, more versatile solutions are also presented, such as having tilt-rotors or tilt-wings.

1.3.2 Aircraft Design

In an aircraft design MDO problem, the most common disciplines used are aerodynamics, structures, weight estimation and propulsion. During the initial stages of conceptual and preliminary design, usually the designers work with simple models such as empirical equations [14–17] or panel methods [18] for aerodynamics, empirical equations [14, 19, 20] or statistical data for weight estimation, statistical approximations [21] for propulsion and analytical equations or simplified numerical equations [22, 23] for structural analysis. As mentioned above, usually some constraints regarding mission performance and requirements are used, and so often geometric models, trim and stability and performance are considered. Geometric models are often used to parametrize the aircraft in aerodynamic or structural analysis [21, 24–26]. Stability is often taken into account by calculating the stability derivatives and comparing them to empirical equations [15, 27–29] or by the use of stability metrics like the static margin [19, 30] and trim is guaranteed by allowing the control surfaces variables to change [31, 32]. Some more disciplines may be considered in the problem, like noise restrictions [3, 4, 33, 34] and emissions [3, 4, 30, 35], especially in UAM problems.

1.3.3 Multidisciplinary Optimization

As the computation capabilities improve, so do the methods to solve complex MDO problems in aircraft design. A survey of the most common practices in recent years can be found in [36]. The research on the topic continues to grow, with different topics being explored, like efficient optimization methods [37–43] and using different architectures [44].

When it comes to MDO applied to aircraft design problems, the most used objectives are related to the overall operation and are associated with weight, aerodynamics, and mission performance [36], and the objective function can be of a single function or a combination of multiple functions, being a multiobjective problem. Concerning the constraints used, they can be regarding mission requirements [31, 45, 46] or performance restrictions, such as noise and/or emissions [3, 4].

1.3.4 Multidisciplinary analysis

Since the computational capabilities are limited, there must be a compromise between the intended accuracy and these limitations. As mentioned above, during the initial stages of design, where a wider exploration of the design space is usually desired, simplified models, Low Fidelity (LF) models are then used [24, 30, 31, 47–50], as they come at a lower computational cost. At a more advanced stage in

the design, during detailed design there is a need for higher accuracy, and so High Fidelity (HF) models need to be used [51–54].

To overcome the loss of accuracy observed in LF models and the high computational burden in HF models, some medium fidelity models can be used. There are two techniques for having this kind of models: refinement of LF simulations [25, 26, 54] or simplification of the HF models [21, 55]. Alternatively to these solution, a Multi-Fidelity (MF) approach can also be used. In such case, usually LF models are used to explore the design space and an HF model is used on specific points of interest [15, 51, 56–59].

1.3.5 Framework architectures

A sequence of the MDAO must be defined, and since multiple disciplines and their influence on one another are being considered, the coupling also needs to be defined.

A survey of different MDAO architectures can be found in [44]. Usually, these different architectures are divided into monolithic and distributed, the first solving a single optimization problem and the latter decomposing the problem into a set of smaller ones. Two examples of monolithic architectures are the Multiple Discipline Feasible (MDF) and the Individual Discipline Feasible (IDF).

IDF architecture applies the Implicit Function Theorem to the constraints and so the coupling and state variables become functions of the design variables and coupling targets. This architecture, despite being simpler to implement than MDF, demonstrates a big disadvantage when a gradient-based optimization is used because of its high computational cost due to the higher number of constraints [60, 61].

MDF architecture is more commonly used as it has a global optimizer and a complete analysis of all disciplines at each global iteration, guaranteeing a convergence of the discipline coupling. Due to this analysis, the method is usually costly to build and run, but it ensures that a discipline converged to a solution at the end of each iteration [19, 21, 25, 28, 33, 45, 59, 62].

1.3.6 Surrogate models

These approximation models are used to decrease the computational cost of an optimization problem, replacing complex models with simplified ones that intend to mimic their behaviour. However, as the models are simplified, there can also be a loss of accuracy, with the surrogate models presenting significant deviations relative to the complex models. The models can also be used to generalize the behaviour of a limited sample of experimental data [63]. A frequently used model is the Kriging model [37, 41, 64, 65] defined by Matheron [63], or some of its adaptations, such as KPLS [41, 42], KPLSK [42], and other variants [47, 56, 57, 66, 67]. Some other examples of different models can be found in [37, 64, 65, 68–71]. The models used in this thesis, RBF and Kriging are presented in section 2.3.

1.3.7 Design of Experiments

Design Of Experiments (DOE) consists of a set of sample points where the objective function is evaluated with the real model, so the surrogate model can then be trained. Different methods [37, 71–74] can

be used to create a sampling plan within the design space, with the most common being the Latin Hypercube Sampling (LHS) [37]. Recently, there have been advances on adaptive sampling plans [39, 43, 75] that use space-filling criteria to update the sampling plan and consequently the surrogate model itself. An example of these criteria is the Expected Improvement (EI) [39, 43, 57], that is based on the probabilistic side of the surrogate model.

1.4 Objectives

The main objective of this thesis is to obtain an optimal solution for the aircraft design problem presented. Three different approaches are going to be used to perform the optimization, to try to find this optimal solution: (i) an optimization using the real functions, built in OAS; (ii) an optimization using surrogate models that mimic the behaviour of the real functions; (iii) an optimization using infill criteria to adapt the surrogate models. Therefore, another macro objective of this thesis is to compare the three different methods employed.

To achieve these two broad objectives, the work can be divided into the following steps:

1. Conceptual design: definition of the initial configuration concept, initial sizing, weight and balance estimations and the propulsive system configuration definition;
2. Problem definition: mission requirements, objective function, design variables and constraints;
3. Adapt the computational models, in OAS, to the problem at hand;
4. Study of different surrogate models and sampling plans with analytical test functions;
5. Assemble the databases to build the surrogate models;
6. Create the surrogate models;
7. Solve the optimization problem using the different approaches;
8. Compare the results of the different approaches.

1.5 Thesis Outline

The structure of this thesis is as follows.

In **chapter 2**, the theoretical aspects of the models used are presented, namely:

- Aerodynamic and structural background of the models used in OAS;
- Basic concepts and definitions of multidisciplinary optimization;
- Surrogate models and surrogate models' search background;
- Brief description of the optimization algorithms used.

In **chapter 3**, the whole process followed to solve this aircraft design problem is presented:

- First, the conceptual design and the decisions made in this phase are presented;
- Then, the optimization problem formulation is stated;
- After this, the MDA implementation schemes are explained, followed by the MDO methodology.

In **chapter 4**, the results obtained for the different case studies are presented and analysed. For each case study, a comparison between the three different optimization approaches is also provided.

In **chapter 5**, an overview of this thesis' achievements is provided. Some major conclusions about the optimization results are also presented. Finally, some suggestions for future work are given.

Chapter 2

Theoretical Overview

2.1 Multidisciplinary Analysis

The aircraft design problem in this study involves two main disciplines, structures and aerodynamics. These two disciplines are coupled since the aerodynamic loads influence the structural analysis which in turn may change the aerodynamic loads a lifting surface is subject to. In this section, these two major disciplines, their coupling and support elements of the problem are addressed.

2.1.1 Structural Analysis

The structural analysis is implemented in the OpenAeroStruct (OAS) [22] framework and it uses a six degrees of freedom (DoF) per node three dimensional spatial beam in a finite element method.

The purpose of this structural analysis is to obtain the displacements of the lifting surfaces knowing the loads they are subjected to. The fundamental equation to compute this deformation is [76]:

$$[K]\{u\} = \{F\} \quad (2.1)$$

where $[K]$ corresponds to the stiffness matrix, $\{u\}$ to the displacement vector and $\{F\}$ to the load vector.

To compute the displacements along the lifting surface the following steps are carried out: first, in the pre-processing phase, the domain is discretized into elements, the local stiffness matrix for each element is calculated and then the global stiffness matrix is assembled; after this, during the processing phase, equation (2.1) is solved, by using the sparse LU-decomposition to invert the matrix; in the post-processing phase, the global displacements can then be transformed and the local strains and the stress applied on each element can be computed.

2.1.1.1 Spatial Beam Element

The element used in the structural analysis is a combination of three basic elements [22]: a truss element, a torsional bar element and two plane beam elements. This is possible by superposition of the elements. As a result, the final spatial beam element has two nodes with six DoF each, as shown in

Figure 2.1.

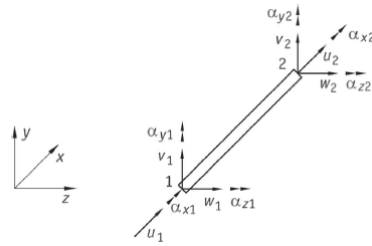


Figure 2.1: Spatial beam representation [22]

The correspondent local stiffness matrix is:

$$[k] = \begin{bmatrix} \frac{E_y A}{L_b} & 0 & 0 & 0 & 0 & 0 & -\frac{E_y A}{L_b} & 0 & 0 & 0 & 0 & 0 & 0 \\ \frac{12E_y I_z}{L_b^3} & 0 & 0 & 0 & 0 & \frac{6E_y I_z}{L_b^2} & 0 & -\frac{12E_y I_z}{L_b^3} & 0 & 0 & 0 & 0 & \frac{6E_y I_z}{L_b^2} \\ \frac{12E_y I_y}{L_b^3} & 0 & -\frac{6E_y I_y}{L_b^2} & 0 & 0 & 0 & 0 & 0 & -\frac{12E_y I_y}{L_b^3} & 0 & -\frac{6E_y I_y}{L_b^2} & 0 & 0 \\ \frac{GJ}{L_b} & 0 & 0 & 0 & 0 & 0 & 0 & 0 & 0 & -\frac{GJ}{L_b} & 0 & 0 & 0 \\ \frac{4E_y I_y}{L_b} & 0 & 0 & 0 & 0 & 0 & 0 & 0 & \frac{6E_y I_y}{L_b^2} & 0 & \frac{2E_y I_y}{L_b} & 0 & 0 \\ \frac{4E_y I_z}{L_b} & 0 & 0 & 0 & 0 & 0 & -\frac{6E_y I_z}{L_b^2} & 0 & 0 & 0 & 0 & \frac{2E_y I_z}{L_b} & 0 \\ & & & & & \frac{E_y A}{L_b} & 0 & 0 & 0 & 0 & 0 & 0 & 0 \\ & & & & & & \frac{12E_y I_z}{L_b^3} & 0 & 0 & 0 & 0 & -\frac{6E_y I_z}{L_b^2} & 0 \\ & & & & & & & \frac{12E_y I_y}{L_b^3} & 0 & \frac{6E_y I_y}{L_b^2} & 0 & 0 & 0 \\ & & & & & & & & \frac{GJ}{L_b} & 0 & 0 & 0 & 0 \\ & & & & & & & & & \frac{4E_y I_y}{L_b} & 0 & 0 & 0 \\ & & & & & & & & & & \frac{4E_y I_z}{L_b} & 0 & 0 \end{bmatrix} \quad \text{symm} \quad (2.2)$$

where E_y is the Young's modulus of the beam material, A is the element's cross-sectional area, L_b is the beam's length, G is the material's shear modulus and J is the torsion constant, and I_y and I_z are the second moments of area about y -axes and z -axes. These properties are calculated for the cross-section according to what is explained in [23].

2.1.1.2 Global Stiffness Matrix

As mentioned above, the next step is to transform the local matrices into the global reference frame. This change is achieved by a series of three matrix rotations.

The final global matrix is the combination of all global node entries, and the result matrix has a form represented in Figure 2.2.

2.1.1.3 Failure criterion

To determine if there is a failure at some point in the structure of the wing and horizontal tail, the Von Mises criterion [77] is used. The equivalent Von Mises stress is calculated, with equation (2.3), and is

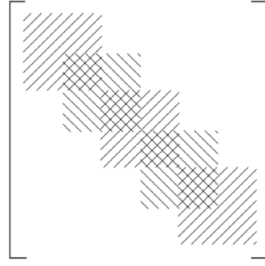


Figure 2.2: Global matrix representation

then compared to the admissible stress, that also considers a safety factor of 1.5.

$$\sigma_{VM} = \sqrt{\frac{1}{2} [(\sigma_{11} - \sigma_{22})^2 + (\sigma_{22} - \sigma_{33})^2 + (\sigma_{33} - \sigma_{11})^2] + 3(\sigma_{12}^2 + \sigma_{23}^2 + \sigma_{31}^2)} \quad (2.3)$$

where σ_{VM} is the equivalent Von Mises stress, σ_{11} , σ_{22} and σ_{33} are the direct stresses; and σ_{12} , σ_{23} , and σ_{31} are the shear stresses.

2.1.2 Aerodynamic Analysis

In this subsection a brief description of the aerodynamic model used in the framework of OpenAeroStruct is given. The methodology here explained is presented in detail by Anderson [78].

The fundamentals of aerodynamics used to explain the methods used in this work are shown in Appendix A.

2.1.2.1 Vortex Flow Element

This is a flow element where the streamlines are concentric circles in the anticlockwise direction, as it can be seen in Figure 2.3:

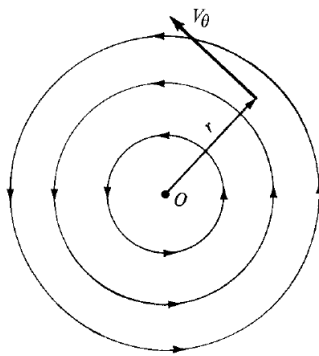


Figure 2.3: Vortex flow element [78]

In this kind of flow, the induced tangential velocity, V_θ , is inversely proportional to the distance between the point considered and the vortex origin, r , and the radial velocity, V_r is zero:

$$\begin{cases} V_\theta = \frac{const}{r} \\ V_r = 0 \end{cases} \quad (2.4)$$

Since the circulation is defined as:

$$\Gamma = \oint \vec{V} \cdot ds = -2\pi r V_\theta \quad (2.5)$$

Now, the induced tangential velocity can be determined as a function of the circulation:

$$V_\theta = -\frac{\Gamma}{2\pi r} \quad (2.6)$$

As the problem in hand is a three-dimensional one, now a vortex filament must be considered, instead of a plane vortex flow. An example of a vortex filament can be seen in Figure 2.4.

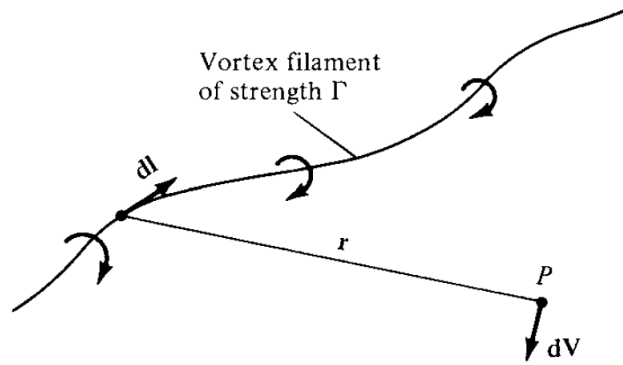


Figure 2.4: Vortex filament of strength Γ [78]

Given the rotational nature of the flow, the Biot-Savart law [78] can now be used to determine the velocity gradient:

$$d\vec{V} = \frac{\Gamma}{4\pi} \frac{d\vec{l} \times \vec{r}}{\|\vec{V}\|^3} \quad (2.7)$$

where \vec{V} is the flow velocity, $d\vec{l}$ is the finite filament size and \vec{r} is the position vector. Now the induced velocity at any point can be found by integrating equation (2.7).

To study an inviscid, incompressible flow using this approach, first two important theorems need to be introduced, the Helmholtz's vortex theorems [78]:

1. The strength of a vortex filament is constant along its length.
2. A vortex filament cannot end in a fluid; it must extend to the boundaries of the fluid (be they finite or infinite) or form a closed path.

2.1.2.2 Lifting Line Theory

It is now possible to apply this approach to a finite wing model, using one single vortex filament, thus using Prandtl's lifting line theory [78]. This theory can be applied to wings that present a twist distribution, a chord distribution and a variable airfoil along the span, but it does not consider dihedral or sweep. As said before, it is assumed that the flow is incompressible and the theory gives good approximations when used for wing with an aspect ratio greater than four, $AR \geq 4$ [78].

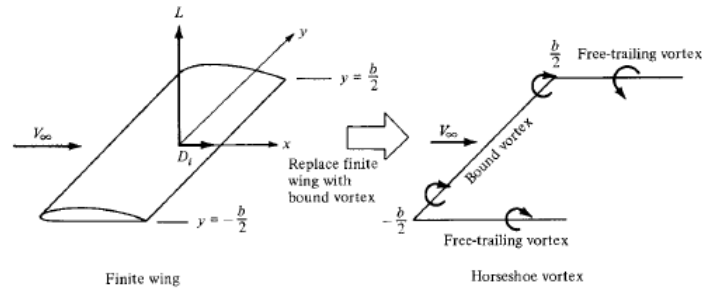


Figure 2.5: Single horseshoe vortex modelling [78]

The theory states that the wing can be represented by a bound vortex with constant strength, Γ . As stated by Helmholtz, a vortex cannot end in a fluid, so this bound vortex needs to continue in the form of two trailing vortices that go from the wing tip to infinity. This system of vortex filaments is called a horseshoe vortex and is illustrated in Figure 2.5. Now, if the wing is discretized along its span, this theory leads to a larger number of horseshoe vortices, as it can be seen in Figure 2.6, that can be superimposed to study the flow.

From Figure 2.6, a single bound vortex, with strength Γ_1 , acts from point A to F. As said before, this continues to the trailing vortices, so the vortex filaments at the wing tips have the same strength. Between points B and E, another vortex is superimposed, and the strength of the bound vortex is now $\Gamma_1 + \Gamma_2$, and because of these two additional trailing vortices need to start from these two points with a strength Γ_2 . This way the lifting surface is represented by a single lifting line that is discretized only in the spanwise direction. This theory as explained here is the basis to the Vortex Lattice Method explained above.

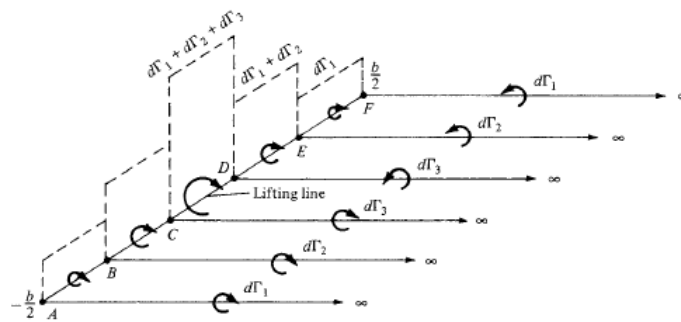


Figure 2.6: Superimposition of horseshoe vortices along the lifting line [78]

2.1.2.3 Vortex Lattice Method

To overcome the fact that the Lifting Line Theory only allows for a spanwise distribution, another method can be used, the Vortex-Lattice Method (VLM) [78, 79]. This method uses a series of lifting lines instead of just one. Now the wing is discretized along the span and along the chord leading to lifting panels. Each of these is represented by a single horseshoe of constant unknown strength. A representation of one of these lifting panels is illustrated in Figure 2.7.

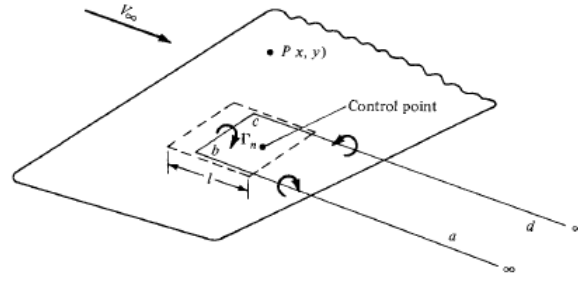


Figure 2.7: Lifting panel schematic with one horseshoe vortex [78]

The bound vortex is located at one quarter of the panel's chord and there are two trailing vortices as before that begin at each side of the panel. A control point is defined at the center line of the panel with respect to the spanwise direction and at the three-quarter panel's chord from the front.

The tangency condition at the control points specifies that the normal velocity at the panel must be zero. This way:

$$\vec{V}_\infty \cdot \vec{n} + u_n = 0 \quad (2.8)$$

where \vec{V}_∞ is the freestream velocity, \vec{n} is the normal to the panel and u_n is the induced flow velocity component.

The induced flow velocity u_n at every control point is a result of a linear combination given by:

$$u_n = \sum_{j=1}^N A_{i,j} \Gamma_j \quad (2.9)$$

where N is the total number of vortices (corresponding to the number of panels) and $A_{i,j}$ represents a row of the aerodynamic influence coefficient (AIC) matrix, which represents the induced flow on panel i due to the vortex on panel j .

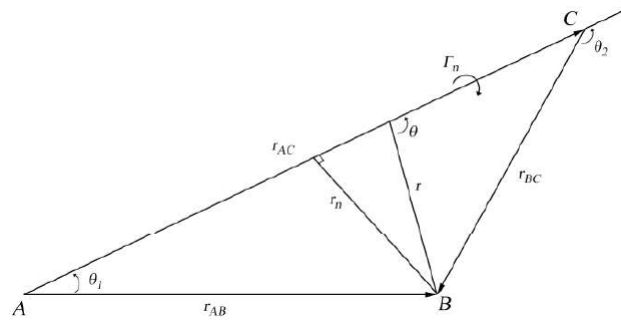


Figure 2.8: Influence of the vortex Γ_n on point B [78]

These coefficients can be calculated using only the grid information, as shown in Figure 2.8. From the Biot-Savart equation (2.7) and knowing that $dl = r d\theta$:

$$dV = \frac{\Gamma_n dl r \sin \theta}{4\pi \|\vec{r}\|^3} \Leftrightarrow dV = \frac{\Gamma_n dl \sin \theta}{4\pi \|\vec{r}\|^2} \Leftrightarrow dV = \frac{\Gamma_n \sin \theta d\theta}{4\pi \|\vec{r}\|} \quad (2.10)$$

Integrating, knowing that the normal distance between B and the vortex line is r_n , the induced velocity

in B because of the vortex line AC is:

$$V = \int_{\theta_1}^{\theta_2} dV = \frac{\Gamma_n}{4\pi} \int_{\theta_1}^{\theta_2} \sin \theta d\theta \Leftrightarrow V = \frac{\Gamma_n}{4\pi} (\cos \theta_1 - \cos \theta_2) \quad (2.11)$$

This way, the influence of a vortex on a specific control point can be computed.

Returning to the tangential condition equation (2.8) and using equation (2.9), and now that the AIC is known, the entire circulation distribution can be calculated:

$$\sum_{j=1}^N A_{i,j} \Gamma_j = -V_\infty \sin \alpha \quad (2.12)$$

where α is the angle between the freestream velocity and the panel.

With the circulation distribution known, now the loads applied on the panels can be determined, using the Kutta-Joukowski theorem:

$$\vec{F}_i = \rho(\vec{V}_\infty + \vec{v}_i) \Gamma_n \times \vec{b}_i \quad (2.13)$$

where \vec{v}_i is the induced velocity by the vortices and \vec{b}_i is the vector describing the bound vortex for the panel.

This force distribution can then be decomposed into lift and drag distributions, which can then also be integrated to calculate the total aerodynamic forces and their coefficients.

2.1.2.4 Compressible Correction

Now that the incompressible aerodynamic coefficients are available, to achieve the compressible flow coefficients, the Prandtl-Glauert [78, 79] theory is employed.

This transformation consists of changing the reference frame from the physical domain xy , used to compute the linearised potential equation, equation (A.19), to a reference frame $\xi\eta$, where: $\xi = x$ and $\eta = \beta y$. The velocity potential, $\bar{\phi}$ is now:

$$\bar{\phi}(\xi, \eta) = \beta \hat{\phi}(x, y) \quad (2.14)$$

and the transformed derivatives are:

$$\frac{\partial \hat{\phi}}{\partial x} = \frac{\partial \hat{\phi}}{\partial \xi} \frac{\partial \xi}{\partial x} + \frac{\partial \hat{\phi}}{\partial \eta} \frac{\partial \eta}{\partial x} = \frac{\partial \hat{\phi}}{\partial \xi} \quad (2.15)$$

$$\frac{\partial \hat{\phi}}{\partial y} = \frac{\partial \hat{\phi}}{\partial \xi} \frac{\partial \xi}{\partial y} + \frac{\partial \hat{\phi}}{\partial \eta} \frac{\partial \eta}{\partial y} = \frac{1}{\beta} \frac{\partial \hat{\phi}}{\partial \eta} \quad (2.16)$$

Finally, combining equations (2.14), (2.15) and (2.16), the following is obtained:

$$\begin{cases} \frac{\partial \hat{\phi}}{\partial x} = \frac{1}{\beta} \frac{\partial \bar{\phi}}{\partial \xi} \\ \frac{\partial \hat{\phi}}{\partial y} = \frac{\partial \bar{\phi}}{\partial \eta} \end{cases} \quad (2.17)$$

The same procedure is used to calculate the second derivatives and so the new potential equation, derived from equation (A.19) for compressible flow in the new reference plane becomes:

$$\frac{\partial^2 \bar{\phi}}{\partial \xi^2} + \frac{\partial^2 \bar{\phi}}{\partial \eta^2} = 0 \quad (2.18)$$

which corresponds to the Laplace's equation.

To compute the lift and drag coefficients, firstly, the pressure coefficient is defined by:

$$C_p \equiv \frac{p - p_\infty}{q_\infty} \quad (2.19)$$

where p is the pressure at the considered point, p_∞ is the pressure at the undisturbed flow and q_∞ is the dynamic pressure at the undisturbed flow given by $q_\infty = \frac{1}{2} \rho_\infty V_\infty^2$.

This dynamic pressure can be written in terms of M_∞ and considering that $a^2 = \gamma \frac{p_\infty}{\rho_\infty}$ the pressure coefficient defined on equation (2.19) becomes:

$$C_p = \frac{2}{\gamma M_\infty^2} \left(\frac{p}{p_\infty} - 1 \right) \quad (2.20)$$

Using the isentropic relations and considering that $\left(\frac{\hat{u}}{V_\infty} \right)^2, \left(\frac{\hat{v}}{V_\infty} \right)^2, \left(\frac{\hat{w}}{V_\infty} \right)^2 \ll 1$, the pressure coefficient can now be written as:

$$C_p = -\frac{2\hat{u}}{V_\infty} = \frac{2}{V_\infty} \frac{\partial \hat{\phi}}{\partial x} = -\frac{2}{V_\infty} \frac{1}{\beta} \frac{\partial \bar{\phi}}{\partial \xi} = \frac{1}{\beta} \left(-\frac{2\bar{u}}{V_\infty} \right) \quad (2.21)$$

Note that $-\frac{2\bar{u}}{V_\infty}$ is simply the linearised pressure coefficient for the incompressible flow, and so the pressure coefficient for compressible flow is:

$$C_p = \frac{C_{p,0}}{\beta} = \frac{C_{p,0}}{\sqrt{1 - M_\infty^2}} \quad (2.22)$$

where $C_{p,0}$ is the linearised pressure coefficient for incompressible flow.

2.1.2.5 Viscous empirical corrections

Since the methods used during the aerodynamic analysis assume an inviscid flow, some viscous corrections are applied to the drag calculation, based on empirical equations [80, 81].

The skin friction coefficient on a flat-plate of a laminar flow [80] is given by:

$$c_{f_{lam}} = \frac{0.664}{\text{Re}^{1/2}} \quad (2.23)$$

On the other hand, considering a turbulent flow with a Mach number higher than 0.3, the skin friction coefficient [80] is:

$$c_{f_{turb}} = \frac{0.455}{(\log_{10} \text{Re})^{2.58} (1 + 0.144 M^2)^{0.65}} \quad (2.24)$$

With equation (2.23) and (2.24) the drag coefficient can then be calculated:

$$c_d = c_{d_{lam}} + c_{d_{turb}} = c_{d_{lam}}(x_{crt}) + c_{d_{turb}}(L_p) - c_{d_{turb}}(x_{crt}) \quad (2.25)$$

where x_{crt} is the point where the transition starts and L_p is the flat-plate length.

This calculated flat-plate skin friction drag coefficient is then adjusted to take into account the pressure drag using a form factor for lifting surfaces [81]:

$$FF_{surf} = \left[1 + \frac{0.6}{(x/c)_{max}} \left(\frac{t}{c} \right)_{max} + 100 \left(\frac{t}{c} \right)_{max}^4 \right] [1.34M^{0.18}(\cos \Lambda)^{0.28}] \quad (2.26)$$

where $(x/c)_m$ is the chordwise location of the airfoil maximum thickness point, $(t/c)_{max}$ is the maximum thickness-to-chord ratio, and Λ is the wing sweep.

2.1.3 Fluid Structure Interaction

In the previous sections, the aerodynamic and structural models were discussed. During the multidisciplinary analysis, information from one analysis is passed to the other and so there is a need to define the Fluid Structure Interaction (FSI).

Knowing the aerodynamic and structural solution at iteration k , the coupled solution at iteration $k + 1$ can be obtained following the next steps [82]:

1. Solve aerodynamic system for the current iteration;
2. Integrate aerodynamic loads onto structural domain;
3. Solve structural analysis with the aerodynamic loads as input;
4. Displacement transfer from the structural analysis to the aerodynamic surface mesh;
5. Update the mesh and start from step 1 again, until convergence is achieved.

The implementation of the FSI in the OAS model is fully described in [22].

2.2 Multidisciplinary Optimization

In this subsection, the basic concepts of multidisciplinary design optimization will be introduced based on [83].

2.2.1 Basic Concepts

- Objective function: function f to be minimized (or maximized) during the optimization process. It allows the designer to compare different designs.
- Design variables: Is through these variables that the solver may vary the objective function. This way, the optimization process consists of finding the values for the set of design variables that minimize or maximize the objective function (subjected to the constraints, which are explained below). All possible combinations of the different design variables' values form the design space.

The k -dimensional vector corresponding to the different k design variables will be denoted as x , and defines each design point.

- Constraints: Metrics used to restrict the possible solution. Constraints are the way to ensure that the obtained optimized solution is feasible. Most engineering applications are constrained problems. These constraints can be limits on the design variables values directly, and in this case they are called bounds, or they may limit the results indirectly, for example having a restricted static margin. In this latter case, the constraints may be equalities and/or inequalities.

This way, the optimization problem can be formulated as in [83]:

$$\begin{aligned}
 &\text{minimize} && f(x) \\
 &\text{w.r.t} && x \in \chi \\
 &\text{subject to} && g_i(x) \leq 0 \quad i = 1, \dots, n_g \\
 &&& h_j(x) = 0 \quad j = 1, \dots, n_h
 \end{aligned} \tag{2.27}$$

where g are the inequality constraints vector, that includes also the design variables' bounds, h are the equality constraints vector and χ is the design space.

2.2.2 MDO architectures

The MDO architecture sets the structure of how the MDAO problem is going to be solved, it defines the sequence of the optimization.

Architectures can be monolithic or distributed. When using the first approach, there is a single optimization problem. On the other hand, when using a distributed architecture, the optimization problem is divided into smaller sub-problems with a smaller number of design variables and constraints [44]. The latter approach is not going to be used in this thesis.

As mentioned, in a monolithic architecture, a single optimization problem is solved. Therefore, only one optimizer is used to find the design variables values that minimize (or maximize) the objective function, while guaranteeing that the constraints are satisfied. The architecture in the scope of this thesis is the Multi Discipline Feasible (MDF).

2.2.2.1 Multi Discipline Feasible

The architecture was suggested by [84] and it ensures that each optimization iteration is multidisciplinary feasible, *i.e.*, that in each iteration the coupling constraints are satisfied. The optimization problem that is solved when using this architecture is the standard, presented in equation (2.27).

2.3 Surrogate Models

In early stages of aerostructural design it is necessary for the designer/optimizer to have as much information as possible. That means a huge amount of simulations/experiments has to be done in order to give enough information about the design space.

Even though the computational power is increasing significantly every year, solving optimization design problems in aircraft engineering is often very costly [85]. These problems, involving a multiple number of disciplines, such as structural or aerodynamic design and analysis, generally are associated with a high number of variables and constraints. Furthermore, the search for an optimal aircraft design may lead to unconventional solutions, where unaccounted phenomena such as non-linearities might become relevant. As said before, in an early stage of design, the optimizer is interested in exploring the design space as much and as fast as possible.

According to [69] there are three ways of performing heavy simulations in optimization problems:

- Using supercomputers, which are very expensive, especially when the management of the down-time is poorly made
- Using Cloud computing
- Building surrogate models

A surrogate model is an approximation model that tries to mimic the behaviour of the real model. This surrogate model is cheaper to evaluate than the original one. These models, also known as metamodels are being used to replace the complex simulation-based models [37, 74].

To build such model, there are three main steps [86]. First, a set of training points must be generated, by performing a Design of Experiments and a modeling technique has to be chosen. The second main step in constructing a metamodel is the training of the model itself on the given points. After building it, the model must be validated and tested. For this validation purposes, different metrics can be used to evaluate the performance of the model, see section 2.3.3.

2.3.1 Sampling Techniques

Sampling strategies evolved in the past years, consequence of the increasing in using these strategies to explore an input space. In the beginning, experiments were planned by using the one factor or variable factor at a time approach or by using a trial and error approach [73]. These strategies were too expensive and the latter did not even guarantee to find the best sample points location [37].

Fisher [72] introduced the Design of Experiments to plan the experiments in order to understand the behaviour of agricultural crops systems. He defined three basic principles, randomization, replication and blocking [37]. These new strategies were planned when only physical experiments (which can be biased) were made. With the emergence of computational experiments, the need of replication was lost, since simulation-based experiments are deterministic [73].

Montgomery [73] outlined these three basic principles of DOE:

- Randomization - The order of the runs and each run material experiment have to be randomly determined. This principle ensures an alleviation of bias by external factors.
- Blocking - Is a technique that reduces the unexplained variability, i.e, the variability that cannot be overcome is mixed with an interaction to eliminate its influence on the experiment. This is done

by using groups/blocks of runs that have similar nuisance factors (that are not the scope of the experiment).

- Replication - This concept has two properties. First, it allows for a determination of an eventual experimental error. Second, by using the mean of one parameter, replication gives the experimenter the chance to obtain a more precise value for the real response of the parameter.

The DOE sampling strategies can be classified into two main groups [73]:

- Classical DOE – Examples: Full/fractional factorial design, Central Composite Design (CCD), Box-Behnken design and Orthogonal Arrays (OA). The first is explained below and the others can be found in [73];
- Modern DOE – Main groups: Random designs, Quasi-random designs, Projection-based designs, Uniform designs, Miscellaneous designs and Hybrid designs [73].

2.3.1.1 Classical Design of Experiments

Classic DOE are sampling techniques that assume an uniform distribution of training points. This ensures a fixed number of samples and so the influence of the random error term in posterior simulations is minimized. In this category, the Full and Fractional Factorial Designs will be presented.

Full and Fractional Factorial Designs

In a Full Factorial (FF) design, in each run of the experiment, every possible combination of factor levels has to be tested. For example, if the problem has two factors, one with x levels and another with y levels, in each run there are xy possible combinations.

This sampling technique can be implemented in Python, using the Surrogate Modelling Toolbox referred in [74]. The number of levels used in industrial experiments is commonly 2 or 3, i.e, 2-levels (2^k) and 3-levels (3^k) factorial designs, where k is the number of factors/design variables. A geometrical view of a 2^3 full factorial design is presented in Figure 2.9.

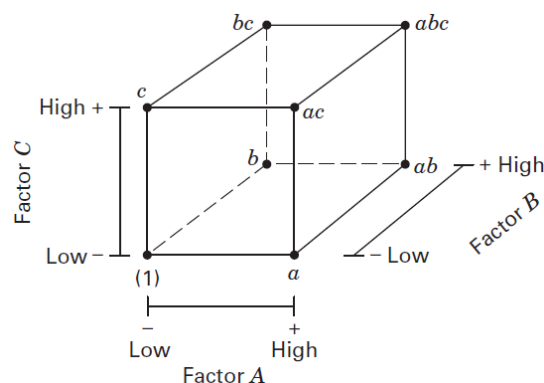


Figure 2.9: 2^3 Full-factorial design geometrical view [73]

These designs are used when the optimizer desires to fully explore the design space. However they have some limitations [37]:

- The computational cost is high because the size of the experiment depends on the number of design variables.
- The response of a 2-levels full factorial design is approximately linear over the range of the design variables.

As a way to reduce the size of the experiment, and if the designer knows *a priori* that certain high-order interactions are negligible, instead of running the whole experiment, only a fraction of it may be tested. Thus, the relevant information can still be obtained and the time to run the experiment is reduced.

These designs are known as fractional factorial designs and are usually represented by $2^{(k-p)}$, for a 2-levels fractional factorial design with k design variables and where $1/(2^p)$ represents the fraction of the full factorial design. To generate a fractional factorial design, the experimenter has to choose the criteria to select the fractions. The most used ones are the highest resolution possible and the minimum aberration [73].

2.3.1.2 Modern Design of Experiments

Modern DOE are also known as space-filling or exploratory designs. These DOE have been replacing the classical ones mainly because of their expensive cost. These techniques tend to locate more training points in the interior of the design space [73].

Random Designs

The methods in this category generate training points which have an equal probability to appear in any sample n from a population N . [87]

The most common methods from this group are the Monte Carlo methods. Such methods include for example the Markov Chain Monte Carlo (MCMC) samplings, Gibbs sampling and the Metropolis Hastings sampling [73].

Monte Carlo Methods

These methods are used to evaluate mathematical/physical expressions through the use of experiments with random numbers. [87]

The methods can only be used when there is no missing data because they tend to show poor coverage regions in high dimensions. They are advantageous when used in complex systems, particularly with a high level of simultaneous correlations among the design variables. [37]

Latin Hypercube Sampling

Latin Square is $N \times N$ grid containing sample points in which there is only one point per each row and column. Latin Hypercube Sampling (LHS) [37] is a generalization of this concept to higher dimensions. This design is a variant of stratified random samplings, which uses a constraint Monte Carlo sampling to solve the uncertainty quantification of some problems.

This is the most used simulation-based design in aerodynamics because of its flexibility. However it

has some disadvantages, for example it may not always be space-filling. This drawback can be solved by using it in combination with orthogonal arrays, suitable space-filling criteria or by the construction of another LHS within small regions of the design space.

2.3.1.3 Hybrid Designs

Hybrid designs are a combination of some techniques aforementioned, either classical or modern, to overcome their individual drawbacks. There is a great effort to improve LHS and so there are several hybrid designs which are based on it such as Nearly Orthogonal Latin Hypercubes and Minimax/Maximin Latin Hypercubes [37].

The maximin LHS uses space-filling metrics to provide a good cover of the design space. The metric is based on the pairwise distances between any two points (x and x') of the sampling plan. All the distances, equation (2.28), are calculated based on the Euclidean norm [86].

$$d(x, x') = \sqrt{\frac{\sum_{i=1}^k \left(\frac{x_i - x'_i}{x_{i_{max}} - x_{i_{min}}} \right)^2}{k}} \quad (2.28)$$

where k is the number of dimensions and $x_{i_{max}}$ and $x_{i_{min}}$ are the maximum and minimum values of the i_{th} dimension of x .

Using the maximin criterion, a set of different sampling plans is built, and then, the one that maximizes the minimum distance between every two points is selected.

2.3.1.4 Adaptive sampling

The aforementioned techniques are used to generate a sampling plan which is static, *i.e* which does not change during the evolution of an optimization. However, some points can be added to some areas of interest, for example where the objective function is expected to be improved or where there are few sample points. When points are added to the initial sampling plan, according to some criterion at choice, the sampling is called adaptive. Some criteria that can be used for this purpose are explained in section 2.4.

2.3.2 Surrogate Modelling Techniques

A surrogate model is a cheaper to evaluate approximation of the real model. These models have been becoming more used in optimization problems in aircraft engineering (examples in [19, 38, 39, 67]) because they allow for a more efficient design exploration in early stages of design.

These models can be classified according to the nature of the design variables and to the methodology [37]. When looking to the methodology, the models use different methods to determine the relationship between the different design variables:

- Regression
- Interpolation

- Projection

On the other hand, when analysing the nature of the design variables, the methods can be [86]:

- Parametric - depend explicitly on the model structure and presuppose a global functional relationship between the training set and responses. Examples: Polynomial regression [37, 65] and Multivariate Adaptive Regression Splines (MARS), [37, 69, 70, 86].
- Non-parametric - combine local information and implicitly construct the model. Examples: Radial Basis Function (RBF) [64, 65, 68, 70, 71, 74] and Support Vector Regression (SVR) [37, 64, 69].

In the following subsections the surrogate models used during this thesis, the Kriging models and two of its variants and the Radial Basis Function, are presented.

2.3.2.1 Kriging

Kriging [88] is a statistical interpolation method, suggested by Krige in 1951 [89] and formulated by Matheron in 1963 [63], which assumes that a deterministic response, $y(x)$ can be a realization of a stochastic process $Y(x)$, that includes a regression model, $f(x)$, and a random process, $Z(x)$:

$$Y(x) = f(x) + Z(x) \quad (2.29)$$

This random process is assumed to have a mean zero, *i.e.* $E[Z(x)] = 0$, and a non-zero covariance, given by:

$$\text{cov}[Z(x), Z(x')] = \sigma^2 R[Z(x), Z(x')] \quad (2.30)$$

where σ^2 is the process variance, $R[\cdot, \cdot]$ is the correlation, also known as kernel function, and x and x' are two points in χ .

The correlation between two points, depends solely on the distance between them, and it can be calculated using different kernel functions [65]. The most common one, and the one used during this work, is the squared exponential kernel function $k_{se}(x, x')$:

$$R[Z(x), Z(x')] = k_{se}(x, x') = \sum_{l=1}^d \exp(-\theta_l (x_l - x'_l)^2) \quad (2.31)$$

where $\theta_l \in \mathbb{R}$ is the hyperparameter correspondent to the l design variable and d is the number of design variables.

This way, a correlation matrix, $[\Psi]$, for the observed data can be defined by:

$$[\Psi] = \begin{pmatrix} R[(x^{(1)}, x^{(1)})] & \cdots & R[(x^{(1)}, x^{(n)})] \\ \cdots & \ddots & \cdots \\ R[(x^{(n)}, x^{(1)})] & \cdots & R[(x^{(n)}, x^{(n)})] \end{pmatrix} \quad (2.32)$$

where n is the number of sample points and x^i are the sample points locations; which leads to a covariance matrix defined by:

$$\text{cov}(\{Z\}, \{Z\}) = \sigma^2[\Psi] \quad (2.33)$$

Depending on the regression model used, the Kriging model can be:

- Simple Kriging [88] - presupposes a known constant regression term;
- Ordinary Kriging [66] - assumes a constant unknown regression term;
- Universal Kriging [65, 74] - the regression model is given by: $f(x) = \sum_{i=1}^n k_i f_i(x)$;
- Blind Kriging [66] - as commonly the full behaviour of the real model is unknown, it is complicated to choose a trend function. The main goal of blind Kriging is to find the basis/trend functions that capture the most variance in the sample data;
- Gradient-Enhanced Kriging (GEK) [47] - is an extension of Kriging model where the gradients' information is used during the construction of the model. This improves the accuracy of the prediction. There are two different ways to integrate the gradient information at samples: direct GEK and indirect GEK. In the direct approach the information is introduced directly to the model equation system by adding the weighted sum of the gradients to the weighted sum of the data. In indirect GEK, a finite difference step size has to be determined for using derivative information;
- Co-Kriging [47] - The Co-Kriging method was created to predict an under-sampled primary variable of interest by better sampled auxiliary variables. It was then extended to variable-fidelity surrogate modelling [67].

In this thesis, an ordinary Kriging is considered, and so equation (2.29) becomes:

$$Y(x) = \mu_m(x) + Z(x) \quad (2.34)$$

where μ_m is the mean of the response at a sampled design point.

The aforementioned hyperparameters are used to control the performance of the Kriging model. They can be estimated by maximizing the likelihood function [74]. This function [86], presented in equation (2.35), is a measure of the goodness of the fit for a given set of sample data and the unknown parameters.

$$Lh = \frac{1}{(2\pi\sigma^2)^{n/2} |\Psi|^{1/2}} \exp \left[-\frac{(\{y\} - \{1\}\mu_m)^T [\Psi]^{-1} (\{y\} - \{1\}\mu_m)}{2\sigma^2} \right] \quad (2.35)$$

where $\{y\}$ is the vector of sample points response and $\{1\}$ a $n \times 1$ column vector of ones. Equation (2.35) can then be simplified by taking the natural logarithm. By deriving the resulting equation and setting it to zero, one can obtain the maximum likelihood estimates (MLE) for μ_m and σ^2 :

$$\hat{\mu}_m = \frac{\{1\}^T [\Psi]^{-1} \{y\}}{\{1\}^T [\Psi] \{1\}} \quad (2.36)$$

$$\hat{\sigma}^2 = \frac{(\{y\} - \{1\}\hat{\mu}_m)^T [\Psi]^{-1} (\{y\} - \{1\}\hat{\mu}_m)}{n} \quad (2.37)$$

If we substitute these results back in equation (2.35) and by taking its logarithm, the concentrated ln-likelihood function is obtained:

$$\ln(Lh) \approx -\frac{n}{2} \ln(\hat{\sigma}^2) - \frac{1}{2} \ln |[\Psi]| \quad (2.38)$$

which depends only on the unknown hyperparameters $\{\theta\}$. The hyperparameters can therefore be found by maximizing equation (2.38), using numerical optimization.

The Kriging model can now predict the true function on an unsampled point, that has to be consistent with the observed data and with the correlation parameters found. Hence, the prediction is such that it maximizes the likelihood of the sample data and the prediction, thus the prediction \hat{y} is:

$$\hat{y}(x) = \hat{\mu}_m + \{\psi\}^T [\Psi]^{-1} (\{y\} - \{1\} \hat{\mu}_m) \quad (2.39)$$

where $\{\psi\}$ is the vector of correlations between the sampled data and the new prediction:

$$\{\psi\} = \begin{pmatrix} R[Y(x^{(1)}), Y(x)] \\ \vdots \\ R[Y(x^{(n)}), Y(x)] \end{pmatrix} = \begin{pmatrix} \psi^{(1)} \\ \vdots \\ \psi^{(n)} \end{pmatrix} \quad (2.40)$$

The model can also be used to estimate the variance of the prediction:

$$\hat{s}^2(x) = \hat{\sigma}^2 \left[1 - \{\psi\}^T [\Psi]^{-1} \{\psi\} + \frac{1 - \{1\}^T [\Psi]^{-1} \{\psi\}}{\{1\}^T [\Psi]^{-1} \{1\}} \right] \quad (2.41)$$

The approach for the estimation of the hyperparameters can be computationally heavy and the optimizer can be trapped between local minima. To solve these problems, cross-validation was presented as an alternative [37]. With this, Kriging was combined with other methods such as the Partial Least Squares (PLS) to produce faster estimates for the hyperparameters. Hence, new methods such as KPLS and KPLSK were developed. PLS is a method that searches the direction that maximizes the variance between the input and output variables. In KPLS, the PLS method is included in the Kriging correlation matrix to scale the number of inputs by reducing the number of hyperparameters [41]. KPLSK is an improvement of KPLS method which is less accurate than the original Kriging model in some cases, especially for multimodal functions. This method uses an additional step. The first step is to construct the KPLS model and estimate the hyperparameters in the reduced space. After this, the estimated hyperparameters are expressed in the original space and used as a starting point to optimize the likelihood function of a standard Kriging model. This method was proposed by Bouhlef et al. [42].

2.3.2.2 Radial Basis Function

Radial Basis Function model is used to interpolate scattered multivariate data. Each training point has an associated RBF and the model is a linear combination of all these functions. The response of these functions depends only on the distance from the prediction point to the training point in question, they decrease (or increase) monotonically with this distance [71, 74]. A common way to represent the

prediction equation for RBF is:

$$\hat{y}(x) = \sum_{i=1}^n a_i \phi_{bf}(d(x, x_i)) \quad (2.42)$$

where a_i is the weighted coefficient for the i -th basis function, n is the number of training points, $(d(x, x_i))$ is the Euclidean distance (other equivalent metric can be used) between the i -th training point x_i and a testing point x and ϕ_{bf} is a basis function. The coefficients a_i are calculated during the training stage. The basis functions can be, for example, Gaussian, multi-quadric, or inverse multi-quadric.

2.3.3 Error metrics

Since a surrogate model is just an approximation of a real function, it is important to evaluate the accuracy of the model in mimicking the real behaviour of a function. For that purpose, there are some commonly used metrics, like the Root Mean Squared Error (RMSE), and its normalized version (NRMSE), and cross-validation [90, 91].

The surrogate model can be tested in some additional test points, that also need to be evaluated with the real function. To compare the two, the RMSE, calculated using equation (2.43), is used.

$$RMSE = \sqrt{\frac{1}{n_{test}} \sum_{i=1}^{n_{test}} (f(x_{test}^i) - \hat{y}(x_{test}^i))^2}, \quad \text{for } i = 1, \dots, n_{test} \quad (2.43)$$

where n_{test} is the number of test points used, x_{test} is the sampling test point, $f(x_{test})$ is its corresponding real function value, and $\hat{y}(x_{test})$ is its surrogate prediction value.

On the other hand, instead of using computational time to compute additional test samples, the surrogate accuracy can be evaluated using the sample points itself, using cross-validation. A leave-one-out cross validation error corresponds to an error measured at a sample point using the surrogate built with all samples apart from that point. This can be done for every sample point, and the global cross-validation error measure is obtained. This error measure is called PRESS [90, 91].

2.4 Surrogate Search

After having the surrogate model built, now an optimization can be performed so that the new, approximated, objective function is minimized.

However, the surrogate model can also be used as an initial prediction and then be updated in some areas of interest. This is done by adding points to the sample set using infill criteria. The criteria used during this work are briefly explained next.

2.4.1 Expected Improvement

This criterion balances the exploitation and exploration of the design space by taking into consideration the mean and the variance provided by the Kriging model [85]. The optimizer uses the Expected Improvement (EI) function, given by equation (2.46), to add a new sample point where the EI is maximum.

According to [83], considering that the best solution know so far is x^* , and its value is $f(x^*) = y_{min}$, the improvement of a new point x for the objective function $f(x)$ is given by:

$$I(x) = \max(f(x^*) - f(x), 0) \quad (2.44)$$

which means that, if $f(x) \geq f(x^*)$ there is no improvement, and on the other hand if $f(x) < f(x^*)$, the improvement will be the possible decrease of the objective function.

The probability of this improvement is given by:

$$P[I(x)] = \frac{1}{\hat{s}\sqrt{2\pi}} \int_{-\infty}^0 e^{-[I(x)-\hat{y}(x)]^2/(2s^2)} dI \quad (2.45)$$

At a sample point, there is no probability of improvement as the function is already known there, and so the EI will also be null. The expected improvement using the distribution predicted by the Gaussian process is then given by:

$$E[I(x)] = \begin{cases} (y_{min} - \hat{y}(x))\Phi\left(\frac{y_{min} - \hat{y}(x)}{\hat{s}(x)}\right) + \hat{s}(x)\phi\left(\frac{y_{min} - \hat{y}(x)}{\hat{s}(x)}\right), & \text{if } \hat{s}(x) > 0 \\ 0, & \text{if } \hat{s}(x) = 0 \end{cases} \quad (2.46)$$

where $\Phi(\cdot)$ is the cumulative distribution function and $\phi(\cdot)$ is the probability density function of the standard normal distribution.

The expression is a trade-off between exploitation of the model and exploration of the design space. The criterion ensures that, if enough iterations are carried out, the global minimum is found. This happens because, even if the optimizer gets trapped in a local minimum at a given iteration, on the next iteration it can “jump” to a new area, where there is a lack of sample points and the variance is therefore high.

2.4.2 Watson and Barnes

The EI criterion is a multimodal function, and so the optimization can be quite costly [39]. Therefore, an alternative is presented, the Watson and Barnes criterion (WB2), proposed in [92]. The criterion aims to improve the efficiency of the optimization [43] by smoothing the EI criterion, which is done by using the prediction of the surrogate as well as the EI, resulting in an objective function given by:

$$WB2(x) = \begin{cases} \hat{y}(x) - E[I(x)], & \text{if } \hat{s}(x) > 0 \\ 0, & \text{if } \hat{s}(x) = 0 \end{cases} \quad (2.47)$$

Even though the criterion is less multimodal and leads to a more efficient optimization, it may not steer to a global minimum, and instead yield to a local minimum. This may happen because after some iterations, the magnitude of the Expected Improvement decreases, as the quality of the surrogate model gets higher, and so the algorithm focuses on exploitation.

2.5 Optimization Algorithms

After having the real and the surrogate models defined, as well as the method for surrogate search, is time now to define the optimization algorithm to be used to find the optimal solution.

The optimization process requires an iterative method, in which the guess of the optimal value is varied until a solution is obtained. What differentiates the different algorithms is their strategies to move between consecutive iterations. [83, 93].

The most common classification used to characterize optimization algorithms is by dividing them into deterministic (which can be divided into gradient-free and gradient-based) or heuristic algorithms, depending on whether or not they include a random parameter generation in the algorithm [83]. In section 2.5.1, some examples of deterministic algorithms are presented. In section 2.5.2, the genetic algorithm, heuristic, is then briefly explained.

2.5.1 Deterministic Algorithms

2.5.1.1 Gradient-free

The approach in this category is to move from a point to the next one, if the value of the objective function in the new one is smaller than before [83]. This strategy presents a high computational cost when the problem has a high number of design variables since it takes a lot of function evaluations. However, these methods can offer some advantages when solving noisy or non-differentiable function problems.

2.5.1.2 Gradient-based

Instead of using solely the objective function value at a certain point, and compare with the next point to move, these algorithms use both the objective function and its derivatives with respect to the design variables to compute the search direction.

Though they are usually faster and need fewer iterations to find the optimal solution, they require a smooth objective function and they only guarantee to converge to a local optimum. The order of the method is defined by the order of the derivatives used, for example, the steepest descent method only uses first order derivatives while Newton algorithms use second order derivatives [83, 93].

To compute the derivatives, if needed, the number of function evaluations increases, especially when using second-order methods. Therefore, to overcome this issue, while maintaining a higher accuracy, new methods were developed – the quasi-Newton algorithms. Such methods, like Davidon-Fletcher-Powell (DFP) or Broyden-Fletcher-Goldfarb-Shanno (BFGS) [83, 93], use only first order derivatives and approximate the Hessian matrix with the function and gradient values from previous iterations, hence generating second-order information.

The choice of the algorithm to be used to find the optimal solution depends also on the type of problem, which can be unconstrained or constrained. Usually, engineering problems are constrained, thus some algorithms to solve this type of problems are presented [83, 93]:

- Projection

- Sequential Quadratic Programming (SQP)
- Penalty and Barrier

In this thesis, the algorithm used is the Sequential Least-Square Quadratic Programming (SLSQP) [94], implemented on OpenMDAO [95], which allows to consider a constrained problem with both bounds, equality and inequality constraints. This algorithm simplifies the original non-linear optimization problem into simpler quadratic sub-problems. A brief description of this algorithm is given next, based on what is presented in [83].

Considering an equality constrained optimization problem, the Lagrangian function of this problem can be defined as:

$$\mathcal{L}(x, \lambda) = f(x) + h(x)^T \lambda \quad (2.48)$$

where λ is the vector of Lagrange multipliers.

The Karush-Kuhn-Tucker (KKT) conditions are necessary to solve the constrained optimization problem. These conditions are defined as the derivatives of equation (2.48) set to zero:

$$\begin{cases} \frac{\delta \mathcal{L}}{\delta x_i} = \frac{\delta f(x)}{\delta x_i} + \sum_{j=1}^l \lambda_j \frac{\delta h_j(x)}{\delta x_i} = 0, & \text{for } i = 1, \dots, k \\ \frac{\delta \mathcal{L}}{\delta \lambda_j} = h_j(x) = 0, & \text{for } j = 1, \dots, l \end{cases} \quad (2.49)$$

where k is the number of variables and l is the number of equality constraints. By solving these two conditions, the optimization problem is addressed as an unconstrained problem with $k + l$ variables, instead of a constrained problem with k variables and l (equality) constraints.

The quadratic problem in an optimization is one with a quadratic objective and linear constraints. A quadratic sub-problem at a design point x_i is defined as:

$$\begin{aligned} & \text{minimize} && \frac{1}{2} \{p\}^T [W]_i \{p\} + \{b_f\}_i^T \{p\} \\ & \text{subject to} && [Q]_i \{p\} + h_i = 0 \end{aligned} \quad (2.50)$$

where $\{p\}$ is the only unknown, $W(x, \lambda) = \nabla_{xx}^2 \mathcal{L}(x, \lambda)$, $b_f(x) = \nabla f(x)$ and $Q(x) = \nabla h(x)$.

This problem has only one unique solution, given by solving:

$$\begin{cases} [W]_i \{p\} + \{b_f\}_i - [Q]_i^T \{\lambda\}_i = 0 \\ [Q]_i \{p\} + \{h\}_i = 0 \end{cases} \quad (2.51)$$

and $\{p\}_i$ and $\{\lambda\}_i$ are the solutions of the equations.

The non-linear equations can then be solved using Newton's method $H \times st = -jb$, where H represents the Hessian matrix and jb the Jacobian vector of the Lagrangian, and st is the finite difference step-size:

$$\begin{bmatrix} W_i & -A_i^T \\ A_i & 0 \end{bmatrix} \begin{bmatrix} p_i \\ \lambda_{i+1} \end{bmatrix} = \begin{bmatrix} -b_i \\ -h_i \end{bmatrix} \quad (2.52)$$

The set of variables p_i is used to update the design point:

$$x_{i+1} = x_i + p_i \quad (2.53)$$

The value of the design point is also updated in the same way, but by using λ_{i+1} .

A SQP algorithm relies on the calculation of the Hessian of the Lagrangian, $W(x, \lambda)$. The Newton method uses an exact Hessian matrix. However this can be costly, and an approximation may be used instead, and so the method becomes Quasi-Newton. The SLSQP algorithm used in this work, employs such an approximation by updating the matrix using BFGS method. Each quadratic sub-problem is then replaced by yet another sequence of linear squares sub-problems, using a stable LDL^T -factorization of the matrix W . This method is fully explained in [94]. The method can be extended to handle inequality constraints by linearising them and using an active-set approach. This allows to only consider the active constraints at a given iteration, and then check if some constraints are not satisfied.

2.5.2 Heuristic Algorithms

Heuristic or stochastic methods try to mimic some natural behaviour and use a certain amount of randomness to avoid getting trapped at a local optimum [96]. They are generally used in problems with different local optima, or when the gradients cannot be calculated. In the case of this work, an heuristic method, a Genetic Algorithm (GA), implemented on OpenMDAO [95] is used in the case of the adaptive sampling, where the SLSQP could not present good results.

Genetic algorithms [97] are based on natural genetics and the process of natural selection. The most important steps on the algorithm are now explained. An initial population with different individuals (design points) is generated using LHS. Each individual has a score according to the objective function, and the ones with the best scores have more probability of passing their information, chromosome, to the next algorithm iteration, called a generation. The process of passing this information is achieved by means of crossover and mutation processes. The algorithm implemented on the framework does not have a stopping criteria based on convergence, and it stops only when the number of generations reaches the number of maximum generations specified by the user.

2.5.3 Sensitivity Analysis

Sensitivity analysis allows to know how the outputs vary with the given inputs. In an optimization process it is important to have this information and so the derivatives of the objective function with respect to the design variables should be computed. Since the computational cost is highly dependent on the function evaluations, and the most demanding step in the optimization is the gradient calculations, having the right approach to compute the derivatives is of utmost importance. The most common method is using finite differences for their easy implementation although they lack accuracy. In the work here developed, which has a considerable amount of design variables and constraints, the derivatives must be computed in a more efficient way for the computational cost not to be extremely high. Hence automatic differentiation is used [62]. This method consists on calculating the derivatives by resorting to the chain

rule. OpenAeroStruct uses the OpenMDAO [95] framework to compute derivatives. To this end, the framework relies on a Modular Analysis and Unified Derivatives (MAUD) architecture [98]. The method uses the chain rule, the direct and adjoint method, a couple form of the chain rule and hybrid methods which are explained in [22]. The main advantage of using this architecture is that the OpenAeroStruct only needs the user to specify the partial derivatives of each module's outputs with respect to its inputs.

Chapter 3

Implementation

The sequence of the aircraft design and optimization developed in this thesis is summarized in Figure 3.1.

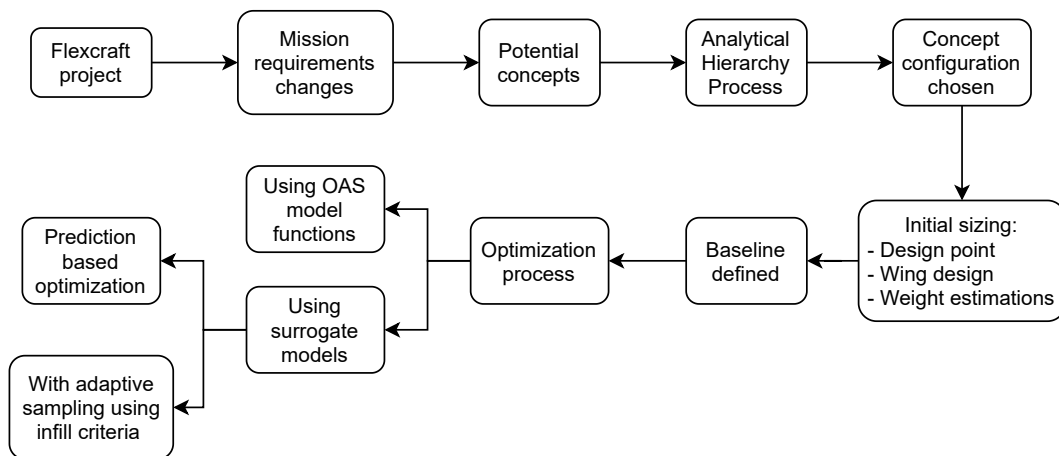


Figure 3.1: Implementation process flowchart

Firstly, the Flexcraft project concept and the changes in the mission are analysed, and some potential concepts to be used for the new mission are studied. The best concept is chosen by using an Analytical Hierarchy Process (AHP) and then an initial sizing is done. This initial sizing is performed by using design point equations, analysing stability conditions to define a baseline for the wing, and every components' weight and position are estimated so that the centre of gravity of the new concept can be calculated. This way, a baseline for the optimization is set. Then the optimization process starts, using the OpenMDAO framework [95], and it can be done either using the real OAS model functions, or using the surrogate models. The latter also presents two possible ways, and so the surrogate-based optimization can occur using the surrogate model itself (prediction-based) or using infill criteria functions.

3.1 Conceptual Design

As said before, in section 1.2, the concept of the aircraft is based on the Flexcraft project concept, whose configuration is shown in Figure 3.2. However, since the mission has changed, new variants of

the original concept were studied. These concepts allow to integrate the new propulsive system, with VTOL capability. First, five concepts are analysed and compared using an Analytical Hierarchy Process, explained in section 3.1.1. After this, the best concept is used and an initial sizing is done by means of design point equations, presented in section 3.1.2, weight and balance estimations, in section 3.1.3 and by doing an initial wing design, presented in section 3.1.4. A brief description of the aircraft's propulsive system architecture is also shown in section 3.1.5.

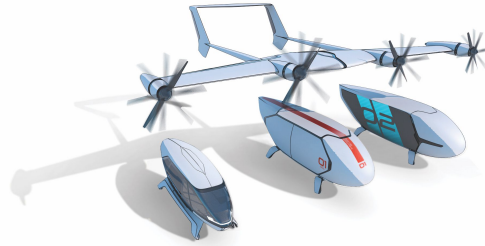


Figure 3.2: Flexcraft configuration [99]

3.1.1 Analytical Hierarchy Process

The selection of the aircraft concept was based on an Analytical Hierarchy Process, that was proposed by Saaty [100]. This systematic method consists on breaking down the problem using chosen criteria and making pairwise comparisons.

Considering the optimization objective function and the mission itself the criteria chosen to evaluate the relative strength of each concept were:

- **Aerodynamics** - When assuming a constant weight, specific fuel consumption, velocity and range, the fuel consumption decreases with the increase of the aerodynamic efficiency, L/D .
- **Weight and Structures** - The concept should be a result of a compromise between structural stiffness and robustness and its weight.
- **Propulsion** - The propulsive system efficiency has to be taken into account as it has a large impact on the fuel and battery consumption.
- **Manufacturing and Maintenance** - The more complex the aircraft's systems are, the more expensive its maintenance and manufacturing will be. For example the maintenance costs depend on the number of engines and electric motors, increasing the expenses as the level of complexity grows.
- **Stability and Control** - Given that the mission does not require high manoeuvrability, the stability of the concept is favoured. The control during the VTOL parts of the mission also impacts the decision making process on the initial concept.
- **Take-off and Landing capabilities** - The regulations for this kind of vehicle here considered are not well developed yet. Based on regulations for general aviation, an evaluation on the capabilities

to take-off and particularly land in critical conditions (such as motor inoperative) were taken into consideration.

- **Noise** - Since the goal is to design an UAV with VTOL capacity to be used in regional connections between urban centres, the noise produced by the system (especially during the mission phase inside cities) has also an impact on the choice of the concept.

The pairwise comparisons are made using qualitative judgements based on a scale of relative importance:

Table 3.1: Scale of relative importance [100]

Intensity	Definition
1	Equal importance
3	Moderate importance of one over another
5	Essential or strong importance
7	Demonstrated importance
9	Extreme importance

The even numbers between the aforementioned can also be used when necessary.

To find the priority vector of the criteria chosen, a pairwise comparison matrix has to be built. This is done by defining the relative importance between different criteria using the scale presented on Table 3.1. The reciprocal property, $a_{ij} = 1/a_{ji}$, has to be respected when building the matrix. Then, the priority vector is the normalized principal eigenvector.

The comparison between the criteria used is presented in Table 3.2, which corresponds to the global priority data matrix, where “Aerodynamics” present a slightly higher importance than “Propulsion” as seen in the first row of the data from the table, in column 3.

Table 3.2: Pairwise comparison between the different criteria

Criteria	A	B	C	D	E	F	G	Priority Vector	
Aerodynamics	A	1	1	2	9	3	7	3	0.29
Structures and Weight	B	1	1	2	7	3	5	3	0.26
Propulsion	C	1/2	1/2	1	7	3	3	3	0.18
Manufacturing and Maintenance	D	1/9	1/7	1/7	1	1/2	1/5	1/5	0.026
Stability and Control	E	1/3	1/3	1/3	2	1	2	3	0.099
Takeoff and Landing	F	1/7	1/5	1/3	5	1/2	1	3	0.080
Noise	G	1/3	1/3	1/3	5	1/3	1/3	1	0.066

Five concepts, shown in Figure 3.3 are going to be analysed, using these criteria, to evaluate which one represents the best configuration:

- **Concept I:** Tilt rotor with four rotors on the wing.
- **Concept II:** Tilt rotor with four rotors, two on the wing tips and two on the horizontal stabilizer tips.
- **Concept III:** Lift + Cruise with two fixed rotors for cruise on the wing, two fixed rotors for vertical take off and landing on the tail booms and two tilt rotors on the wing tips.

- **Concept IV:** Lift + Cruise with two fixed rotors for cruise on the wing, one fixed rotor for vertical take off and landing on an additional surface between the tail booms and two tilt rotors on the wing tips.
- **Concept V:** Lift + Cruise with two fixed rotors for cruise on the wing, one fixed rotor to increase stability during vertical take-off and landing on the horizontal stabilizer and two tilt rotors on the wing tips.

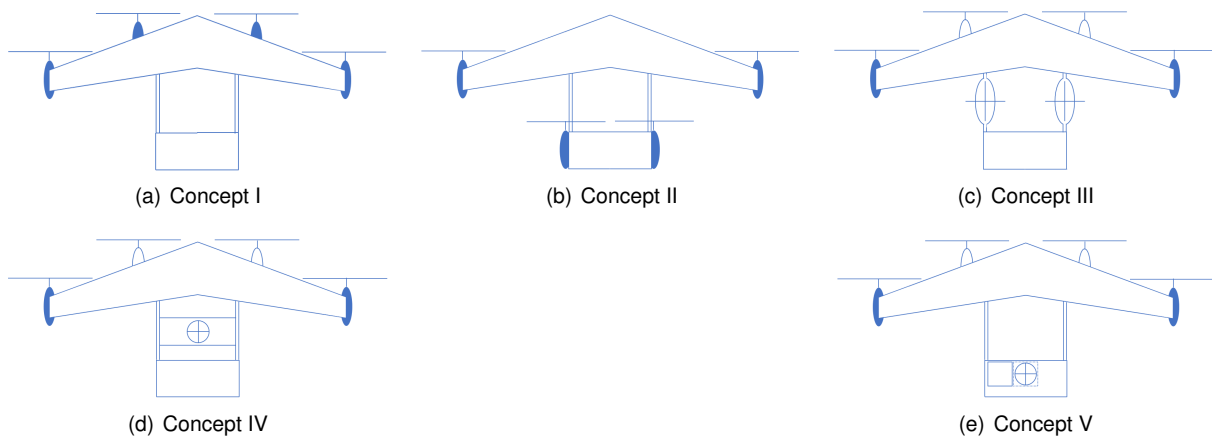


Figure 3.3: Configurations analysed during the conceptual design phase. The rotors with a solid colour have tilting capability.

For each criterion used, a pairwise comparison of the five concepts needs to be done and so, for each criterion, there will be a comparison matrix, that are shown in C.1. Having the priority vectors correspondent to all the criteria, and the global priority vector, now it is possible to assess what configuration is best. That is achieved by multiplying each criterion priority vector by the global priority vector. The global comparison and the rank of each concept are presented in Table 3.3.

Table 3.3: Global comparison of the concepts

	A	B	C	D	E	F	G	Priority Vector	Rank
I	0.218	0.459	0.312	0.117	0.447	0.051	0.472	0.321	1
II	0.480	0.208	0.496	0.266	0.041	0.107	0.270	0.320	2
III	0.035	0.058	0.037	0.045	0.171	0.281	0.047	0.075	5
IV	0.062	0.121	0.078	0.521	0.171	0.281	0.106	0.123	4
V	0.205	0.154	0.078	0.051	0.171	0.281	0.106	0.161	3

With this final rank, the conclusion is that the first concept is the potential best for the considered mission and it is the one to use.

3.1.2 Design Point

Having chosen a concept for the general configuration of the aircraft, now some general dimensions can be defined. This is done using the design point equations, for both vertical and forward flight. A more detailed explanation of the design point analysis can be found in [81]. The parameters used in the following equations are presented in Table 3.4.

The weight of the aircraft is considered to be the same as the Flexcraft as a first approach, which means that the Maximum Take Off Mass (MTOM) is 3500 kg. This is the value used to find the design point.

First, the forward flight is considered, where the Wing Loading and the Power Loading that satisfy all the mission requirements are estimated. The Wing Loading (WL) is $WL = W/S$ and Power Loading (PL) is $PL = W/P$, where W is the aircraft's weight, S is the wing area, and P is the required power.

The wing loading affects some parameters of aircraft performance, such as the stall speed or range, and so it has to be chosen according to the mission requirements.

The first condition used to size the initial concept is the stall speed, presented in equation (3.1):

$$\left(\frac{W}{S}\right)_{stall} \leq \frac{1}{2}\rho V_{stall}^2 C_{L_{max}} \quad (3.1)$$

where V_{stall} is the stall speed, defined by the aviation regulations [101], and $C_{L_{max}}$ is the maximum lift coefficient.

The second condition is the aircraft's range. This condition is assessed with equation (3.2):

$$\left(\frac{W}{S}\right)_{range} \leq \frac{1}{2}\rho V_{cr}^2 \sqrt{\frac{C_{D_0}}{k}} \quad (3.2)$$

where V_{cr} is the cruise speed, C_{D_0} is the zero-lift drag coefficient and k is the induced drag factor, which corresponds to $k = \frac{1}{\pi AR e}$, where AR is the aspect ratio and e is the Oswald's efficiency factor.

The power loading also plays an important role in the aircraft's performance, and there are some conditions that can be imposed so that it satisfies all the requirements. The conditions used are the maximum power loading at climb angle requirement and cruise, presented in equations (3.3) and (3.5), respectively.

$$\left(\frac{W}{P}\right)_{ca} \leq \frac{1}{\frac{V_{ca}}{\eta_p} \left[\sin \gamma_{ca} + \frac{\rho V_{ca}^2 C_{D_0}}{2 \left(\frac{W}{S}\right)} + \frac{2k}{\rho V_{ca}^2} \frac{W}{S} \right]} \quad (3.3)$$

with V_{ca} being:

$$V_{ca} = \sqrt{\frac{2}{\rho} \left(\frac{W}{S}\right)} \sqrt{\frac{k}{3C_{D_0}}} \quad (3.4)$$

$$\left(\frac{W}{P}\right)_{cr} \leq \frac{1}{\frac{1}{\eta_p} \left[\frac{\rho V_{cr}^3 C_{D_0}}{2 \left(\frac{W}{S}\right)} + \frac{2k}{\rho V_{cr}} \frac{W}{S} \right]} \quad (3.5)$$

where η_p is the propulsive system efficiency, and γ_{ca} is the climb angle.

Having these four conditions, the design space can be plotted as shown in Figure 3.4. In the plot, it is possible to identify the point where all the conditions are satisfied and the wing loading and power

loading are maximum, which corresponds to the design point (where the cruise line intersects the stall condition). Now, knowing WL and PL and the weight of the aircraft, the wing area necessary and the required power can be determined.

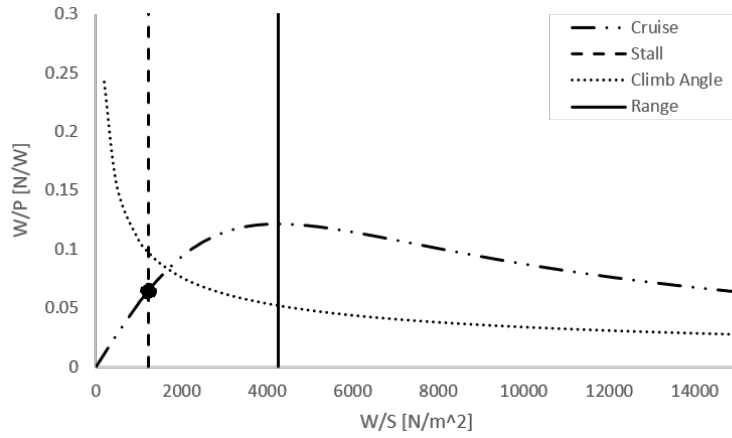


Figure 3.4: Design space for forward flight

Now, the vertical flight conditions are considered, where the power loading and the Disc Loading (DL) need to satisfy once again the mission requirements, with the disc loading being $DL = W/A_R$, where A_R is the total rotor area.

Four conditions are considered. The first one is the maximum disc loading, which in this thesis is chosen to be $DL_{max} = 600 \text{ N m}^{-2}$ which is a typical value for a tilt rotor [102].

Another requirement is the maximum power loading at vertical climb, given by equation (3.6):

$$\left(\frac{W}{P}\right)_{vc} \leq \frac{1}{\left(V_{vc} - \frac{k_i}{2}V_{vc} + \frac{k_i}{2}\sqrt{V_{vc}^2 + \frac{2DL}{\rho}} + \frac{\rho V_{tip}^3}{2DL} \left(\frac{\sigma_r C_{dblade}}{8}\right)\right)} \quad (3.6)$$

where V_{vc} is the vertical climb speed, $k_i \approx 1.2$ is the induced power factor, used to include the effects of drag and inefficiencies, like the rotor tip losses, V_{tip} is the rotor's tip velocity, σ_r is the rotors' solidity ratio and C_{dblade} is the average blade's drag coefficient.

For the hover condition, this maximum power loading is given by equation (3.7):

$$\left(\frac{W}{P}\right)_{hover} \leq \frac{1}{k_i \sqrt{\frac{DL}{2\rho}} + \rho \frac{V_{tip}^3}{DL} \left(\frac{\sigma_r C_{dblade}}{8}\right)} \quad (3.7)$$

The last condition to be considered is the maximum power loading to satisfy the transition condition from equation (3.8):

$$\left(\frac{W}{P}\right)_{tr} \leq \frac{1}{\frac{k_i}{\sin(\theta_{tilt})} \sqrt{\frac{-V_h^2}{2} + \sqrt{\left(\frac{V_h^2}{2}\right)^2 + \left(\frac{DL}{2\rho \sin(\theta_{tilt})}\right)^2} + \frac{\rho V_{tip}^3}{DL} \left(\frac{\sigma_r C_{dblade}}{8} (1 + 4.6\mu^2)\right) + X} \quad (3.8)$$

where θ_{tilt} is the rotor tilt angle measured clock-wise from horizontal axes, V_h is the horizontal component of the forward flight velocity, μ is the advance ratio given by equation (3.9) and X is given by equation (3.10).

$$\mu = \frac{V_h}{V_{tip}} \quad (3.9)$$

$$X = \frac{1}{2}\rho V_\infty^3 C_{D0} \frac{1}{WL} + \frac{2WL}{(\pi AR e)\rho V_\infty} \quad (3.10)$$

The condition of transition should be evaluated at different tilt angles, with different corresponding velocities.

As it was done before for the forward flight phase, now the design space can be plotted, as shown in figure 3.5. The point corresponding to the intersection between the vertical climb condition and the maximum disc loading represents the design point.

Table 3.4: Initial sizing based on the design point considerations

Parameter	Units	Value	Parameter	Units	Value
V_{stall}	$m s^{-1}$	40	k_i	-	1.2
V_{cr}	$m s^{-1}$	111.11	e	-	0.8
V_{vc}	$m s^{-1}$	3	AR	-	7.98
V_{tip}	$m s^{-1}$	204	σ_r	-	0.09
C_{Lmax}	-	1.4	η_p	-	0.85
C_{D0}	-	0.02	ρ (cruise)	$kg m^{-3}$	1.088
C_{dblade}	-	0.03	ρ (hover)	$kg m^{-3}$	1.223
γ_{ca}	$^\circ$	5	ρ (ground)	$kg m^{-3}$	1.225

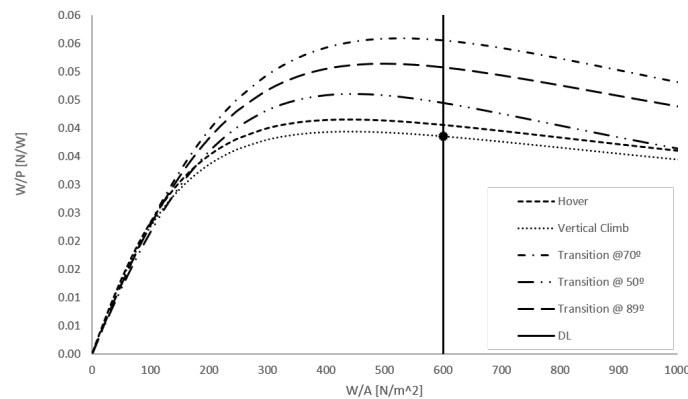


Figure 3.5: Design space for vertical flight

Combining the two design points, an initial sizing of the aircraft is done and the results are presented in Table 3.5.

Table 3.5: Initial sizing based on the design point considerations

$\left(\frac{W}{P}\right)_{ff}$	$\left(\frac{W}{S}\right)$	$\left(\frac{W}{P}\right)_{vf}$	$\left(\frac{W}{A_R}\right)$	W	P_{ff}	P_{vf}	S	A_R
$[\text{N W}^{-1}]$	$[\text{N m}^{-2}]$	$[\text{N W}^{-1}]$	$[\text{N m}^{-2}]$	$[\text{N}]$	$[\text{kW}]$	$[\text{kW}]$	$[\text{m}^2]$	$[\text{m}^2]$
0.0641	1218	0.0386	600	34335	535	890	28.18	57.23

3.1.3 Weight and Balance Estimations

The total mass of the aircraft was assumed to be 3500 kg as mentioned before. However, until this point there is no breakdown of the total weight for each aircraft's component. In this section, an estimation of the weight of each component is given. The estimates were made using either empirical equations (presented in [81] or in [20]) and they are presented in Tables C.8, C.9, C.10, C.11 in the Appendix C, section C.2. A position for each component is also presented, and this position is taken with respect to the wing's leading edge at root and to ground level (the referential used can be observed in Figure 3.6).

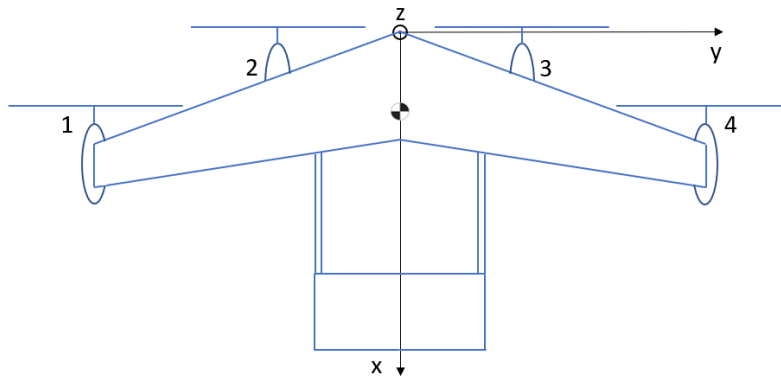


Figure 3.6: Schematics of the aircraft and the referential used

With the weights and position of every component, the center of gravity (CG) location can now be determined. This position is presented in Table 3.6, as well as the updated total weight.

Table 3.6: Total mass and CG position

Total mass [kg]	CG Position		
	x [m]	y [m]	z [m]
3530.56	2.00	0	2.097

3.1.4 Wing Design

As mentioned in section 1.2, the airfoils of the lifting surfaces were kept for this work. However, now the wing area is different from the one on the Flexcraft project, and the mission has changed too. The taper ratio (TR) of the wing was maintained, being $TR = 0.4$ and the wingspan was also kept the same and equal to 15 m, to obey helipads limitations. With the CG position known, an estimation of the neutral point for different sweep angles is done, so that it is possible to have a reasonable value for the static

margin, $K_n = \frac{x_N - x_{CG}}{\bar{c}}$, with x_N being the longitudinal position of the neutral point, x_{CG} is the longitudinal position of the CG and \bar{c} is the mean aerodynamic chord.

The neutral point was calculated using XFLR5 software, that performs aerodynamic analysis using panel methods [103]. The wing used for this study is characterized by the dimensions presented in Table 3.7. The wing sweep angle is going to be varied from 10 to 20 degrees.

Table 3.7: Wing dimensions

Parameter	Nomenclature	Value	Units
Span	b	15	m
Mean aerodynamic chord	\bar{c}	1.994	m
Root chord	c_{root}	2.684	m
Tip chord	c_{tip}	1.074	m
Taper ratio	TR	0.4	—
Sweep	Λ	10-20	°
Dihedral	Γ_d	2	°

The horizontal stabilizer dimensions used are the same as the Flexcraft aircraft, and are presented in Table 3.8.

Table 3.8: Horizontal stabilizer dimensions

Parameter	Nomenclature	Value	Units
Span	b	4	m
Root chord	c_{root}	1.86	m
Taper ratio	TR	1	—
Sweep	Λ	0	°
Dihedral	Γ_d	0	°

The static margin is then evaluated with the different sweep angle of the wing varying. The results are presented in figure 3.7.

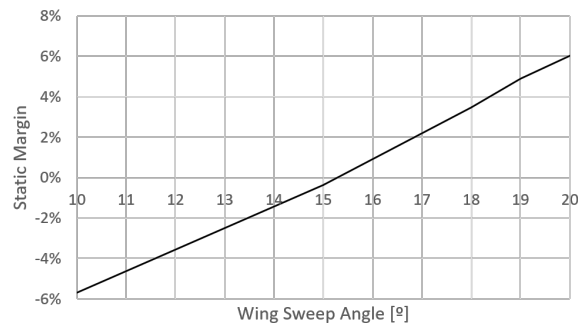


Figure 3.7: Static margin variation with respect to the wing sweep angle

As baseline, it was chosen to have a wing with 20° of sweep angle in order to have a reasonable value for the static margin.

3.1.5 Propulsive System Architecture

Even though a detailed study on the propulsive systems is out of the scope of this thesis, a brief description of the general architecture of the system is here provided.

The propulsive system consists on an hybrid series configuration, shown in Figure 3.8. In this configuration, the internal combustion engine burns fuel and rotates an AC generator. The power generated can be used to charge the batteries and to be delivered to the AC electric motors that drive the propellers.

The series configuration allows for a separation of power and thrust generation and also to have different flight modes [104], *i.e.* to have flight phases where only the electric energy of the batteries is used to propel the aircraft, and other phases where only the Internal Combustion Engine (ICE) is the provider of the necessary energy. This way, the vertical climb, hover, transition and vertical descent are driven using the batteries and the forward flight phases are carried out using only fuel energy.

Therefore, the ICE and generator can be sized for only cruise, which allows the system to be working at a steady state in most of the mission, and so it is working with the same specific fuel consumption (SFC), at the optimal engine point. However, this system implies an increase of the propulsive system weight and its complexity.

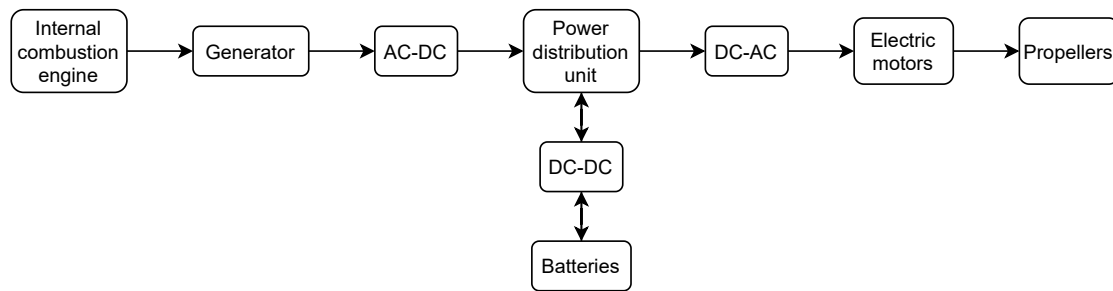


Figure 3.8: High-level representation of the propulsive system

3.2 Optimization Problem Formulation

Now that the concept for the aircraft is chosen, and the general dimensions for the baseline are defined, the next step is to perform the optimization from this baseline. In this section, the formulation used to solve this problem is presented.

3.2.1 Mission Requirements

Initially, the mission requirements are set. Based on these, the objective function and the design variables can then be chosen, as well as the constraints can be set.

The mission requirements considered are as follows:

- Cruise speed: The cruise speed was set to be the same as for the Flexcraft project, which is 110 m s^{-1} .

- Range: The aircraft's range was slightly decreased, in comparison to the Flexcraft project, being reduced from 1000 km to 800 km. This change results from the limitations found with the electrical vertical take off and landing, and the weight of batteries that this requires.
- Payload: As it happened with the range, the amount of payload also suffered a reduction, going from 900 kg to 500 kg. Once again, this happens because of the increase in batteries weight and the tilt system that now needs to be employed.
- Stability: Even though in this thesis there is not a comprehensive study on the matter, the aircraft must at least be able to fly trimmed and with a guaranteed reasonable value for the static margin. Therefore, it was decided that the static margin should be between 5 % and 20 %, and the pitching moment coefficient should be zero at the cruise phase.
- Structural integrity: The aircraft must be able to withstand the VTOL phases and also a pull-up manoeuvre of 3.8g.

3.2.2 Objective Function

With the range fixed, one main objective is to minimize the fuel consumption. Also, since VTOL phases play a major role in the power required, which in turn influences the weight of the rotors and batteries, this power should also be considered. In order to deal with these different possible objectives, an energetic objective function is used, combining the energy spent during both cruise and VTOL operations.

The mass of consumed fuel is estimated by using the Breguet equation for a propeller aircraft [81, 105], shown in equation (3.11). This equation does not present the propeller efficiency that is generally used, since this is not implemented on OAS.

$$m_{fuel} = \frac{W_0}{g} \left[\exp \left(\frac{-R \cdot g \cdot SFC}{V_{cr}} \frac{C_D}{C_L} \right) - 1 \right] \quad (3.11)$$

where W_0 is the aircraft's weight without the fuel, R is the fixed range and SFC is the specific fuel consumption.

The corresponding energy can be calculated using the fuel's specific energy density, $E_{spec\ fuel}$, which is assumed to be equal to 43.28 MJ kg^{-1} , according to [106].

The energy for the VTOL phases of the mission is estimated using the required power, that comes from the equations presented in section 3.1.2 and the time that each phase takes. It was considered to have a vertical climb to obstacle height of 5 seconds and a hover time of 60 seconds. The transition phase was also considered, by adding a fixed term to the total energy. A preliminary study of the necessary energy needed during transition was done, but since this term is relatively small in comparison to the total energy obtained for each configuration, the transition energy will not play a role in the optimized solution.

The final expression for the objective function is then given by equation (3.12):

$$E = m_{fuel} \times E_{spec\ fuel} + P_{vc} \times t_{vc} + P_{hover} \times t_{hover} + E_{tr} \quad (3.12)$$

3.2.3 Design Variables

Various case studies are going to be performed, using different numbers of Design Variables (DV). Consequently, in this section, all the DV are presented.

The wing planform is defined using a linear distribution for the chord, by controlling the chord at the root, $(c_{root})_{wing}$, and the chord at the tip $(c_{tip})_{wing}$. The same happens for the horizontal tail planform, using $(c_{root})_{tail}$ and $(c_{tip})_{tail}$.

The wingbox structure is defined by the thickness of the spars and the skins. Using the OAS model for the wingbox, the rear and front spar thicknesses, $(t_{spar})_{wing}$, are considered to be the same, as well as the upper and lower skin thicknesses, $(t_{skin})_{wing}$. A constant thickness is considered along the span for both the spars and the skins. This consideration was taken because of manufacturing restrictions. Once again, the same happens for the horizontal tail, thus adding two more design variables, $(t_{spar})_{tail}$ and $(t_{skin})_{tail}$.

The angle of attack at cruise condition, α , is also used as a design variable in one of the case studies.

3.2.4 Constraints

The constraints of the problem are related to the mission requirements, explained on section 3.2.1.

To ensure a longitudinally stable aircraft, the static margin, estimated according to [81], K_n , will have to be between 5 and 20 % as mentioned before. Directional and lateral stability are not considered on this thesis, since the vertical stabilizers are not being considered in the optimization problem, and are assumed to be equal to the ones on the Flexcraft project.

Additionally, in order to have a trimmed flight during cruise, a constraint regarding the pitching moment coefficient, C_M , is used, and is also imposed that lift must be equal to the total weight. During the pull-up manoeuvre considered, an additional constraint is imposed, so that the lift is equal to the total weight multiplied by the pull up load factor, $n = 3.8g$. Two load cases are considered: the vertical climb, and a pull-up of 3.8g. The four critical points on the wingbox, explained on section 3.3.3, must satisfy the structural failure criterion at these ultimate load cases. The criterion used is the Von-Mises failure criterion, presented in section 2.1.1.3. Finally, a constraint regarding the volume of the necessary fuel is employed. This, ensures that the volume occupied by the fuel is smaller than the available volume inside the wingbox structure of the wing.

The constraints' equations were arranged in a manner that to be satisfied they need to be negative (apart from the fuel volume constraint, which needs to be positive). Since there are computational errors and limitations, each equality constraint was transformed into two inequality constraints. The limiting values of the constraints used in the optimization are presented in Table 3.9. The bound of the design variables are also set, and they are presented in Table 3.10.

3.2.5 Optimization Problem Statement

Having defined the objective function in section 3.2.2, the design variables presented in section 3.2.3, and set the constraints and bounds of these design variables in section 3.2.4, it is now possible to state

Table 3.9: Constraints' minimum and maximum allowable values

Constraint	Minimum value	Maximum value
K_n	0.05	0.2
C_M	-0.01	0.01
Failure criterion	-	-0.001
L=W (Cruise)	-0.1	0.01
L=nW (Pull up)	-0.1	0.01
Fuel volume	0.001	-

Table 3.10: Design variables bounds

Design variable	Units	Lower bound	Upper bound
$(c_{tip})_{wing}$	m	0.5	2
$(c_{root})_{wing}$	m	1.5	3.5
$(t_{spar})_{wing}$	m	0.001	0.01
$(t_{skin})_{wing}$	m	0.001	0.01
$(c_{tip})_{tail}$	m	1.15	2.5
$(c_{root})_{tail}$	m	1.15	2.5
$(t_{spar})_{tail}$	m	0.0005	0.01
$(t_{skin})_{tail}$	m	0.0005	0.01
α	°	-1.5	0.5

the optimization problem in the form explained in section 2.2.1 in equation (2.27). This statement is presented in equation (3.13).

$$\begin{aligned}
 &\text{minimize} && m_{fuel} \times E_{spec_{fuel}} + P_{vc} \times t_{vc} + P_{hover} \times t_{hover} + E_{tr} \\
 &\text{w.r.t} && (c_{tip})_{wing}, (c_{root})_{wing}, (t_{spar})_{wing}, (t_{skin})_{wing}, \\
 &&& (c_{tip})_{tail}, (c_{root})_{tail}, (t_{spar})_{tail}, (t_{skin})_{tail}, \alpha \\
 &\text{subject to} && 0.05 \leq K_n \leq 0.2 \\
 &&& (C_M)_{cr} \approx 0 \\
 &&& L_{cr} \approx W \\
 &&& L_{pull} \approx nW \\
 &&& \text{Von-Mises criterion (VTOL)} \lesssim 0 \\
 &&& \text{Von-Mises criterion (pull-up)} \lesssim 0 \\
 &&& \text{Fuel volume} < \text{Available volume}
 \end{aligned} \tag{3.13}$$

3.3 MDA implementation

The analysis performed during the optimization includes structural and aerodynamic analysis. In this section, the architecture of the MDA is explained.

3.3.1 Discipline coupling

In the beginning of the MDA, performed at each iteration of the optimization, the lifting surfaces' geometries are set using the inputs of the design variables. An aerodynamic analysis is then performed. Using

the outputs from the aerodynamic analysis, the aerodynamic loads, a structural analysis is then carried out. With the displacements computed in this analysis, a new aerodynamic shape is used to perform the aerodynamic analysis once again. This process repeats until convergence, between aerodynamics and structures, occurs.

There are two main approaches to solve the MDA: fixed-point and Newton [107]. By using a fixed-point approach each analysis is solved individually and the data from other disciplines is fixed when solving a certain analysis. Two examples of this approach are the Jacobi and the Gauss-Seidel approach [107]. In the first one, the outputs used from the other analysis correspond to the previous iteration. In contrast, the Gauss-Seidel approach uses the most recent outputs. The latter approach generally converges faster. On the other hand, in the Newton approach [107], all the analyses are solved simultaneously in each optimization iteration.

In [22], a comparison between different approaches for solving a coupled aerostructural system for level flight and pull-up (2.5g) using OAS is presented. The authors compared a Newton approach, a Non-Linear Block Gauss-Seidel (NLBGS) and a NLBGS approach with Aitken relaxation. They concluded that the best approach is NLBGS with Aitken relaxation, and so this is the approach used in this thesis. A diagram of the approach can be consulted in Figure 3.9.

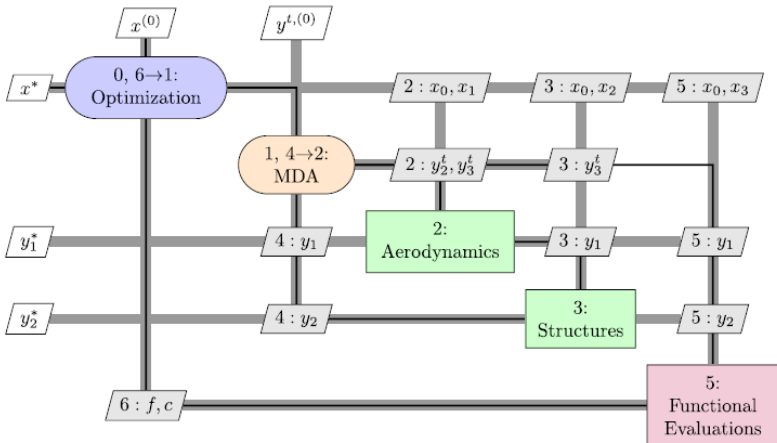


Figure 3.9: eXtended Design Structure Matrix (XDSM) diagram [108] for aerostructural optimization using a Gauss-Seidel approach. The x vectors are design variables and the y vectors are states, where * represents the values at the design optimum. Figure from [22].

3.3.2 Aerodynamic analysis

The OAS framework uses a VLM for the aerodynamic analysis. The inputs used are both design variables or outputs from the geometric models. Also, some corrections in the drag calculations are considered regarding viscosity and compressibility, as explained in section 2.1.2. The loads carried by the lifting surfaces are evaluated at two different load cases, a vertical climb condition and a pull-up manoeuvre of 3.8g.

3.3.3 Structural analysis

To evaluate the failure criterion, a Finite Element Analysis (FEA) is employed using the elements explained in section 2.1.1. The cross-section is a wingbox structure, with a thin walled spar and skin, represented in Figure 3.10.

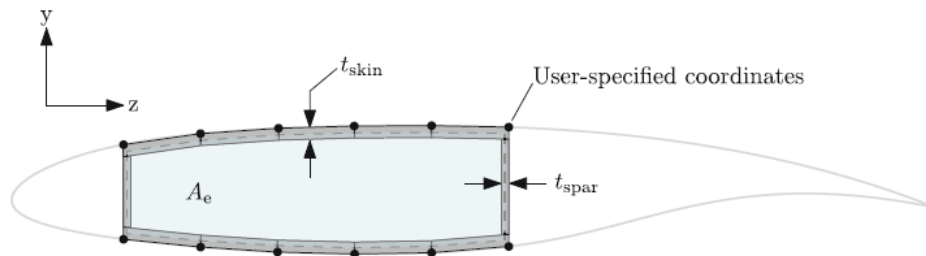


Figure 3.10: Wingbox representation [23]

The lifting surface is discretized according to the user-specified number of panels, and the FEA elements used can be observed in Figure 3.11.

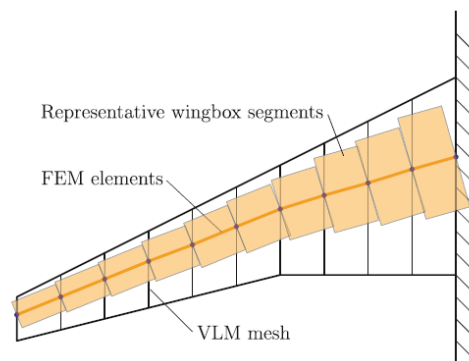


Figure 3.11: Aerodynamic and structural discretization [23]

For the cross-section in each discretized element, its area, the area moments of inertia about two axes, and the torsion constant are calculated [23]. These are estimated using the normalized user-specified coordinates of the wingbox.

The failure criterion, presented in section 2.1.1.3, is checked at the root of the two lifting surfaces, wing and horizontal stabilizer, in four critical points, shown in Figure 3.12.

In addition to the already calculated failure criterion, it is also possible to obtain the CG position of both lifting surfaces.

3.3.4 Mesh convergence

The number of panels, for both chordwise and spanwise directions, is given by the user. In this thesis, the number of panels for either the aerodynamic and structural analysis are considered the same, since this is the only option available on OAS, so far.

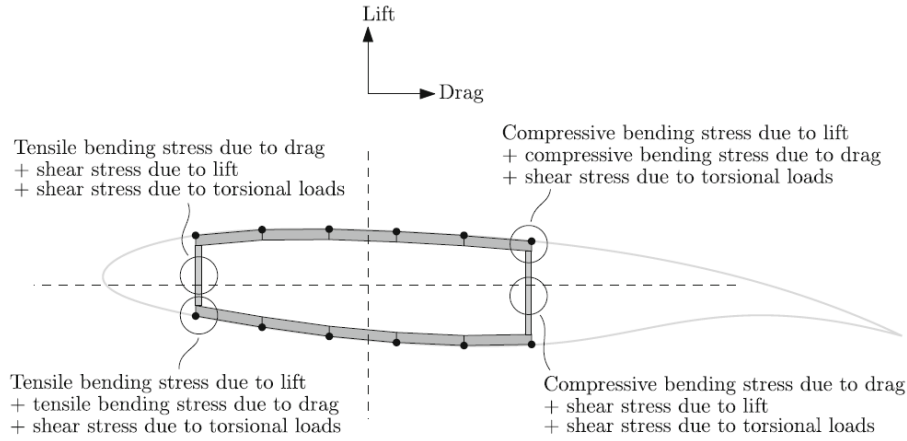


Figure 3.12: Critical stress combinations [23]

Considering that the number of divisions in the spanwise direction is n_y , and in the chordwise direction is n_x , a study on the influence of the number of panels chosen on the aerodynamic and structural parameters is performed.

The parameters considered are lift and drag coefficients, as well as the average tip displacements in both the wing and tail.

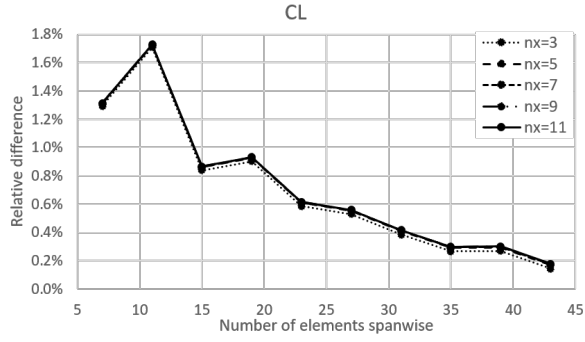
For both lifting surfaces n_x is considered to be the same, and it will be varied from 3 to 11. As for the spanwise discretization, the number of panels in the horizontal tail is considered to be two-thirds of the wing panels, but always ensuring that $(n_y)_{tail}$ is at least equal to 7. It is also ensured that n_y is always an odd number, which is a requirement of the framework used.

The results of the parameters considered are compared to the ones obtained when using a mesh with the following characteristics: $n_x = 17$, $(n_y)_{wing} = 99$ and $(n_y)_{tail} = 67$. The deviations in form of percentages to this reference mesh are shown in Figure 3.13.

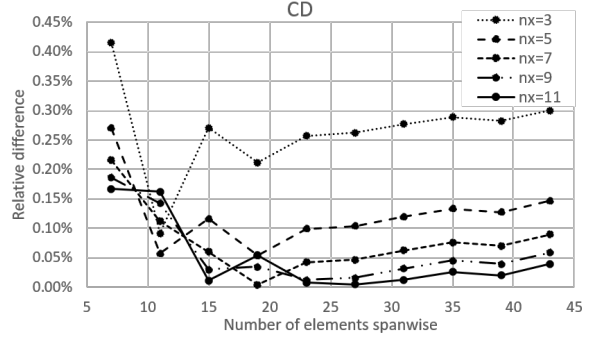
Based on the results, and having in mind that by increasing the number of panels the computational costs also increases, it was chosen to have a mesh with the following parameters: $(n_y)_{wing} = 27$, $(n_y)_{tail} = 19$ and $n_x = 7$.

3.4 MDO methodology

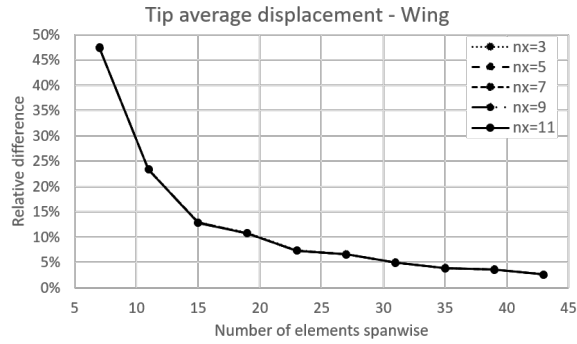
Two different approaches of the optimization, implemented on OpenMDAO [95] are compared in this thesis, one that uses the OAS model to evaluate the objective function and the constraints, and another one that uses surrogate models and different search methods to carry out the optimization. First, the sampling plans and surrogate models were studied using known test functions, like the Branin function. These studies are presented in section 3.4.1, and then the optimization cycle is explained in section 3.4.2.



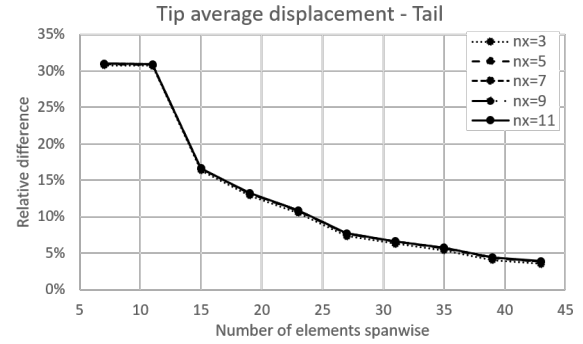
(a) Mesh convergence test evaluating C_L



(b) Mesh convergence test evaluating C_D



(c) Mesh convergence test evaluating the average tip displacement of the wing



(d) Mesh convergence test evaluating the average tip displacement of the horizontal tail

Figure 3.13: Mesh convergence study

3.4.1 Test functions studies

The surrogate models used during the thesis were built in Python, using the Surrogate Modeling Toolbox (SMT) [74]. The sampling plans were also generated using the same toolbox.

First, in order to study different sampling plans and surrogate models, a study with analytical test functions was carried out. The functions used were the Branin, equation (3.14) and the Rosenbrock, equation (3.15), functions [86]. The latter was evaluated using different numbers of design variables, n_x .

$$f(x) = \left(x_2 - \frac{5.1}{4\pi^2} x_2 + \frac{5}{\pi} x_1 - 6 \right)^2 + 10 \left[\left(1 - \frac{1}{8\pi} \right) \cos x_1 + 1 \right], \quad x_1 \in [-5, 10], \quad x_2 \in [0, 15] \quad (3.14)$$

$$f(x) = \sum_{i=1}^{n_x-1} [(x_{i+1} - x_i^2)^2 + (x_i - 1)^2], \quad -2 \leq x_i \leq 2, \quad \text{for } i = 1, \dots, n_x \quad (3.15)$$

Three different types of sampling plans were used, the LHS (with a *maximin* criterion), FF and a random design sampling plan. Different numbers of sample points were used to evaluate their influence on the surrogate models built. Four different surrogate models were tested, the Kriging model, the KPLS, KPLSK and RBF models.

When evaluating the surrogates built using the Branin and the two variables Rosenbrock function, a test sample set was used, with 200 sample points. The test samples were generated using LHS with

the *maximin* criterion. The results of the average relative error evaluated on those test points are shown in the following tables and figures.

To understand the influence of the sampling plan, first the surrogate model used is fixed, and three sampling plans for each value of training points are built, one using LHS, one using FF and another one using a random design. Figure 3.14 shows the relative errors obtained with each sampling plan, when using a Kriging surrogate model.

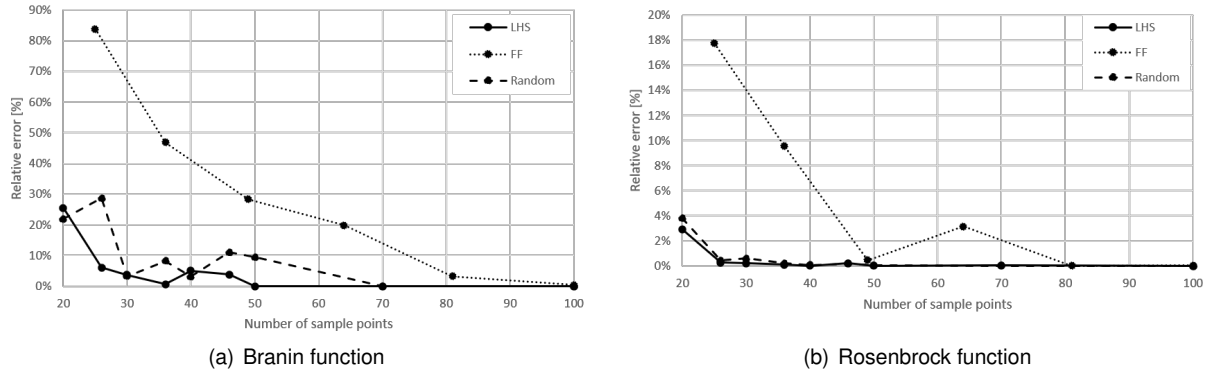


Figure 3.14: Average relative error with the different sampling plans using a Kriging surrogate model to represent the Branin function and the Rosenbrock function with 2 design variables

When using a Full Factorial sampling plan, usually it is necessary to have more training points to get good results but, by doing so, the computational cost increases. This trend is also seen when other surrogate models (KPLS, KPLS and RBF) are used, and when using the Rosenbrock test function. The results can be seen in the Appendix B, in figures B.1 and B.2.

From this study, the sampling plan chosen was the LHS plan. Using this plan, the accuracy of the different surrogate models itself were then studied.

Table 3.11: Average relative error obtained with the different surrogate models representing the Branin function

# Training points	Kriging	KPLS	KPLSK	RBF
20	26 %	54 %	37 %	296 %
26	6.04 %	16.45 %	5.95 %	277 %
30	3.69 %	15.57 %	9.24 %	257 %
36	0.62 %	12.69 %	13.30 %	292 %
40	5.03 %	16.65 %	15.20 %	259 %
46	3.82 %	25.07 %	18.17 %	211 %
50	0.021 %	22.27 %	23.82 %	191 %
70	0.019 %	10.35 %	9.85 %	163 %
100	0.002 %	0.003 %	0.002 %	129 %

From Table 3.11, it is observed that the relative error associated with the RBF surrogate model is significantly higher than the others. This trend is observable when using both test functions (the rest of the results are shown in the Appendix B in tables B.1 and B.2). Therefore, the RBF model will not be used. It can also be concluded that the Kriging model is the one that needs less training points to have good matching results with the real function. For example, for the Branin function, the Kriging model needs 46 training sample points to achieve an average relative error smaller than 5 %, while the KPLS

and KPLSK models need more than 70.

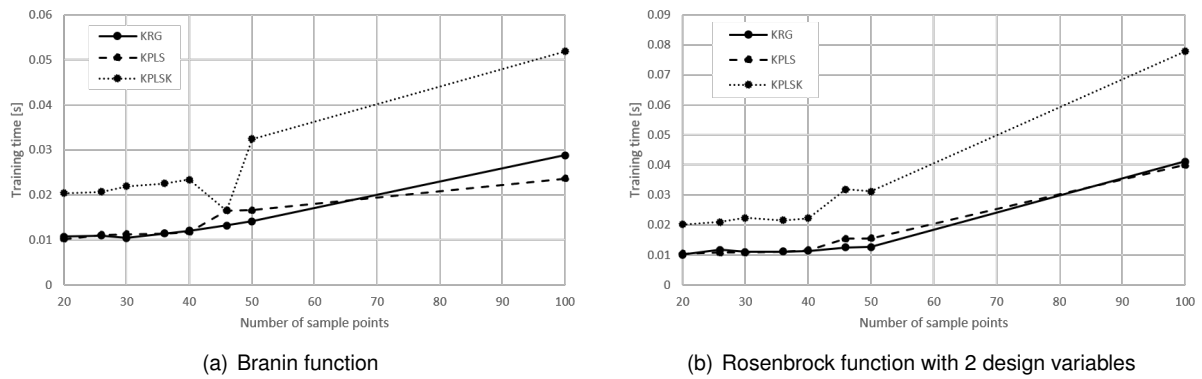


Figure 3.15: Training time to build the different surrogate models represent the Branin function and the Rosenbrock function with 2 design variables

The training time needed to built the different surrogate models is presented in Figure 3.15. As it is shown, the Kriging model and the KPLS model are the ones that take less time, *i.e.*, they imply less computational cost. Since the Kriging model shows the smaller average relative errors between these two models, it will be the chosen surrogate model to use in the aircraft design optimization problem.

3.4.2 Optimization cycle

Before building the surrogate models, and solving the optimization problem using these approximated functions, the problem is solved using the real functions and its analytical derivatives.

In summary, the optimization cycle when using the real functions is described by the following steps:

1. Model setup, using OAS: set the flow conditions, material's properties, the mission performance values (e.g. vertical climb velocity) and the initial values of the design variables (from the baseline already defined).
2. Search direction: Computed with the gradient information of the objective function and constraints to find the next iteration point.
3. Point evaluation: MDA in the point chosen, using a scheme represented in Figure 3.9.
4. Assessment: Constraints and convergence criteria assessment.
5. Repeat steps 2 to 4 until convergence is achieved.

The results from this optimization problem are then compared with the results obtained when surrogate models are used.

The optimization using the surrogate models is described in Figures 3.16 and 3.17, for when no infill criterion is used, and for when there is an adaptive sampling plan based on the infill criterion chosen, respectively.

In the first case, the objective function of the optimization problem is the surrogate model itself, without adding any additional sample points.

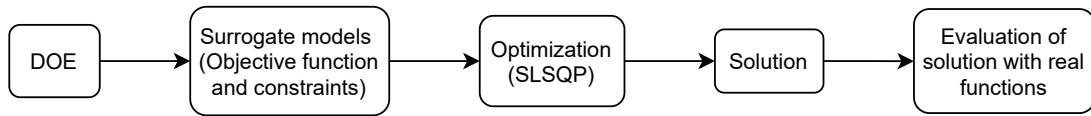


Figure 3.16: Optimization cycle with the surrogate models functions

As shown in Figure 3.16, firstly the DOE is generated and the surrogate models, for the objective functions and every constraint, are built. Having the new, approximated, functions, the optimization problem is then solved using the SLSQP algorithm.

The final solution is then evaluated with the real model to check if there are any major discrepancies.

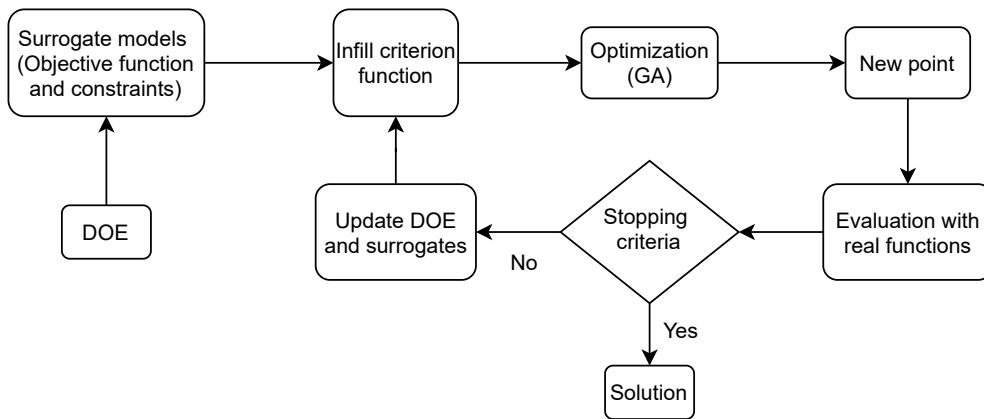


Figure 3.17: Optimization cycle with the surrogate models functions using an adaptive sampling plan

On the other hand, instead of using the objective function surrogate model as the function to be minimized, an infill criteria function, explained in section 2.4, can be used. The constraints used in the problem correspond to the constraints' surrogate models.

As shown in Figure 3.17, an initial DOE is generated and the initial surrogate models are built. After this, the infill criteria function is defined, using the objective function (total energy) surrogate model. At this point, the objective function, for the optimizer to minimize, becomes the infill criterion function itself. The optimization problem is solved using a genetic algorithm, and the solution obtained is then evaluated with the real model and a new sample point is added to the DOE. The surrogate models, and consequently the infill criterion function, are then updated and the process starts over again until convergence is achieved.

Chapter 4

Results

As mentioned before, the results from the optimization using the real functions and using the surrogate models are compared. In fact, several optimization problems were solved, each with different parameters as design variables. First, three case studies (cases 2.1, 2.2 and 2.3) using only two design variables were carried out. These studies allowed to have a deeper knowledge of the problem, meaningly, the objective function and constraints behaviour. After this, a case study using four design variables (case 4) was performed, and lastly a case with eight design variables (case 8) was done. In this chapter, the results of these different case studies are presented and discussed.

4.1 Baseline

The results presented in the following sections will be compared to the baseline characterized by the parameters presented in Table 4.1. The angles of attack used as baseline are: $\alpha = -0.8^\circ$ for cruise, $\alpha_{vc} = -0.3^\circ$ for vertical climb and $\alpha_{pull} = 6^\circ$ for pull up.

Table 4.1: Baseline geometric parameters

Parameter	Units	Value	Parameter	Units	Value
Wing root chord	m	2.684	Tail root chord	m	1.86
Wing tip chord	m	1.074	Tail tip chord	m	1.86
Wing skin thickness	m	0.0038	Tail skin thickness	m	0.00255
Wing spar thickness	m	0.0038	Tail spar thickness	m	0.00255
Wing sweep	°	20	Tail sweep	°	0
Wing span	m	15	Tail span	m	4
Wing dihedral	°	2	Tail dihedral	°	0

The performance parameters, obtained using the OAS model for this baseline configuration are presented in Table 4.2.

Table 4.2: Baseline performance

Wing structural mass [kg]	Horizontal tail structural mass [kg]	Fuel [kg]	Total mass [kg]	L/D	Total energy [MJ]
408.35	37.68	407.07	3524.10	13.36	17937.11

4.2 Case studies conditions

In this section, the design variables used in each case study, presented in the following sections, are identified. The objective function is always considered to be the total energy minimization, its surrogate model or the infill criterion based on this surrogate model. The constraints are also always the same functions, explained before in Chapter 3, or their surrogate models. The design variables used in each case study carried out are the following:

- **Case 2.1** - wing root chord (range: 1.5 m to 3.5 m); wing skin thickness (range: 0.001 m to 0.01 m);
- **Case 2.2** - wing tip chord (range: 0.5 m to 2 m); wing spar thickness (range: 0.001 m to 0.01 m);
- **Case 2.3** - wing root chord (range: 1.5 m to 3.5 m); angle of attack at cruise phase (range: -1.5° to 0.5°);
- **Case 4** - wing tip chord (range: 0.5 m to 2.0 m); wing root chord (range: 1.5 m to 3.5 m); wing skin thickness and the wing spar thickness (range: 0.001 m to 0.01 m);
- **Case 8** - wing tip chord (range: 0.5 m to 2.0 m); wing root chord (range: 1.5 m to 3.5 m); wing skin thickness and the wing spar thickness (range: 0.001 m to 0.01 m); tail tip chord and tail root chord (range: 1.15 m to 2.5 m); tail skin and spar thicknesses (range: 0.0005 m to 0.01 m).

4.3 Cases with 2 design variables

4.3.1 Surrogate models' accuracy

4.3.1.1 Case 2.1

To test the accuracy of the surrogate models' predictions, a sample test set of 100 points was generated using LHS. Then, the sampling plans with which the surrogate models are built were generated, using an increasing number of sample points. The accuracy of the corresponding surrogate model was evaluated with the average relative error, calculated for each test point. The results of the average relative error obtained with the different sample sets are shown in Figure 4.1. The results of the constraints that are not presented here, because of space limitations, follow the same trend as the ones shown in Figure 4.1, and the same happens on the following cases.

The behaviour of the objective function is well captured even with a reduced number of sample points. However, some constraints, like the wing failure criterion for both the vertical climb phase and pull up manoeuvre, for example, need more sample points to give good results. This can be explained by the non-linear behaviour of these two functions, depicted in Figure 4.2. However, the general trend for every

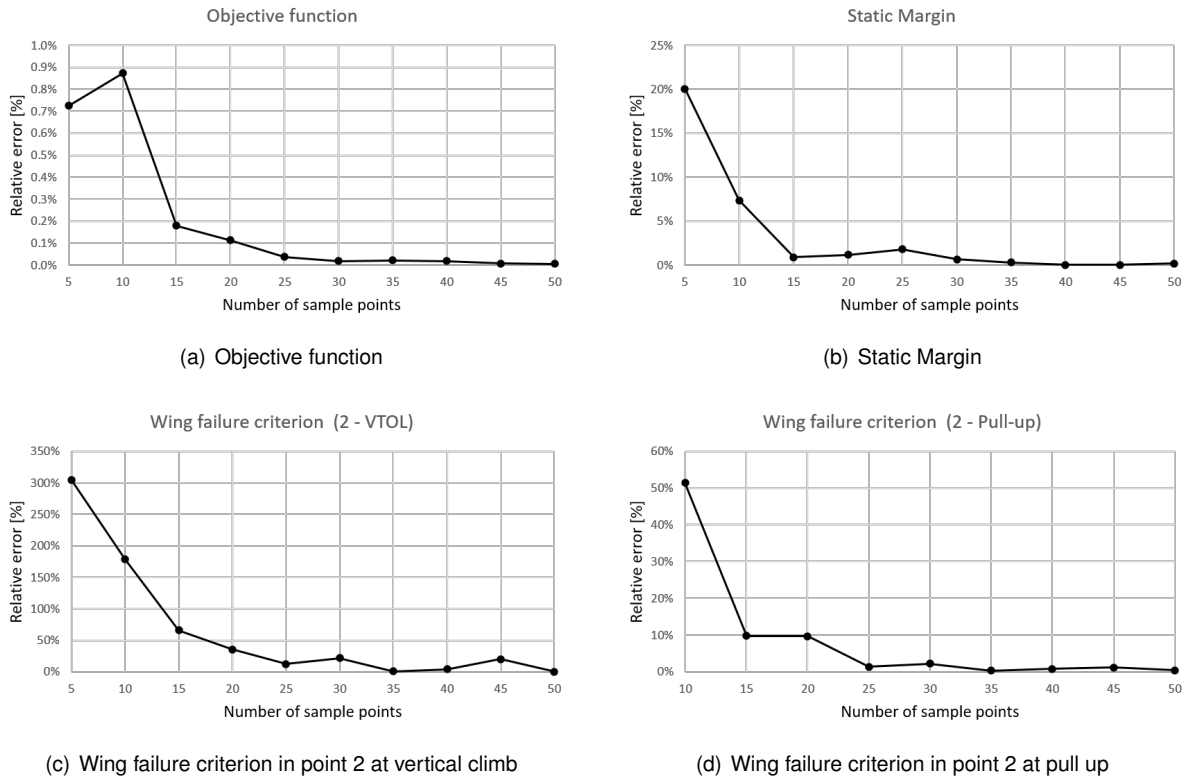


Figure 4.1: Average relative error of different functions vs number of sample points used for case 2.1

constraint and the objective function is for the average relative error to decrease with the increase in number of sample points, as expected. The number of sample points needed so that the total energy and every constraint function presents a relative error smaller than 5% is 35.



Figure 4.2: Behaviour of the real functions varying with the two design variables used in case 2.1

4.3.1.2 Case 2.2

As it was done in the first case study, initially the quality of the surrogate models when varying the number of sample points to built them is analysed. Again, a test sample set was used, generated with LHS and using 100 test points. The results of the average relative error of some of the surrogate models built are shown in Figure 4.3.

As it was seen before in case 2.1, there is a clear trend of the relative error, decreasing with the

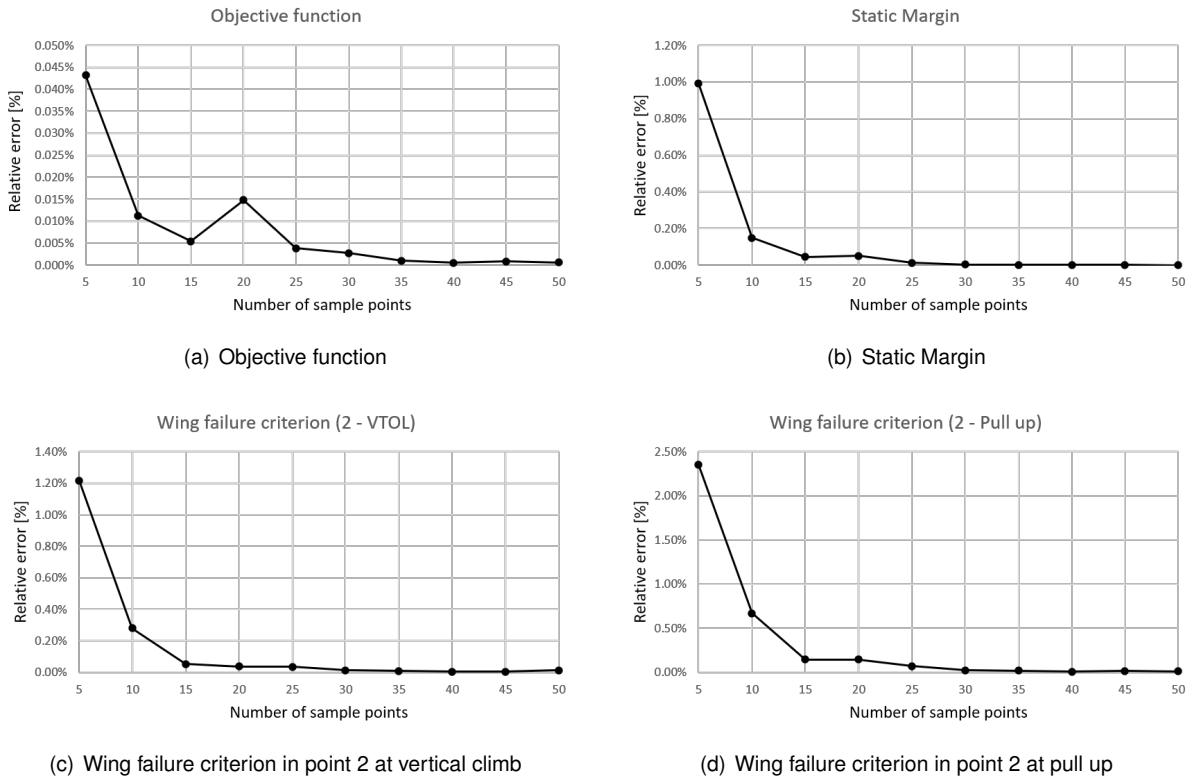


Figure 4.3: Average relative error of different functions vs number of sample points used for case 2.2

increase of sample points used, as expected. Unlike case 2.1, all the surrogate models present an average relative error smaller than 5% even when only using 10 sample points. This suggests a more linear behaviour of the functions with respect to these two design variables, which can be confirmed in Figure 4.4.

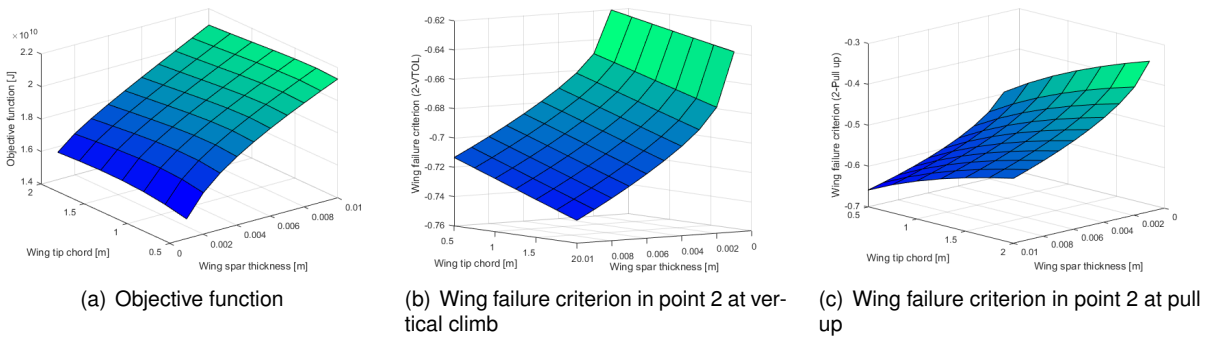


Figure 4.4: Behaviour of the real functions varying with the two design variables used in case 2.2

4.3.1.3 Case 2.3

As it was done in cases 2.1 and 2.2, another set of test points with 100 points was generated with LHS. The result of the surrogate models' predictions for each function were compared with the real functions on those points, and the results of the average relative error are presented in Figure 4.5.

The relative errors tend to decrease with the increase of number of sample points used, and to

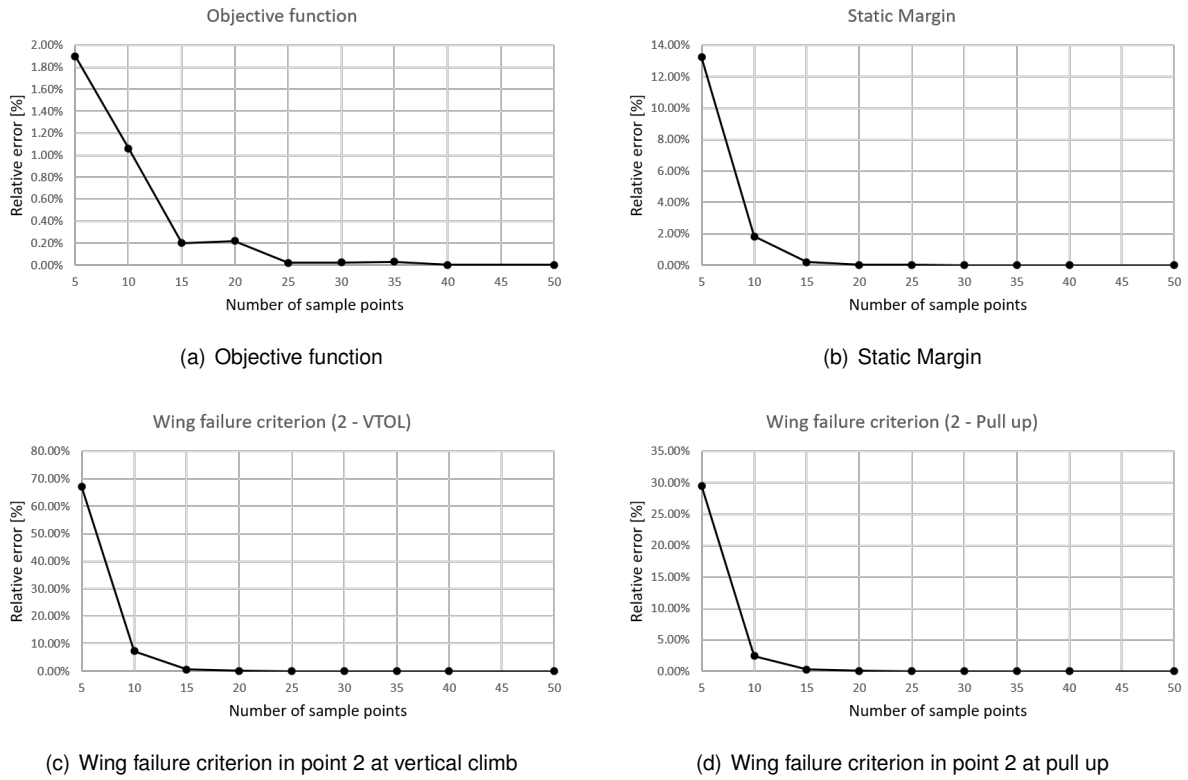


Figure 4.5: Average relative error of different functions vs number of sample points used for case 2.3

converge to zero, as expected. The number of sample points necessary, so that the relative error associated with every function is lower than 5%, is around 25. As in case 2.2, the behaviour of the real functions is more linear than in case 2.1, and so the surrogate models can mimic the results more easily, *i.e.* requiring less samples. The behaviours of the objective function, and two wing failure criteria are shown in Figure 4.6. From these figures it is also possible to conclude that, when the angle of attack is a design variable, its influence on the objective function is much more significant than the wing root chord variable. For this reason, when using the angle of attack as a design variable in more complex cases, it was noted that the surrogate models were not able to depict well the real function behaviour and therefore the angle of attack was dropped out, and in cases 4 and 8 it is not used.

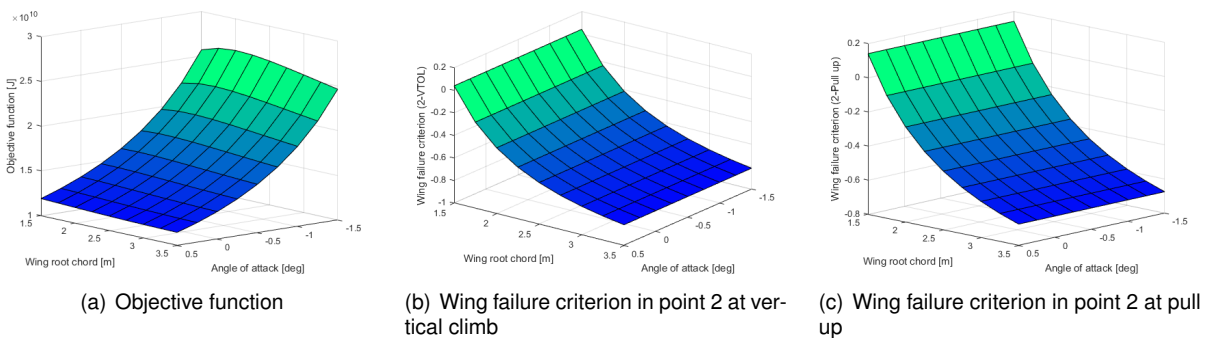


Figure 4.6: Behaviour of the real functions varying with the two design variables used in case 2.3

4.3.2 Optimization results

The optimization results for the cases 2 are here presented. Also, a comparison of the different approaches, the optimization using the real functions, optimization using the surrogate models, and optimization using the adaptive sampling, is presented.

4.3.2.1 Case 2.1

The optimization problem is first solved using the real functions and its derivatives, using the SLSQP algorithm and the adjoint method. The optimal solution found is presented in Table 4.3, and the optimization history of the objective function (total energy), the design variables and active constraints are shown in Figures 4.7 and B.3, respectively. It is possible to see that the optimal solution corresponds to a higher wing root chord and a smaller wing skin thickness. It is noticeable that in some iterations there was, at least, a constraint which was violated. This is explained because of how the SLSQP algorithm works, it first minimizes the objective function and only then it tries to obtain a feasible solution.

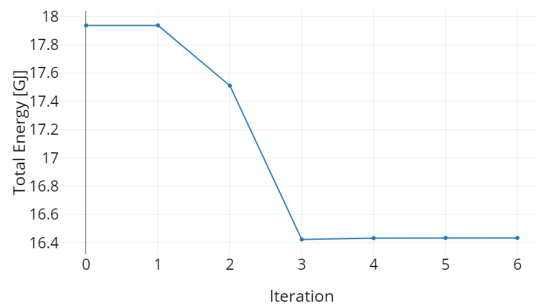


Figure 4.7: Optimization history of the objective function in case 2.1 (when using the real functions)

In the case of the second approach, where the objective function is a surrogate model of the total energy function and the constraints are the corresponding surrogate models as well, the problem was solved using the different sampling plans, *i.e.*, with the different number of sample points presented before, to build the surrogate model. Only the best result is presented here, and it corresponds to when the number of sample points used is 50, the largest database considered. In this approach the algorithm used is the SLSQP and it uses the prediction values of the surrogate models and its derivatives estimates as well. The results of the optimization are presented in Table 4.3. It should be noted that the performance data corresponds to the real function values evaluated at the optimum solution obtained with the surrogate models.

In last approach, the sampling plan, with which the surrogate models are built, is an adaptive plan, *i.e.*, there are points that are added to the plan, according to some criterion (WB2 in this case), as it was explained in section 3.4.2 and shown in Figure 3.17. Bearing in mind the quality study of the surrogates explained before, different number of starting sample points were chosen for different functions, since the WB2 criterion is based on the total energy and the constraints are assumed to be good enough to represent their corresponding real functions. For the total energy (previous objective function) the number of initial sample points is 5, for the constraints which have a linear or almost linear behaviour the

surrogates were built using 20 starting sample points, and for the constraints that, in the accuracy study shown a difficulty in mimicking their real function (such as the wing failure criteria), the number of starting sample points is 50. Once the starting surrogate models were built, the new objective function is defined as the WB2 criterion. The algorithm used in this optimization process is the GA, since the analytical derivatives of this function are too complex. A penalty function is added to the objective function, when a constraint or more are not respected, which corresponds to the absolute value of the constraint multiplied by a fixed scalar, 1^{30} . To ensure that the design space is well explored, the population was chosen to be composed by 200 individuals and the maximum number of generations was set to 100. For each iteration of the global optimization cycle a new point is added to the sampling plans (using OAS to evaluate the real functions at that point), the surrogate models are built again, and the GA looks for a new minimum. The stopping criterion used was the number of added points. A convergence criterion was not used because the WB2 presents a balance between the exploitation and exploration, and so, even if there is convergence in two consecutive iterations, in the next iteration the optimizer might tend to explore another area of the design space with a lower total energy needed. The number of added points for this case was set to 50. However, it was then observed that the optimal solution for the considered 50 iterations was found after adding just 3 points and the points found by the GA were very similar in most iterations. Even so, the 50 points were added to explore other regions and ensure that the best solution was found. The results of the history of the optimization are presented in Figure 4.8.

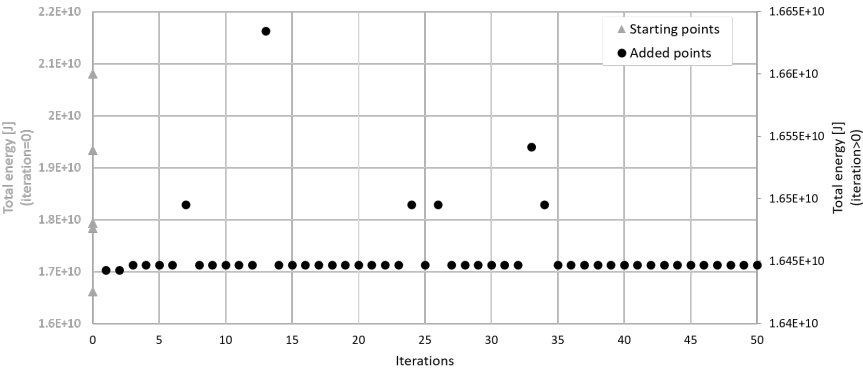


Figure 4.8: Optimization history of the total energy in Case 2.1 using the adaptive sampling approach

In Figure 4.8, it is possible to see the value of the total energy of the 5 initial sample points (triangles) and the total energy of the points that were being added to the sampling plans (circles). The first two points added correspond to unfeasible solutions, and the third is the optimal solution for this case. This solution is characterized by the parameters found in Table 4.3.

All of the three approaches employed lead to an improvement in comparison to the baseline, and the differences between the three solutions is very small (less than 1 % in the total energy). This validates the results obtained with the surrogate models, either when using the models as the objective function and constraints and when using the WB2 criterion, since the solutions found present very similar values for the design variables.

The benefits of using the surrogate models, in terms of computational cost (Table 4.4), are not verified in this case, since the optimization using the real functions when using the SLSQP takes only 6 iterations

Table 4.3: Results of the different solutions of case 2.1

	Wing root chord [m]	Wing skin thickness [m]	Wing structural mass [kg]	Fuel [kg]	Total mass [kg]	L/D	Total energy [MJ]
Baseline	2.684	0.0038	408.35	407.07	3524.10	13.36	17937.11
Real functions	2.739	0.00155	228.68 -44.00 %	378.10 -7.12 %	3315.47 -5.92 %	13.54 1.35 %	16433.35 -8.38 %
Surrogate search	2.739	0.00154	228.26 -44.10 %	378.02 -7.14 %	3314.96 -5.93 %	13.54 1.38 %	16429.71 -8.40 %
Adaptive sampling	2.739	0.00157	230.06 -43.66 %	378.42 -7.04 %	3317.16 -5.87 %	13.54 1.38 %	16446.95 -8.31 %

to find the optimum, which corresponds to 6 function and gradient evaluations. On the other hand, the second approach takes 44 surrogate model predictions and 50 real function evaluations to build the surrogate models, while the adaptive sampling approach takes 10^5 surrogate model predictions plus 100 real functions evaluations (50 to build the initial surrogate models and one for each of the 50 points added).

Table 4.4: Computational cost of the four methods for case 2.1

	Real functions (SLSQP)	Surrogate search	Adaptive sampling
Iterations	6	11	50
Function evaluations	6	44 (+50)	1000000 (50+50)
Gradient evaluations	6	11	0

4.3.2.2 Case 2.2

When using the SLSQP and the real functions, the solution found is again an improvement in comparison to the baseline. The values of the design variables of the optimal solution are presented in Table 4.6. In this table, the results of the general performance of the aircraft are also shown. In Figure 4.9, the optimization history of the total energy can be observed, and the history of the design variables and the active constraints during the process are shown in Figure B.4.

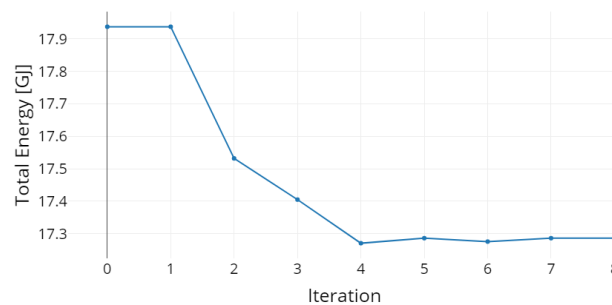


Figure 4.9: Optimization history of the objective function in case 2.2 (when using the real functions)

It is observed that the total energy converges to the optimal solution, varying very little in the last

iterations, where the optimizer is just trying to find a feasible solution near the region where it found the minimum.

When considering the approach that uses the surrogate models, as before, the optimized solution presented next, corresponds to the best solution found with the different sampling plans. The best solution is found when 10 sample points are used, and is presented in Table 4.5.

As it was explained in case 2.1, the third approach used corresponds to the adaptive sampling plan, using the WB2 criterion as the objective function of the optimization and adding sample points to the surrogate models according to this criterion, in order to find the optimal solution. The number of starting sample points used to build the total energy surrogate model is 5, and the number of the starting points used to build the constraints' surrogate models is 20, since the accuracy with this number of sample points is reasonable, as seen before in section 4.3.1. Once again, the GA was used as the optimization algorithm and were used a population with 200 individuals and a maximum number of generations of 100. Since in case 2.1, the number of added points, 50, turned out to be excessive, and because of time constraints, in this case only 25 points were added to the sampling plans. The result of the optimization is presented in Table 4.5, and the optimal solution corresponds to the point added on the 6th iteration. The total energy through the different iterations is shown in Figure 4.10.

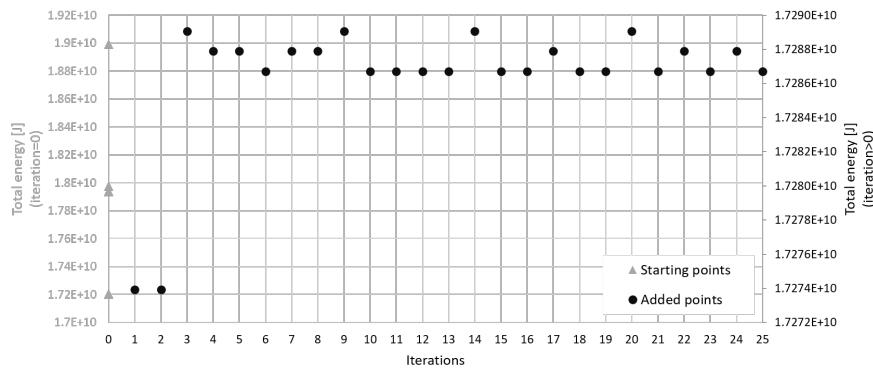


Figure 4.10: Optimization history of the total energy in Case 2.2 when using the adaptive sampling approach

The first points, in iteration 0, correspond to the starting sample points used to build the total energy surrogate model. The points corresponding to the first two iterations present a lower value of the total energy than the optimal solution, but they are unfeasible. Once again, the points added to the sampling plans are very similar to each other, which suggests that probably the global minimum was found, or that there is a very small feasible area that was not found by the GA.

All the approaches reach a better solution than the baseline, and the differences between the three solutions found are very small. In every optimization, the wing tip chord is increased, to similar values, and the wing spar thickness is reduced, being very close to the lower boundary of that design variable. The solution obtained using the surrogate models is slightly better than the other two, reducing the total energy in 3.72 % in comparison to the baseline. In terms of computational cost, a comparison between the different approaches is presented in Table 4.6.

Similarly to the previous case, the optimization with the real functions presents the smallest computa-

Table 4.5: Results of the different solutions of Case 2.2

	Wing tip chord [m]	Wing spar thickness [m]	Wing structural mass [kg]	Fuel [kg]	Total mass [kg]	L/D	Total Energy [MJ]
Baseline	1.074	0.0038	408.35	412.76	3529.79	13.19	17937.11
Real functions	1.340	0.00108	363.58 -10.96 %	397.75 -3.64 %	3470.01 -1.69 %	13.47 2.18 %	17286.07 -3.63 %
Surrogate search	1.347	0.00100	362.06 -11.34 %	397.39 -3.73 %	3468.13 -1.75 %	13.48 2.20 %	17270.45 -3.72 %
Adaptive sampling	1.341	0.00111	364.38 -10.77 %	397.76 -3.63 %	3470.82 -1.67 %	13.47 2.18 %	17286.72 -3.63 %

Table 4.6: Computational cost of the different approaches for Case 2.2

	Real functions	Surrogate search	Adaptive sampling
Iterations	8	3	25
Function evaluations	10	4 (+10)	500000 (+20+25)
Gradient evaluations	8	3	0

tional cost, having only 10 real functions' evaluations, while the optimization using the surrogate models need only 4 surrogate model predictions but it also needs 10 real functions evaluations to build models. The adaptive sampling approach is the most costly, needing $50 \cdot 10^4$ surrogate model predictions, plus 20 real function evaluations to build the total energy and the constraints initial surrogate models, plus the 25 real functions evaluations (one for each added point). In this case, the computational cost of the first two approaches is very similar since the real functions optimization takes 10 real function evaluations, which is the same value needed to build the surrogate models, and it takes only 4 more surrogate models predictions in the second approach.

4.3.2.3 Case 2.3

Once again, the optimization algorithm used in the real functions approach, is SLSQP. The evolution of the objective function as well as the design variables' values and the active constraint ($L = nW$ at pull up) through the optimization problem can be seen in Figures 4.11 and B.5, respectively. The solution obtained is presented in Table 4.7.

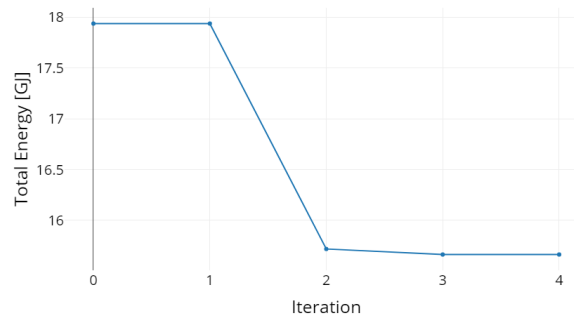


Figure 4.11: Optimization history of the total energy in Case 2.3 (when using the real functions)

From the optimization history, it is possible to observe that the optimizer converges to the solution in a small amount of iterations. This can indicate that either the objective function and the constraints are linear or almost linear (which is verified from the results shown in section 4.3.1) or, that the optimizer got trapped in a local minimum.

For the second approach, the optimization problem was solved with the different surrogate models created before, and the best result is presented in Table 4.7, and was found when considering 10 sample points to build the surrogates.

In the last approach, the adaptive sampling is used, where new points are added to the sampling plans and the surrogate models are updated accordingly. In this case, as it happened before, the number of starting sample points is different for the total energy function, and the constraints. The starting plan for building the total energy surrogate model has 5 points, while the sampling plan for all the constraints, except the pitching moment coefficient, uses 25 sample points, and the sampling plan used to build the latter constraint uses 40 sample points at the start. Once again, the WB2 criterion plus a penalty function was used as the objective function, optimized using the GA available in OpenMDAO. The number of individuals on each population and the maximum number of generations were again set to 200 and 100, respectively. The number of added points to each sampling plan, and consequently to the surrogate models, was 25. Once again, a convergence stopping criterion was not used, for the same reasons as before.

The best solution was found after adding 6 points to the sampling plans. The total energy of the optimal solution found in each iteration is found in Figure 4.12.

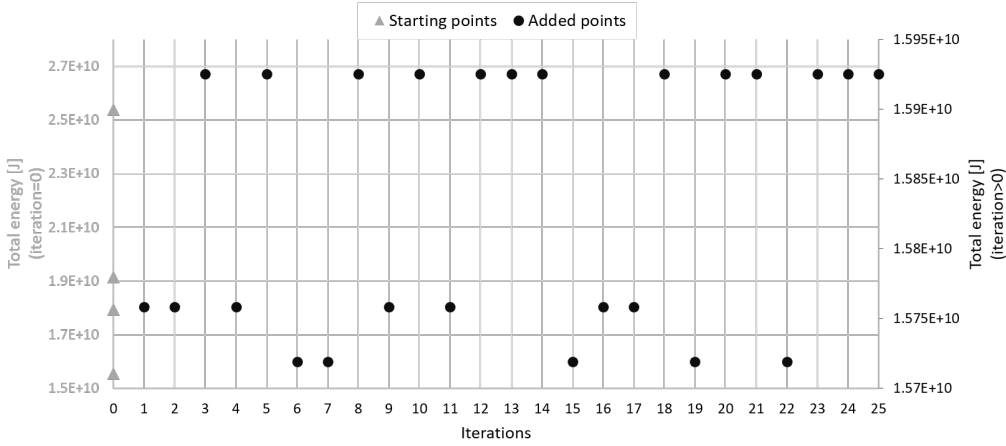


Figure 4.12: Optimization history of the total energy in case 2.3 using the adaptive sampling plan

The points presented in iteration 0 correspond to the starting points of the total energy sampling plan. Every point added corresponds to a feasible solution, and as said previously, the best solution is found in iteration 6, which is characterized by the parameters in Table 4.7. Once more, the points added are very similar to each other in different iterations which leads to believe that the global minimum was found, or that a feasible small region was not found.

As noticed for cases 2.1 and 2.2, every optimization process lead to a solution which shows an improvement, when compared to the baseline configuration. The difference between the three obtained

Table 4.7: Results of the different solutions of Case 2.3

	Wing root chord [m]	Angle of attack [°]	Wing structural mass [kg]	Fuel [kg]	Total mass [kg]	L/D	Total energy [MJ]
Baseline	2.684	-0.8	408.35	407.07	3524.10	13.36	17937.11
Real functions	2.500	-0.455	388.29 -4.91 %	360.28 -11.49 %	3457.25 -1.90 %	14,91 11.59 %	15664.39 -12.67 %
Surrogate search	2.500	-0.454	388.29 -4.91 %	360.23 -11.51 %	3457.20 -1.90 %	14.91 11.61 %	15662.03 -12.68 %
Adaptive sampling	2.512	-0.465	389.57 -4.60 %	361.54 -11.18 %	3459.79 -1.82 %	14.87 11.30 %	15719.06 -12.37 %

solutions can be found in Table 4.7. The best solution is the one obtained when using the total energy surrogate model as the objective function, but the difference between the three solutions are again very small, around 0.3 %, which validates the results. Previously, it was said that the optimizer in the real functions problem could be trapped in a local minimum because it took a very small amount of iterations. However, the results when using the GA in the adaptive sampling criterion, suggest that a global minimum was found.

Again, in terms of computational costs (shown in Table 4.8), the real functions optimization presents a lower number of real function evaluations, 4, while the surrogate based optimization needs only 3 iterations, but it takes 4 surrogate models predictions and 10 real functions evaluations to build the surrogate models. As for the adaptive sampling it takes $50 \cdot 10^4$ surrogate models predictions to find the minimum, plus 40 real functions evaluations to build the initial sampling plans, plus 25 real functions evaluations, one for each added point.

Table 4.8: Computational cost of the three methods for case 2.3

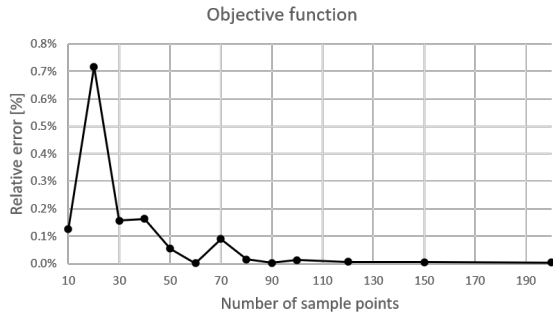
	Real functions	Surrogate search	Adaptive sampling
Iterations	4	3	25
Function evaluations	4	4 (+10)	500000 (+40+25)
Gradient evaluations	4	3	0

4.4 Case 4

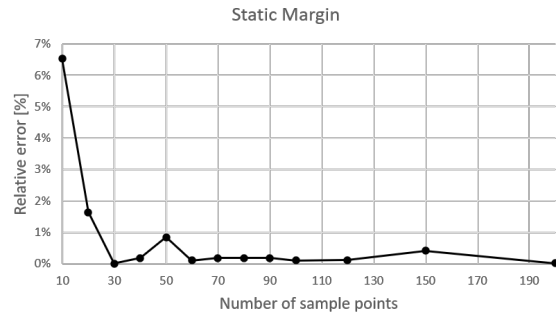
4.4.1 Surrogate models' quality

The quality of the surrogate models built is once again tested, but now using a set of 400 test points, generated with LHS. The results of the average relative errors of four examples of the surrogate models are presented in Figure 4.13. The models which are not here represented, follow the same trends as the ones depicted here.

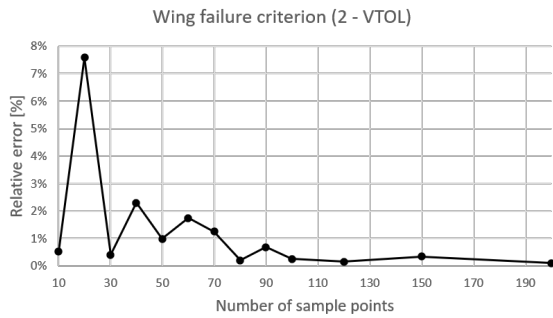
The objective function and static margin functions relative errors show a clear trend of decreasing with the number of sample points. On the other hand, the wing failure criteria, both in VTOL and Pull up,



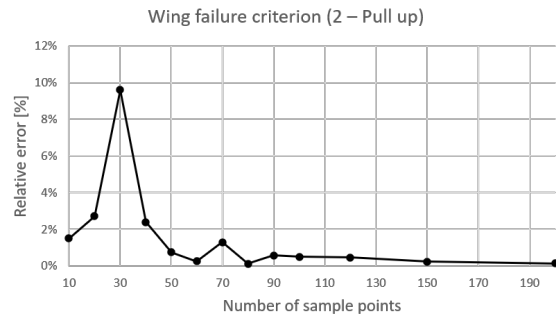
(a) Objective function



(b) Static Margin



(c) Wing failure criterion in point 2 at vertical climb



(d) Wing failure criterion in point 2 at pull up

Figure 4.13: Average relative error of different functions vs number of sample points used for case 4

show some oscillations with a lower number of sample points, but the average relative error is always smaller than 1 % for 80 or more sample points. As seen before, in the cases with less variables, these two criteria present non-linear behaviour, that explains the increased difficulty in getting an accurate surrogate model when using fewer sample points.

4.4.2 Optimization results

The real functions optimization, once again, uses the SLSQP algorithm and the adjoint method. The optimization history of the problem can be seen in Figures 4.14 and B.6, where the total energy and the design variables and active constraints in each iteration are shown. The optimal solution's design variables values are presented in Table 4.9, where the corresponding performance parameters are also shown. It is again observed, that the optimizer first finds a minimum and in the last iterations there is only a fine tuning of the design variables, so that every constraint is satisfied.

The optimization problem, in the case when using the surrogate models, was solved using the different sampling plans and the best result is presented in Table 4.9, and was found when using 50 sample points to build the surrogate models.

The adaptive sampling plan approach, consists in continuously adapting the sampling plan and consequently the surrogate models, as explained before. In this case, the starting sampling plan to build the total energy surrogate model has 10 sample points, while the sampling plans to build the constraints have 30 sample points, except two of the failure criteria of the wing in the pull-up manoeuvre, in which case the initial surrogate models are built using 40 sample points. As it happened in the previous cases,

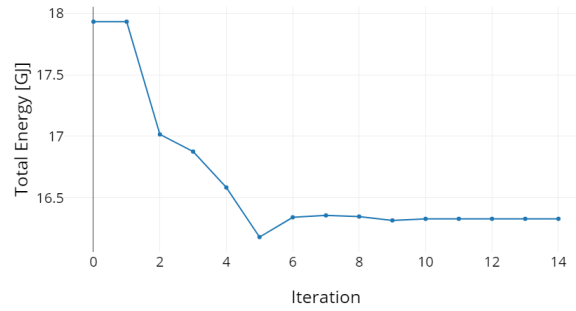


Figure 4.14: Optimization history of the total energy in case 4 (when using the real functions)

the objective function considered is the WB2 criterion, and the optimizer used is the GA of OpenMDAO. The population size used was 300 and the maximum number of generations was set to 100. The number of added sample points to the surrogate models was 50. The total energy history throughout the optimization is shown in Figure 4.15.

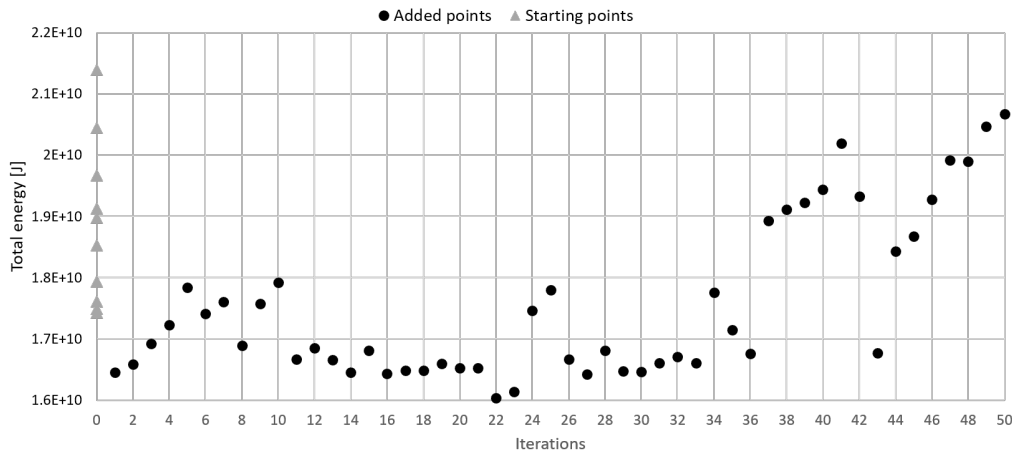


Figure 4.15: Optimization history of the total energy in Case 4

The best feasible solution obtained was found after 29 iterations, *i.e.*, after the 29 real functions evaluations were done, and is characterized by the parameters shown in Table 4.9. The number of unfeasible solutions found was much more significant than on the cases with less variables. Since the point is considered as feasible by the surrogate predictions, but then it is after all unfeasible, when evaluated with the real functions, it shows that there are still some errors in the surrogate models' predictions. This happens even though the surrogate models' accuracy shown before, in section 4.4.1, seems very high (average relative error lower than 3%). This can be explained by the complexity of the problem, and the wide design space that is being considered. Even though the relative errors may be low, it can happen that the test points are close to the points used to build the surrogates, and so, there might be some unsampled areas of the design space. Contrary to what happened before, in this case, the added points show different results in almost every iteration. This can mean that the design space was not yet completely explored and thus is not ensured that a global minimum was found.

Since in the last cases, there was a clear difference between the approaches where the adjoint method was used and where the GA was used, in this case and the next one, the approach that uses

the real functions is also carried out by using the GA. In this case, the number of individuals used was significantly smaller than the one used in the adaptive surrogate model approach, because the evaluations are more expensive. Therefore, the number of individuals and the number of generations used was 130 and 50, respectively.

Table 4.9: Results of the different solutions obtained in Case study 4

	Wing tip chord [m]	Wing root chord [m]	Wing spar thickness [m]	Wing skin thickness [m]	Wing structural mass [kg]	Fuel [kg]	Total mass [kg]	L/D	Total energy [MJ]
Baseline	1.074	2.684	0.0038	0.0038	408.35	407.07	3524.10	13.36	17937.11
Real functions	0.972	2.812	0.00196	0.00171	191.99 -52.98 %	375.72 -7.70 %	3275.66 -7.05 %	13.46 0.75 %	16329.59 -7.69 %
Surrogate search	0.982	2.818	0.00155	0.00186	194.64 -52.33 %	376.78 -7.44 %	3280.10 -6.92 %	13.44 0.60 %	16375.18 -7.43 %
Adaptive sampling	0.959	2.825	0.00245	0.00178	210.41 -48.47 %	378.99 -6.90 %	3298.08 -6.41 %	13.43 0.52 %	16471.23 -6.89 %
Real functions (GA)	1.176	2.653	0.00227	0.00118	220.85 -45.92 %	380.03 -6.64 %	3309.56 -6.09 %	13.44 0.60 %	16516.66 -6.63 %

Each of the four approaches leads to an improvement of the total energy needed to complete the aircraft's mission. The spar and skin thicknesses are much smaller than the ones from the baseline and so the structural mass of the wing is significantly smaller, in comparison to the baseline this mass is around half in every solution. The improvement on the aerodynamic efficiency, L/D , which consequently leads to a decrease on the necessary fuel, and the decrease in the wing structural mass, leads to a significant reduction of the total energy necessary to complete the mission.

The differences between the several solutions are not very significant (around 1%), but the best solution corresponds to the one found when the real functions are used. As stated before, the solution found with the third approach may correspond to a local minimum because the population sizes or the number of generations are smaller than needed, or the number of points added is too low. The small amount of individuals, generations and points added is explained by the time existing constraints. In the approach where the surrogate models are used, and the optimization problem is solved using the SLSQP, the optimizer may get trapped in a local minimum as well, since, even though the starting point is the same as the one used in the real functions approach, the prediction of the derivatives or the functions can show some errors, and so the optimizer is guided to a slightly different solution.

In this case, it is noticeable that when using the real functions but with the GA instead, the difference between the real functions and the adaptive sampling are smaller than when comparing to the results with the SLSQP.

Table 4.10: Computational cost of the different optimization approaches for case 4

	Real functions	Surrogate search	Adaptive sampling	Real functions (GA)
Iterations	14	21	50	50
Function evaluations	21	34 (+50)	1500000 (+40+50)	6500
Gradient evaluations	14	17	0	0

In terms of computational cost, the surrogate models still do not shown an advantage when in com-

parison with the real functions using the SLSQP. The real functions approach takes only 21 real functions evaluations, while the surrogate model approach needs 34 surrogate models' predictions plus 50 real functions evaluations to build the models, the third approach takes $15 \cdot 10^5$ surrogate models' predictions plus 40 real functions evaluations to build the initial sampling plans plus a real functions evaluation for each of the 50 points added, and lastly, the final approach takes 6500 real functions evaluations. The results show that, in a case where the gradient-based algorithm is not possible to use, or when the objective functions is multi-modal for example, the adaptive sampling shows some advantage in terms of results. In terms of the computational cost, the differences between the two approaches are much less significant (since the time it takes to get a surrogate model prediction is around 100 times lower than the time it takes to evaluate the real functions).

4.5 Case 8

4.5.1 Surrogate model's quality

The quality of the surrogate models built is tested using a 600 sample points test set, generated with LHS. The results of the average relative error of the objective function (total energy) and some of the constraints functions are presented in Figure 4.16.

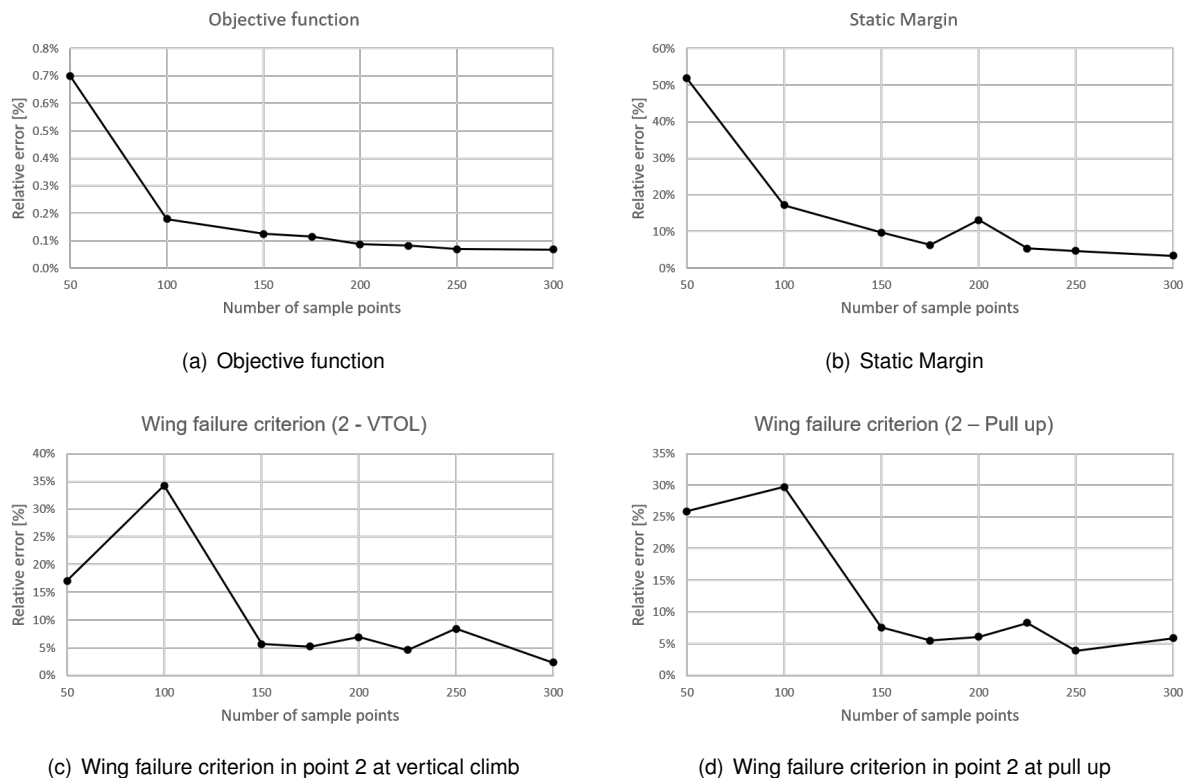


Figure 4.16: Average relative error of different functions vs number of sample points used for case 8

The average relative error of the total energy function clearly tends to decrease with the number of sample points converging to a value near 0 %. The constraints present a higher relative error, needing more sample points to have a surrogate model capable of representing their functions. In some cases,

Table 4.11: Number of starting sample points according to the function

Function	# Samples	Function	# Samples
Energy	50	Wing Failure 1 & 2 (VTOL)	300
S_M	300	Wing Failure 3 & 4 (VTOL)	100
$L_{cr} \approx W$	300	Tail Failure 1 & 2 & 3 & 4 (VTOL)	100
$L_{pull} \approx nW$	300	Wing Failure 1 & 2 (Pull up)	300
C_M	300	Wing and Tail Failure 3 & 4 (Pull up)	100
Fuel volume	100	Tail Failure 1 & 2 (Pull up)	150

it is necessary to have 300 points so that the relative error assumes a reasonable value, smaller or near 5 %, which is the case of the presented constraints in figure 4.16.

4.5.2 Optimization results

In the first approach, the real functions are used and the optimization algorithm is again the SLSQP. The optimal solution found is presented in Tables 4.12 and 4.13. The optimization history of the total energy can be found in Figure 4.17, while the design variables and the active constraints in each iteration are shown in Figure B.7. As it was observed before, the last iterations show that the optimizer is just trying to find a feasible solution near the area where it already found a minimum, *i.e.*, it is exploiting that region.

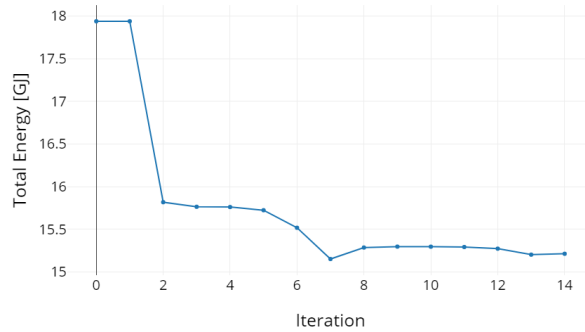


Figure 4.17: Optimization history of the total energy in Case 8 (when using the real functions)

In the second approach, the best result of the optimizations performed with the different sampling plans to build the surrogate models, corresponds to the sampling plan of 200 sample points. The optimal solution found is presented in Tables 4.12 and 4.13.

In the third approach, once again, the sampling plans that are used to build the surrogate models are updated according to the WB2 criterion. The starting sampling plans to build each surrogate model contain the number of sample points indicated in Table 4.11. Once more, the GA was used to solve the problem, and a population of 500 individuals was considered in each iteration, with the number of maximum generations being set to 50. The number of points added to the sampling plan was increased to 200, from the experience gained in case 4.

The total energy values of the solution in each iteration are presented in Figure 4.18. As it happened in case 4, the number of unfeasible solutions found is again very high, corresponding to 160 of the 200 points added. However, there are feasible solutions that improve the total energy function, and the best one corresponds to the first point that is found and added to the sampling plans (1st iteration).

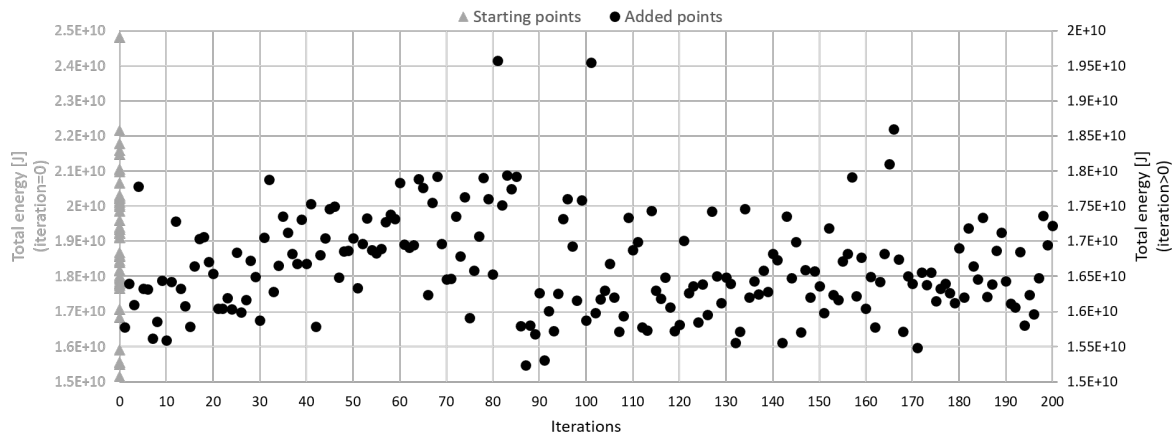


Figure 4.18: Optimization history of the total energy in Case 8

The values of the design variables and the performance parameters corresponding to the best solution found are presented in Tables 4.12 and 4.13, respectively. Even though the number of added points was increased, it is once again noticeable that the added points correspond to different solutions and so, once more, it might be that the global minimum was not found.

Once again, the real functions approach was carried out one more time, but using the GA as optimizer instead, as it was done in case 4. This time, the number of individuals and of generations was set to 260 and 80, respectively.

All the four approaches lead to a significant improvement from the baseline, corresponding to a reduction higher than 10 % of the total energy needed. The differences between the first two approaches are not very significant, thus validating the results obtained with the surrogate models. On the other hand, the solution found with the adaptive sampling strategy shows significant differences from the other two, more than 30 %, when analysing the wing structural mass for example. This confirms that the global minimum was not found in this approach, and that there was a need for more points to be added, or a need to have a bigger population. Once again, the results of the adaptive sampling are closer to the results of the real functions when using the GA than when using the SLSQP, which shows that the adaptive sampling method can be a good approach to some problems where the derivatives can not be used.

The solutions of the first two approaches present a wing tip chord which is slightly increased, in comparison with the baseline, and the wing root chord that is slightly smaller. Overall, this leads to a decrease in the wing area, and since the wingspan is fixed, the aspect ratio increases, which helps to explain the increase of the L/D . Both structural masses decrease significantly, as a consequence of the decrease in the spar and skin thickness of both the wing and the horizontal tail. Therefore, with both an aerodynamic improvement and a reduction of the overall weight of the aircraft, the total energy is much smaller than in the baseline, reducing it more than 14 %.

In terms of computational cost, the surrogate models present a higher cost in comparison with the first approach once again, with the number of real function evaluations in the first approach being only 15, while in the second approach there are 18 surrogate models predictions plus 200 real functions

Table 4.12: Design variables values of the different solutions obtained in case study 8

	Wing tip chord [m]	Wing root chord [m]	Wing spar thickness [m]	Wing skin thickness [m]	Tail tip chord [m]	Tail root chord [m]	Tail spar thickness [m]	Tail skin thickness [m]
Baseline	1.074	2.684	0.0038	0.0038	1.86	1.86	0.00255	0.00255
Real functions	1.230	2.511	0.00199	0.00222	1.15	1.15	0.0005	0.00168
Surrogate search	1.205	2.533	0.0028	0.00203	1.15	1.15	0.0005	0.00089
Adaptive sampling	1.253	2.488	0.00986	0.00132	1.155	1.161	0.00348	0.00054
Real functions (GA)	1.812	2.033	0.00248	0.00354	1.15	1.161	0.0005	0.00069

Table 4.13: Performance parameters of the different solutions obtained in case study 8

	Wing structural mass [kg]	Horizontal mass structural mass [kg]	Fuel [kg]	Total mass [kg]	L/D	Total energy [MJ]
Baseline	408.35	37.68	407.07	3524.10	13.36	17937.11
Real functions	232.82 -42.99 %	7.85 -79.17 %	349.93 -14.04 %	3261.61 -7.45 %	14.45 8.19 %	15213.01 -14.00 %
Surrogate search	237.67 -41.80 %	7.12 -81.12 %	349.70 -14.09 %	3265.48 -7.34 %	14.48 8.41 %	15203.15 -14.06 %
Adaptive sampling	362.52 -11.22 %	13.14 -65.14 %	362.80 -10.87 %	3409.45 -3.25 %	14.58 9.14 %	15772.57 -10.84 %
Real functions (GA)	362.61 -11.20 %	5.87 -84.42 %	359.01 -11.81 %	3398.49 -3.56 %	14.69 9.96 %	15608.34 -11.77 %

evaluations to build the sampling plans of the surrogate models, and in the last approach there are $50 \cdot 10^5$ surrogate models predictions, plus 300 real functions evaluations to build the initial sampling plans, plus 200 real functions evaluations, one for each point being added. In the last approach, the optimization takes 10400 real functions evaluations to find a solution, which is much more significant than the 15 evaluations when using the gradient-based algorithm, and the solution is worse.

Table 4.14: Computational cost of the different optimization approaches for Case 8

	Real functions	Surrogate search	Adaptive sampling	Real functions (GA)
Iterations	14	19	200	80
Function evaluations	15	18 (+200)	5000000 (+300+200)	10400
Gradient evaluations	14	18	0	0

4.6 Optimal solution

The optimal solution found, the one that minimizes the most the total energy needed to complete the defined mission, corresponds to the solution found with the surrogate models in case 8. The proposed

configuration presents a wing structural mass that is around 42 % lighter than the wing structural mass of the baseline, a reduction of around 81 % in the horizontal stabilizer structural mass and a reduction of about 14 % of the fuel mass. This leads to an overall weight mass that is around 7 % smaller than the one of the baseline. The lift-to-drag ratio of this configuration is almost 8.5 % higher than the baseline. The solution presents a significant reduction of the total energy needed, 14.06 %. The two configurations, the baseline and the optimal solution, are shown in Figure 4.19.

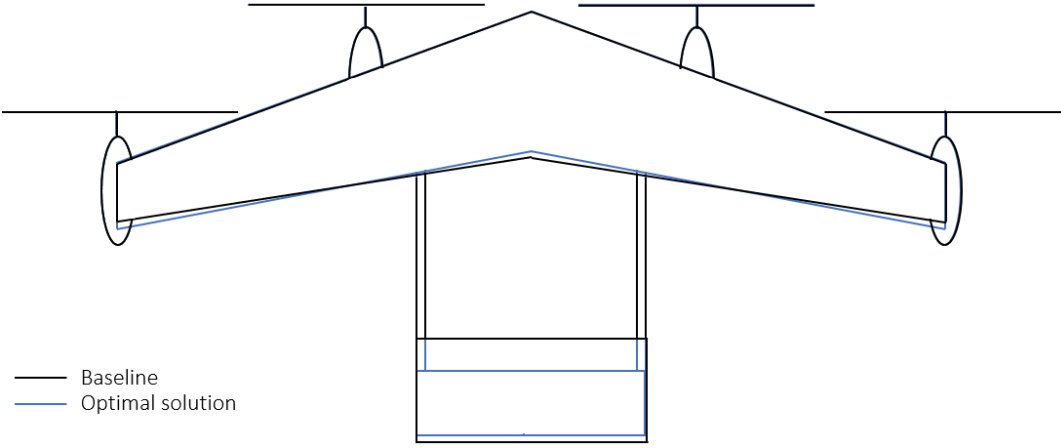


Figure 4.19: Baseline and optimal solution general configurations

Chapter 5

Conclusions

5.1 Achievements

This thesis focuses on solving an aircraft design optimization problem, using different approaches to carry out the optimization process. The aircraft is a variant of the Flexcraft configuration, developed to have VTOL capabilities.

First the concept of the Flexcraft was adapted to the new mission profile, by performing some initial studies, like conceptual sizing of the lifting surfaces, weight and balance estimations, design point analysis and defining the general configuration of the propulsive system. The new concept was then considered as the baseline for the optimization problem.

Then, the optimization problem itself was defined, by identifying the mission requirements which were the base to select the design variables, constraints and objective function. The physical models were then implemented using OAS framework, which presents low-fidelity models for both aerodynamics and structural analysis. The necessary modules, such as the objective function chosen, were added to the framework. To study the different sampling plans and surrogate models available on the SMT, some studies using analytical common test functions were carried out, which lead to the use of the LHS and the Kriging model to solve the optimization problem.

Several case studies were then performed, in order to understand the behaviour of the objective function and constraints and the different approaches. First, the case studies were very simple, having only two design variables, and then the complexity was increased by using four and then eight design variables. For each case study, different databases were generated to build and test the surrogate models for every function. Then each case study optimization problem was solved using the three different approaches at hand, the one using the real functions, the one using the surrogate models of these real functions, and the one using an adaptive sampling plan that uses the WB2 criterion has the objective function, and the surrogate models of the real functions as constraints. On the last two case studies, an additional approach was used: an optimization using the real functions but with a GA as optimizer.

The optimization algorithms used consist of a gradient-based, SLSQP, and a heuristic algorithm,

the GA. The first was used in the optimization using the real functions and in the optimization using its surrogate models. The GA was used on the third approach, where for each iteration the optimizer finds a possible minimum, which is then evaluated by the real functions and added to the sampling plans of the surrogate models.

The solutions obtained with the different approaches are compared for each case study done, and a final configuration, based on the best optimal solution of every case study, is finally presented. For each case study, an analysis of the computational cost taken for each optimization approach is also depicted.

5.2 General conclusions

When comparing the surrogate models based optimization with the real functions gradient-based optimization, the latter shows a smaller computational cost, and even though sometimes its solution is slightly worse, it is not very significant. This means, that for the problem at hand, the surrogate models do not present a relevant advantage over the real functions, which are already simple, since the physical models are of low-fidelity.

This can also be explained because the analytical partial derivatives of each function were possible to give as an input to the optimizer. If for example the derivatives were too complex or not available, the real functions approach may not have been the better strategy.

The design of the wing is also very similar to the baseline used, which can lead to the quick optimization process using the real functions. This can either be happening because the optimization is too constrained, since the number of design variables is relatively small, or because the baseline is already a good design. If a higher design freedom was allowed, multi-modal solutions could have been possible which could favour surrogate-based optimization.

5.3 Future Work

Since the results for the surrogate models, based on the low-fidelity models available on OAS, present good results, one possible idea for future work would be to use these models to explore the design space first, so then higher fidelity models could be employed in some points/areas of interest.

Another aspect that would be interesting to study is the increase in the number of variables. Some suggestions are: to let the wing sweep angle vary, ensuring that the electric motors position along the chord would match with this angle; allow for a wing span variation, and this time ensuring that the electric motors' position in the spanwise direction was also compatible with the new span.

The models used were only from aerodynamics and structures, with an additional consideration of the static margin, but some more complex models could also be employed. For example, some weight estimations could be integrated on the code, to allow for a variation of the tilt system weight with the position of the electric motors relative to the wing. Another idea would be to improve the models of aerodynamics and structures, by including the influence of the rotor's on the wing and tail and including some aeroelastic instabilities' considerations, respectively.

Bibliography

- [1] Flexcraft consortium. FLEXCRAFT - Project's website. <https://flexcraft.pt>. Accessed on June 2020.
- [2] Markets and Markets. Urban Air Mobility Market. <https://www.marketsandmarkets.com/Market-Reports/urban-air-mobility-market-251142860.html>. Accessed on February 2021.
- [3] F. Afonso, I. Ribeiro, A. Ferreira, F. Lau, and A. Suleman. Design considerations for an environmentally sustainable tilt-rotor aircraft for urban air mobility. Submitted to Transportation Research Part D: Transport and Environment in 2021.
- [4] F. Afonso, A. Ferreira, I. Ribeiro, F. Lau, and A. Suleman. On the design of environmentally sustainable aircraft for urban air mobility. *Transportation Research Part D: Transport and Environment*, 91(i):1–24, 2021. doi: 10.1016/j.trd.2020.102688.
- [5] W. Johnson, C. Silva, and E. Solis. Concept vehicles for vtol air taxi operations. In *Proceedings of the AHS International Technical Meeting on Aeromechanics Design for Transformative Vertical Flight 2018*, San Francisco, CA, USA, 2018.
- [6] W. Johnson and C. Silva. Observations from exploration of vtol urban air mobility designs. In *7th Asian/Australian Rotorcraft Forum, ARF 2018*, Jeju, South Korea, 2018.
- [7] Airbus. City airbus. <https://www.airbus.com/innovation/zero-emission/urban-air-mobility/cityairbus.html>. Accessed on June 2020.
- [8] Lilium. Lilium jet - project's website. <https://lilium.com/the-jet>. Accessed on June 2020.
- [9] J. Aviation. Joby aviation - company's website. <https://www.jobyaviation.com/>. Accessed on June 2020.
- [10] V. F. Society. Joby s4. <https://evtol.news/joby-s4/>. Accessed on June 2020.
- [11] S. Rajendran and S. Srinivas. Air taxi service for urban mobility: A critical review of recent developments, future challenges, and opportunities. *Transportation Research Part E: Logistics and Transportation Review*, 143, 2020. doi: 10.1016/j.tre.2020.102090.
- [12] A. Straubinger, R. Rothfeld, M. Shamiyeh, K.-D. Büchter, J. Kaiser, and K. O. Plötner. An overview of current research and developments in urban air mobility – setting the scene for uam introduction. *Journal of Air Transport Management*, 87:101852, 2020. doi: 10.1016/j.jairtraman.2020.101852.

- [13] Y. Zhou, H. Zhao, and Y. Liu. An evaluative review of the vtol technologies for unmanned and manned aerial vehicles. *Computer Communications*, 149:356–369, 2020. doi: 10.1016/j.comcom.2019.10.016.
- [14] D. H. Di Bianchi, T. H. Orra, and P. Paglione. Monte Carlo based robust MDO applied to aircraft conceptual design: A technical-financial coupling optimization strategy. In *15th AIAA Aviation Technology, Integration, and Operations Conference*, Dallas, TX, USA, 2015. doi: 10.2514/6.2015-2737.
- [15] T. Lukaczyk and *et al.* SUAVE: An open-source environment for multi-fidelity conceptual vehicle design. In *16th AIAA/ISSMO Multidisciplinary Analysis and Optimization Conference*, Dallas, TX, USA, 2015. doi: 10.2514/6.2015-3087.
- [16] S. R. Dean, J. J. Doherty, and T. R. Wallace. MDO-based concept modelling and the impact of fuel systems on wing design. In *47th AIAA Aerospace Sciences Meeting including the New Horizons Forum and Aerospace Exposition*, pages 1–12, Orlando FL, USA, January 2009. doi: 10.2514/6.2009-434.
- [17] R. E. Perez and H. T. L. Hugh. Multidisciplinary optimization framework for control-configuration integration in aircraft conceptual design. *Journal of Aircraft*, 43(6):1937–1948, 2006. doi: 10.2514/1.22263.
- [18] A. Ceruti, G. Caligiana, and F. Persiani. Comparative evaluation of different optimization methodologies for the design of UAVs having shape obtained by hot wire cutting techniques. *International Journal on Interactive Design and Manufacturing*, 7(2):63–78, 2013. doi: 10.1007/s12008-012-0164-x.
- [19] N. V. N. et al. Multidisciplinary unmanned combat air vehicle system design using multi-fidelity model. *Aerosp. Sci. Technol.*, 26(1):200–210, 2013. doi: 10.1016/j.ast.2012.04.004.
- [20] D. P. Wells, B. L. Horvarth, and L. A. McCullers. The flight optimization system weights estimation method. *NASA/TM-2017-219627/Volume I*, 2017. <https://ntrs.nasa.gov/search.jsp?R=20170005851>.
- [21] M. Laban and U. Herrmann. Multi-disciplinary analysis and optimization applied to supersonic aircraft part 1: Analysis tools. In *48th AIAA/ASME/ASCE/AHS/ASC Structures, Structural Dynamics, and Materials Conference*, volume 2, pages 1845–1861, Honolulu, HI, USA, April 2007. doi: 10.2514/6.2007-1857.
- [22] J. P. Jasa, J. T. Hwang, and J. R. R. A. Martins. Open-source coupled aerostructural optimization using python. *Structural and Multidisciplinary Optimization*, 57:1815–1827, 2018. doi: 10.1007/s00158-018-1912-8.
- [23] S. S. Chauhan and J. R. R. A. Martins. Low-fidelity aerostructural optimization of aircraft wings with a simplified wingbox model using openaerostruct. In *Proceedings of the 6th International*

- Conference on Engineering Optimization, EngOpt 2018*, Lisbon, Portugal, 2018. doi: 10.1007/978-3-319-97773-7_38.
- [24] S. Choi, J. J. Alonso, U. M. Kroo, and M. Wintzer. Multifidelity design optimization of low-boom supersonic jets. *Journal of Aircraft*, 45(1):106–118, 2008. doi: 10.2514/1.28948.
- [25] D. L. Allison, C. C. Morris, J. A. Schetz, R. K. Kapania, L. T. Watson, and J. D. Deaton. Development of a multidisciplinary design optimization framework for an efficient supersonic air vehicle. *Advances in Aircraft and Spacecraft Science*, 2(1):17–44, 2015. doi: 10.12989/aas.2015.2.1.017.
- [26] Z. T.-t. Zhang, T. g. Wang, W. Huang, and L. Yan. Parameterization and optimization of hypersonic-gliding vehicle configurations during conceptual design. *Aerospace Science and Technology*, 58: 225–234, 2016. doi: 10.1016/j.ast.2016.08.020.
- [27] J. P. Berends, M. J. Van Tooren, and D. N. Belo. A distributed Multi-Disciplinary Optimisation of a blended wing body UAV using a multi-agent task environment. In *47th AIAA/ASME/ASCE/AHS/ASC Structures, Structural Dynamics, and Materials Conference*, pages 114–135, Newport, RI, USA, 2006. doi: 10.2514/6.2006-1610.
- [28] K. Alston, S. Doyle, T. Winter, H. Kim, and S. Ragon. High fidelity multidisciplinary optimization (HFMDO). In *13th AIAA/ISSMO Multidisciplinary Analysis and Optimization Conference 2010*, number September, pages 1–14, Fort Worth, TX, USA, 2010. doi: 10.2514/6.2010-9319.
- [29] K. Reynolds and N. Nguyen. Multi-objective wing shape optimization of an elastically-shaped aircraft concept. In *51st AIAA Aerospace Sciences Meeting including the New Horizons Forum and Aerospace Exposition 2013*, number January, pages 1–16, Grapevine, TX, USA, 2013. doi: 10.2514/6.2013-142.
- [30] R. P. Henderson, J. R. R. A. Martins, and R. E. Perez. Aircraft conceptual design for optimal environmental performance. *Aeronautical Journal*, 116(1175):1–22, 2012. doi: 10.1017/S000192400000659X.
- [31] S. Choi, J. J. Alonso, and H. M. Kroo. Two-level multifidelity design optimization studies for supersonic jets. *Journal of Aircraft*, 46(3):776–790, 2009. doi: 10.2514/1.34362.
- [32] C. G. Pak. Aeroelastic tailoring study of an N+2 low-boom supersonic commercial transport aircraft. In *16th AIAA/ISSMO Multidisciplinary Analysis and Optimization Conference*, pages 1–29, Dallas, TX, USA, June 2015. doi: 10.2514/6.2015-2791.
- [33] J. Brezillon, A. Ronzheimer, D. Haar, M. Abu-Zurayk, M. Lummer, W. Krüger, and F. J. Natterer. Development and application of multi-disciplinary optimization capabilities based on high-fidelity methods. In *53rd AIAA/ASME/ASCE/AHS/ASC Structures, Structural Dynamics and Materials Conference 2012*, number April, pages 1–28, Honolulu, HI, USA, 2012. doi: 10.2514/6.2012-1757.

- [34] J. Colombi, John M.; Miller, Michael E.; Schneider, Michael; McGrogan, Jason; Long, David S.; Plaga. Model Based Systems Engineering with Department of Defense Architectural Framework. *Systems Engineering*, (3):305–326. doi: 10.1002/sys.20180.
- [35] R. E. Perez and J. R. R. A. Martins. pyACDT: An object-oriented framework for aircraft design modelling and multidisciplinary optimization. In *12th AIAA/ISSMO Multidisciplinary Analysis and Optimization Conference*, MAO, Victoria, BC, Canada, September 2008. doi: 10.2514/6.2008-5955.
- [36] A. Papageorgiou, M. Tarkian, K. Amadori, and J. O. Ivander. Multidisciplinary design optimization of aerial vehicles: A review of recent advancements. *International Journal of Aerospace Engineering*, 2018. doi: 10.1155/2018/4258020.
- [37] R. Yondo, E. Andrés, and E. Valero. A review on design of experiments and surrogate models in aircraft real-time and many-query aerodynamic analyses. *Prog. Aerosp. Sci.*, 96:23–61, 2018. doi: 10.1016/j.paerosci.2017.11.003.
- [38] Y. He, J. Sun, P. X. Wang, and A. S. Usmani. Preference-driven kriging-based multiobjective optimization method with a novel multipoint infill criterion and application to airfoil shape design. *Aerosp. Sci. Technol.*, 96, 2020. doi: 10.1016/j.ast.2019.105555.
- [39] N. B. et al. Adaptive modeling strategy for constrained global optimization with application to aerodynamic wing design. *Aerosp. Sci. Technol.*, 90:85–102, 2019. doi: 10.1016/j.ast.2019.03.041.
- [40] N. V. Queipo and E. Nava. A gradient boosting approach with diversity promoting measures for the ensemble of surrogates in engineering. *Struct. Multidiscip. Optim.*, 60(4):1289–1311, 2019. doi: 10.1007/s00158-019-02325-4.
- [41] M. A. Bouhlel, N. Bartoli, A. Otsmane, and J. Morlier. Improving kriging surrogates of high-dimensional design models by partial least squares dimension reduction. *Struct. Multidiscip. Optim.*, (5):935–952, 2016. doi: 10.1007/s00158-015-1395-9.
- [42] M. A. Bouhlel, N. Bartoli, A. Otsmane, and J. Morlier. An improved approach for estimating the hyperparameters of the kriging model for high-dimensional problems through the partial least squares method. *Math. Probl. Eng.*, 2016. doi: 10.1155/2016/6723410.
- [43] M. J. Sasena, P. Papalambros, and P. Goovaerts. Exploration of metamodeling sampling criteria for constrained global optimization. *Engineering Optimization*, 34(3):263–278, 2002. doi: 10.1080/03052150211751.
- [44] J. R. R. A. Martins and A. B. Lambe. Multidisciplinary design optimization: A survey of architectures. *AIAA Journal*, 51(9):2049–2075, 2013. ISSN 00011452. doi: 10.2514/1.J051895.
- [45] J. Yoon, N. V. Nguyen, S. M. Choi, J. W. Lee, S. Kim, and Y. H. Byun. Multidisciplinary general aviation aircraft design optimizations incorporating airworthiness constraints. In *10th AIAA Aviation Technology, Integration and Operations Conference 2010, ATIO 2010*, Fort Worth, TX, USA, September 2010. doi: 10.2514/6.2010-9304.

- [46] S. Rajagopal and R. Ganguli. Multidisciplinary design optimization of a uav wing using kriging based multi-objective genetic algorithm. In *50th AIAA/ASME/ASCE/AHS/ASC Structures, Structural Dynamics, and Materials Conference*, Palm Springs, CA, USA, May 2009. doi: 10.2514/6.2009-2219.
- [47] Z. H. Han, S. Görtz, and R. Zimmermann. Improving variable-fidelity surrogate modeling via gradient-enhanced kriging and a generalized hybrid bridge function. *Aerosp. Sci. Technol.*, 25(1): 177–189, 2013. doi: 10.1016/j.ast.2012.01.006.
- [48] K. Amadori, C. Jouannet, and P. Krus. A framework for aerodynamic and structural optimization in conceptual design. *Collection of Technical Papers - AIAA Applied Aerodynamics Conference*, 1(June):748–757, 2007. ISSN 10485953. doi: 10.2514/6.2007-4061.
- [49] U. lemma and M. Diez. Optimal conceptual design of aircraft including community noise prediction. *Collection of Technical Papers - 12th AIAA/CEAS Aeroacoustics Conference*, 5(May):2855–2864, 2006. doi: 10.2514/6.2006-2621.
- [50] P. W. Jansen, R. E. Perez, and J. R. R. A. Martins. Aerostructural optimization of nonplanar lifting surfaces. *Journal of Aircraft*, 47(5):1490–1503, 2010. doi: 10.2514/1.44727.
- [51] A. Elham and M. J. L. van Tooren. Multi-fidelity wing aerostructural optimization using a trust region filter-sqp algorithm. *Struct. Multidiscip. Optim.*, 55(5):1773–1786, 2017. doi: 10.1007/s00158-016-1613-0.
- [52] P. Piperni, A. DeBlois, and R. Henderson. Development of a multilevel multidisciplinary-optimization capability for an industrial environment. *AIAA Journal*, 51(10):2335–2352, 2013. ISSN 00011452. doi: 10.2514/1.J052180.
- [53] J. M. Longo, R. Dittrich, D. Banuti, M. Sippel, J. Klevanski, U. Atanassov, G. Carrier, P. Dubeau, I. S. El Din, R. Thepot, A. Loubeau, F. Coulouvrat, R. Jarlas, H. Rabia, D. Perigo, and J. Steelant. Concept study for a Mach 6 transport aircraft. *47th AIAA Aerospace Sciences Meeting including the New Horizons Forum and Aerospace Exposition*, (January):1–16, 2009. doi: 10.2514/6.2009-435.
- [54] L. Cavagna, S. Ricci, and L. Travaglini. NeoCASS: An integrated tool for structural sizing, aeroelastic analysis and MDO at conceptual design level. *Progress in Aerospace Sciences*, 47(8):621–635, 2011. ISSN 03760421. doi: 10.1016/j.paerosci.2011.08.006. URL <http://dx.doi.org/10.1016/j.paerosci.2011.08.006>.
- [55] M. Muir, C. Muldal, E. Kolb, G. Robertson, A. Parkinson, O. M. Querin, R. W. Hewson, and V. V. Toropov. The use of MDO and advanced manufacturing to demonstrate rapid, agile construction of a mission optimized UAV. *Collection of Technical Papers - AIAA/ASME/ASCE/AHS/ASC Structures, Structural Dynamics and Materials Conference*, pages 1–21, 2013. ISSN 02734508.
- [56] D. J. J. Toal. Some considerations regarding the use of multi-fidelity kriging in the construction of surrogate models. *Struct. Multidiscip. Optim.*, 51(6):1223–1245, 2015. doi: 10.1007/s00158-014-1209-5.

- [57] S. G. Kontogiannis, J. Demange, A. M. Savill, and T. Kipouros. A comparison study of two multifidelity methods for aerodynamic optimization. *Aerosp. Sci. Technol*, 97, 2020. doi: 10.1016/j.ast.2019.105592.
- [58] Q. Zhou, J. Wu, T. Xue, and P. Jin. A two-stage adaptive multi-fidelity surrogate model-assisted multi-objective genetic algorithm for computationally expensive problems. 37(1):623–639, 2021. doi: 10.1007/s00366-019-00844-8.
- [59] N. V. Nguyen, M. Tyan, and J. W. Lee. A modified variable complexity modeling for efficient multidisciplinary aircraft conceptual design. *Optimization and Engineering*, 16(2):483–505, 2015. ISSN 15732924. doi: 10.1007/s11081-014-9273-7.
- [60] A. Dener and J. E. Hicken. *Revisiting Individual Discipline Feasible using matrix-free Inexact-Newton-Krylov*. doi: 10.2514/6.2014-0110.
- [61] J. E. Hoogervorst and A. Elham. Wing aerostructural optimization using the individual discipline feasible architecture. *Aerospace Science and Technology*, 65:90–99, 2017. doi: 10.1016/j.ast.2017.02.012.
- [62] J. R. R. A. Martins and J. T. Hwang. Review and unification of methods for computing derivatives of multidisciplinary computational models. *AIAA Journal*, 51(11):2582–2599, 2013. doi: 10.2514/1.J052184.
- [63] G. Matheron. Principles of geostatistics. *Economic Geology*, 1963. doi: 10.2113/gsecongeo.58.8.1246.
- [64] X. Song, L. Lv, W. Sun, and J. Zhang. A radial basis function-based multi-fidelity surrogate model: exploring correlation between high-fidelity and low-fidelity models. *Struct. Multidiscip. Optim.*, 60(3):965–981, 2019. doi: 10.1007/s00158-019-02248-0.
- [65] M. R. Kianifar and F. Campean. Performance evaluation of metamodelling methods for engineering problems: towards a practitioner guide. *Struct. Multidiscip. Optim.*, 61(1):159–186, 2020. doi: 10.1007/s00158-019-02352-1.
- [66] I. Couckuyt, A. Forrester, D. Gorissen, F. D. Turck, and T. Dhaene. Blind kriging: Implementation and performance analysis. *Adv. Eng. Softw.*, 49(1):1–13, 2012. doi: 10.1016/j.advengsoft.2012.03.002.
- [67] H. K. Yong, L. Wang, D. J. J. Toal, A. J. Keane, and F. Stanley. Multi-fidelity kriging-assisted structural optimization of whole engine models employing medial meshes. *Struct. Multidiscip. Optim.*, 60(3):1209–1226, 2019. doi: 10.1007/s00158-019-02242-6.
- [68] Z. Wu, D. Wang, W. Wang, K. Zhao, H. Zhou, and W. Zhang. Hybrid metamodel of radial basis function and polynomial chaos expansions with orthogonal constraints for global sensitivity analysis. *Struct. Multidiscip. Optim.*, 2020. doi: 10.1007/s00158-020-02516-4.

- [69] T. Østergård, R. L. Jensen, , and S. E. Maagaard. A comparison of six metamodeling techniques applied to building performance simulations. *Appl. Energy*, 211:89–103, 2018. doi: 10.1016/j.apenergy.2017.10.102.
- [70] R. Jin, W. Chen, and T. W. Simpson. Comparative studies of metamodeling techniques under multiple modeling criteria. *8th Symp. Multidiscip. Anal. Optim.*, (1998):1–13, 2000. doi: 10.2514/6.2000-4801.
- [71] N. V. Queipo, R. T. Haftka, W. Shyy, T. Goel, R. Vaidyanathan, and P. K. Tucker. Surrogate-based analysis and optimization. *Prog. Aerosp. Sci.*, vol. 41(1):1–28, 2005. doi: 10.1016/j.paerosci.2005.02.001.
- [72] R. A. Fisher. *The Design of Experiments*. Hafner Publishing Company, 8th edition, 1966.
- [73] D. C. Montgomery. *Design and Analysis of Experiments*, volume 2. John Wiley & Sons, Inc., 8th edition, 2012.
- [74] M. A. Bouhlef, J. T. Hwang, N. Bartoli, R. Lafage, J. Morlier, and J. R. R. A. Martins. A python surrogate modeling framework with derivatives. *Adv. Eng. Softw.*, 135, 2019. doi: 10.1016/j.advengsoft.2019.03.005.
- [75] M. A. Bouhlef, N. Bartoli, A. Otsmane, and J. Morlier. Efficient global optimization for high-dimensional constrained problems by using the kriging models combined with the partial least squares method. *Engineering Optimization*, 2018. doi: 10.1080/0305215X.2017.1419344.
- [76] J. N. Reddy. *Introduction to the Finite Element Method*. McGraw-Hill Education, 3rd edition, 2006.
- [77] T. H. G. Megson. *Aircraft Structures for engineering students*. Butterworth-Heinemann, 3 edition, 1999. ISBN 9780340705889.
- [78] J. D. Anderson. *Fundamentals of Aerodynamics*. McGraw-Hill, 5th edition, 2010.
- [79] J. Katz and A. Plotkin. *Low-Speed Aerodynamics*. Cambridge University Press, 2001. ISBN 0521665523.
- [80] F. M. White. *Fluid Mechanics*. McGraw-Hill, 7 edition, 2011.
- [81] D. P. Raymer. *Aircraft Design: A Conceptual Approach*. American Institute of Aeronautics and Astronautics, Inc., 4th edition, 2006. ISBN: 1563478293.
- [82] P. Doerffer, G. N. Barakos, and M. M. Luczak. *Fluid–Structure Interaction Simulation*, pages 263–281. Springer International Publishing, Cham, 2017. doi: 10.1007/978-3-319-50568-8_14.
- [83] J. Martins and A. Ning. *Engineering Design Optimization*. Cambridge University Press (to be published), 2021. URL <http://www.umich.edu/~mdolaboratory/pdf/Martins2021.pdf>.
- [84] E. J. Cramer, J. E. Dennis, P. D. Frank, R. M. Lewis, and G. R. Shubin. Problem formulation for multidisciplinary optimization. *SIAM Journal Optimization*, 4(4):754–776, 1994. doi: 10.1137/0804044.

- [85] N. Bartoli, I. Kurek, R. Lafage, T. Lefebvre, R. Priem, M. A. Bouhlef, J. Morlier, V. Stiliz, and R. Regis. Improvement of efficient global optimization with mixture of experts: methodology developments and preliminary results in aircraft wing design. In *17th AIAA/ISSMO Multidisciplinary Analysis and Optimization Conference*, Washington, DC, USA, 2016. doi: 10.2514/6.2016-4001.
- [86] A. I. J. Forrester, A. Sóbester, and A. J. Keane. *Engineering Design via Surrogate Modelling: A Practical Guide*. John Wiley & Sons Ltd., 2008.
- [87] J. E. Gentle. *Random number generation and Monte Carlo methods*. Springer, 2nd edition, 2003.
- [88] J. Sacks, W. J. Welch, T. J. Mitchell, and H. P. Wynn. Design and analysis of computer experiments. *Statistical Science*, (4):409–423, 1989.
- [89] D. G. Krige. A statistical approach to some basic mine valuation problems on the witwatersrand. *Journal of Chemical, Metallurgical and Mining Society of South Africa*, pages 119–139, 1951. ISSN ISSN 0038-223X.
- [90] C. Park, R. T. Haftka, and N. H. Kim. Remarks on multi-fidelity surrogates. *Struct. Multidiscip. Optim.*, 55(3):1029–1050, 2017. doi: 10.1007/s00158-016-1550-y.
- [91] F. A. C. Viana, R. T. Haftka, and V. S. Jr. Multiple surrogates: how cross-validation errors can help us to obtain the best predictor. *Struct. Multidisc. Optim.*, (39):439–457, 2009. doi: 0.1007/s00158-008-0338-0.
- [92] A. G. Watson and R. J. Barnes. Infill sampling criteria to locate extremes. *Mathematical Geology*, 27(5):589–608, 1995. doi: 10.1007/BF02093902.
- [93] J. Nocedal and S. J. Wright. *Numerical Optimization*. Springer, 1999. ISBN 0-387-98793-2.
- [94] D. Kraft. A Software Package for Sequential Quadratic Programming. Technical Report 28, 1988.
- [95] J. S. Gray, J. T. Hwang, J. R. R. A. Martins, K. T. Moore, and B. A. Naylor. OpenMDAO: An Open-Source Framework for Multidisciplinary Design, Analysis, and Optimization. *Structural and Multidisciplinary Optimization*, 59:1075–1104, 2019. doi: 10.1007/s00158-019-02211-z.
- [96] M. Gilli and P. Winker. A Review of Heuristic Optimization Methods in Econometrics. *Swiss Finance Institute Research*, pages 08–12, 2008.
- [97] D. E. Goldberg. *Genetic Algorithms in Search, Optimization and Machine Learning*. Addison-Wesley Longman Publishing Co., Inc., USA, 1st edition, 1989. ISBN 0201157675.
- [98] J. T. Hwang and J. R. R. A. Martins. A computational architecture for coupling heterogeneous numerical models and computing coupled derivatives. *ACM Transactions on Mathematical Software*, 44(4), 2018. ISSN 15577295. doi: 10.1145/3182393.
- [99] SAPO. News about the FLEXCRAFT Project. <https://24.sapo.pt/tecnologia/artigos/flexcraft-a-aeronave-que-muda-de-corpo-conforme-a-missao-que-tem-pela-frente>. Accessed on June 2020.

- [100] T. L. Saaty. *The Analytic Hierarchy Process: Planning, Priority Setting, Resource Allocation*. McGraw-Hill, 1980.
- [101] *CS-23 Amendment 5 and AMC and GM to CS-23 Issue 3*. EASA, July 2020.
- [102] M. D. Maisel, D. J. Giulianetti, and D. C. Dugan. The history of the xv-15 tilt rotor research aircraft: From concept to flight. *NASA SP-2000-4517*.
- [103] *XFLR5 - Analysis of foils and wings operating at low Reynolds numbers*, 2013.
- [104] B. Brelje and J. R. R. A. Martins. Electric, hybrid, and turboelectric fixed-wing aircraft: A review of concepts, models, and design approaches. *Progress in Aerospace Sciences*, pages 1–19, 2019. doi: 10.1016/j.paerosci.2018.06.004.
- [105] J. Roskam and C.-T. E. Lan. *Aircraft Aerodynamics and Performance*. Design, Analysis and Research Corporation, 1997.
- [106] U. Neuling and M. Kaltschmitt. Techno-economic and environmental analysis of aviation biofuels. *Fuel Processing Technology*, 171:54–69, 2018. doi: 10.1016/j.fuproc.2017.09.022.
- [107] R. Barrett, M. Berry, T. Chan, J. Demmel, J. Donato, J. Dongarra, V. Eijkhout, R. Pozo, C. Romine, and H. V. der Vorst. *Templates for the solution of linear systems: building blocks for iterative methods*. SIAM, 1994. ISBN 9780898713282.
- [108] A. Lambe and J. R. R. A. Martins. Extensions to the design structure matrix for the description of multidisciplinary design, analysis, and optimization processes. *Struct Multidisc Optim*, 46, 2012. doi: 10.1007/s00158-012-0763-y.

Appendix A

Aerodynamics

A.1 Fundamentals

The theory used in the aerodynamic analysis is based on the three laws of conservation:

- Mass conservation
- Momentum conservation
- Energy conservation

Analysing a finite control volume in which the balances will be done, one can have a volume fixed in space (Eulerian perspective) or one that moves with the fluid (Lagrangian perspective).

Applying the mass conservation equation to a finite volume fixed in space:

$$\frac{\partial}{\partial t} \int_{\mathcal{V}} \rho d\mathcal{V} + \oint_S \rho \vec{V} \cdot d\vec{S} = 0 \quad (\text{A.1})$$

where t corresponds to time, ρ is the air density, \vec{V} is the fluid's velocity, \mathcal{V} is the finite volume and S is the finite volume's surface.

Since the volume is fixed in space, the limits of integration are also fixed and so the time partial derivative can be placed inside the integral.

$$\int_{\mathcal{V}} \frac{\partial \rho}{\partial t} d\mathcal{V} + \oint_S \rho \vec{V} \cdot d\vec{S} = 0 \quad (\text{A.2})$$

Applying the Gauss Theorem to the surface integral, one obtains:

$$\int_{\mathcal{V}} \left[\frac{\partial \rho}{\partial t} + \nabla \cdot (\rho \vec{V}) \right] d\mathcal{V} = 0 \quad (\text{A.3})$$

For a given arbitrary finite control volume, the only possible solution for the aforementioned equation is:

$$\frac{\partial \rho}{\partial t} + \nabla \cdot (\rho \vec{V}) = 0 \quad (\text{A.4})$$

Considering that the flow analysed is fully developed around the airfoil and therefore is steady, the time derivative becomes null. If one also assumes that the flow is incompressible, i.e, ρ is constant, then:

$$\rho \nabla \cdot \vec{V} = 0 \implies \nabla \cdot \vec{V} = 0 \quad (\text{A.5})$$

Since a subsonic flow across an airfoil can be considered as irrotational, we can consider the flow to be a potential flow:

$$\begin{cases} \nabla \cdot \vec{V} = 0 \\ \nabla \times \vec{V} = 0 \\ \vec{V} = \nabla \phi \end{cases} \quad (\text{A.6})$$

where ϕ is the potential of the velocity and $u = \frac{\partial \phi}{\partial x}$, $v = \frac{\partial \phi}{\partial y}$, $w = \frac{\partial \phi}{\partial z}$.

This leads to Laplace equation:

$$\nabla \cdot \nabla \phi = 0 \implies \nabla^2 \phi = 0 \quad (\text{A.7})$$

Moving onto the momentum equation, one has that:

$$\frac{\partial}{\partial t} \int_V \rho \vec{V} dV = - \oint_S \rho \vec{V} (\vec{V} \cdot \vec{n}) dS - \oint_S p \vec{n} dS + \int_V \rho \vec{f} dV \quad (\text{A.8})$$

where p is pressure, \vec{n} is the normal to the surface, and $\int_V \rho \vec{f} dV$ represents the mass forces.

To simplify, now the Lagrangian differential form of the equation is used:

$$\rho \frac{D\vec{V}}{Dt} = -\nabla p + \rho \vec{f} \quad (\text{A.9})$$

Assuming that $\vec{f} = 0$, $\frac{\partial \vec{V}}{\partial t} = 0$ and using the vectorial identity (for a irrotational flow):

$$\vec{V} \cdot \nabla \vec{V} = \nabla \left(\frac{V^2}{2} \right) - \vec{V} \times (\nabla \times \vec{V}) = \nabla \left(\frac{V^2}{2} \right) \quad (\text{A.10})$$

The momentum equation becomes:

$$\rho d \left(\frac{V^2}{2} \right) = -dp \quad (\text{A.11})$$

The Euler equation is therefore obtained and considering that at a constant entropy $\frac{dp}{d\rho} = a^2$, where a is the speed of sound and $a = \frac{V}{M}$ the following can be derived:

$$\frac{d\rho}{\rho} = -M^2 \frac{dV}{V} \quad (\text{A.12})$$

This equation allows to understand that the Mach number, M , will have an impact on compressibility effects.

Therefore, a step back is needed, to equation (A.5). As stated, the flow is considered to be fully developed and so the time derivative can be dropped:

$$\nabla(\rho \cdot \vec{V}) = 0 \quad (\text{A.13})$$

Considering a flow around an airfoil, like the one represented in Figure A.1, the velocity components in the undisturbed and disturbed flows can be written as follow:

$$\text{Undisturbed flow: } \begin{cases} V_x = V_\infty \\ V_y = 0 \\ V_z = 0 \end{cases} \quad \text{Disturbed flow: } \begin{cases} V_x = V_\infty + \hat{u} \\ V_y = \hat{v} \\ V_z = \hat{w} \end{cases} \quad (\text{A.14})$$

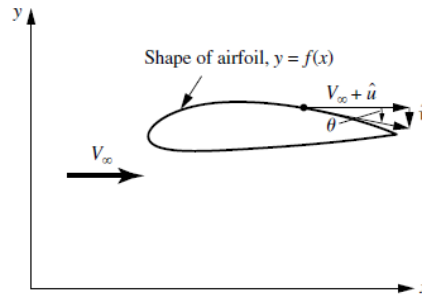


Figure A.1: Airfoil in the physical space [78]

Using the velocity potential, through some algebraic manipulation is possible to obtain from equation (A.13):

$$\rho(\phi_{xx} + \phi_{yy} + \phi_{zz}) + \phi_x \frac{\partial \rho}{\partial x} + \phi_y \frac{\partial \rho}{\partial y} + \phi_z \frac{\partial \rho}{\partial z} = 0 \quad (\text{A.15})$$

Considering the Euler equation (A.11) and the relation between the speed of sound and $\frac{dp}{d\rho}$, one can obtain:

$$\begin{aligned} & \left[a^2 - (V_\infty + \hat{\phi}_x)^2 \right] \hat{\phi}_{xx} + \left[a^2 - (V_\infty + \hat{\phi}_y)^2 \right] \hat{\phi}_{yy} + \left[a^2 - (V_\infty + \hat{\phi}_z)^2 \right] \hat{\phi}_{zz} - \\ & - 2(V_\infty + \hat{\phi}_x) \hat{\phi}_y \hat{\phi}_{xy} - 2(V_\infty + \hat{\phi}_x) \hat{\phi}_z \hat{\phi}_{xz} - 2\hat{\phi}_y \hat{\phi}_z \hat{\phi}_{yz} = 0 \end{aligned} \quad (\text{A.16})$$

$$\frac{a_\infty^2}{\gamma - 1} + \frac{V_\infty^2}{2} = \frac{a^2}{\gamma - 1} + \frac{(V_\infty + \hat{u})^2 + \hat{v}^2 + \hat{w}^2}{2} \quad (\text{A.17})$$

Using the relation between the potential of velocity and the velocity itself, and using the energy equation (A.17) and equation (A.16), one can obtain the potential equation for compressible flow:

$$\begin{aligned}
& (1 - M_\infty^2) \frac{\partial \hat{u}}{\partial x} + \frac{\partial \hat{v}}{\partial y} + \frac{\partial \hat{w}}{\partial z} = \\
& = M_\infty^2 \left[(\gamma + 1) \frac{\hat{u}}{V_\infty} + \frac{\gamma + 1}{2} \left(\frac{\hat{u}}{V_\infty} \right)^2 - \frac{\gamma - 1}{2} \frac{\hat{v}^2 + \hat{w}^2}{V_\infty^2} \right] \frac{\partial \hat{u}}{\partial x} + \\
& + M_\infty^2 \left[(\gamma - 1) \frac{\hat{u}}{V_\infty} + \frac{\gamma + 1}{2} \left(\frac{\hat{v}}{V_\infty} \right)^2 - \frac{\gamma - 1}{2} \frac{\hat{u}^2 + \hat{w}^2}{V_\infty^2} \right] \frac{\partial \hat{v}}{\partial y} + \\
& + M_\infty^2 \left[(\gamma - 1) \frac{\hat{u}}{V_\infty} + \frac{\gamma + 1}{2} \left(\frac{\hat{w}}{V_\infty} \right)^2 - \frac{\gamma - 1}{2} \frac{\hat{u}^2 + \hat{v}^2}{V_\infty^2} \right] \frac{\partial \hat{w}}{\partial z} + \\
& + M_\infty^2 \left[\frac{\hat{v}}{V_\infty} \left(1 + \frac{\hat{u}}{V_\infty} \right) \left(\frac{\hat{u}}{V_\infty} + \frac{\hat{v}}{V_\infty} \right) + \frac{\hat{w}}{V_\infty} \left(1 + \frac{\hat{u}}{V_\infty} \right) \left(\frac{\hat{u}}{V_\infty} + \frac{\hat{w}}{V_\infty} \right) + \frac{\hat{v}\hat{w}}{V_\infty^2} \left(\frac{\hat{v}}{V_\infty} + \frac{\hat{w}}{V_\infty} \right) \right]
\end{aligned} \tag{A.18}$$

For the subsonic regime, some assumptions can be made. The perturbations are going to be considered as much smaller than the velocity of the undisturbed flow: $\hat{u}, \hat{v}, \hat{w} \ll V_\infty \implies \frac{\hat{u}}{V_\infty}, \frac{\hat{v}}{V_\infty}, \frac{\hat{w}}{V_\infty} \ll 1$ and $\left(\frac{\hat{u}}{V_\infty} \right)^2, \left(\frac{\hat{v}}{V_\infty} \right)^2, \left(\frac{\hat{w}}{V_\infty} \right)^2 \ll 1$.

Therefore, the linearised potential equation becomes:

$$(1 - M_\infty^2) \frac{\partial \hat{u}}{\partial x} + \frac{\partial \hat{v}}{\partial y} + \frac{\partial \hat{w}}{\partial z} = 0 \Leftrightarrow (1 - M_\infty^2) \hat{\phi}_{xx} + \hat{\phi}_{yy} + \hat{\phi}_{zz} = 0 \tag{A.19}$$

Appendix B

Surrogate models

B.1 Test functions studies for surrogate models and sampling plans

In this section some complementary results from the accuracy studies done to evaluate the different surrogate models and sampling plans techniques are presented.

The first results figure B.1 shown are relative to the study done using the Branin test function to evaluate the influence of the sampling plan on the surrogate models' predictions.

The results shown in Figure B.2, are relative to the same study but using the Rosenbrock test function instead.

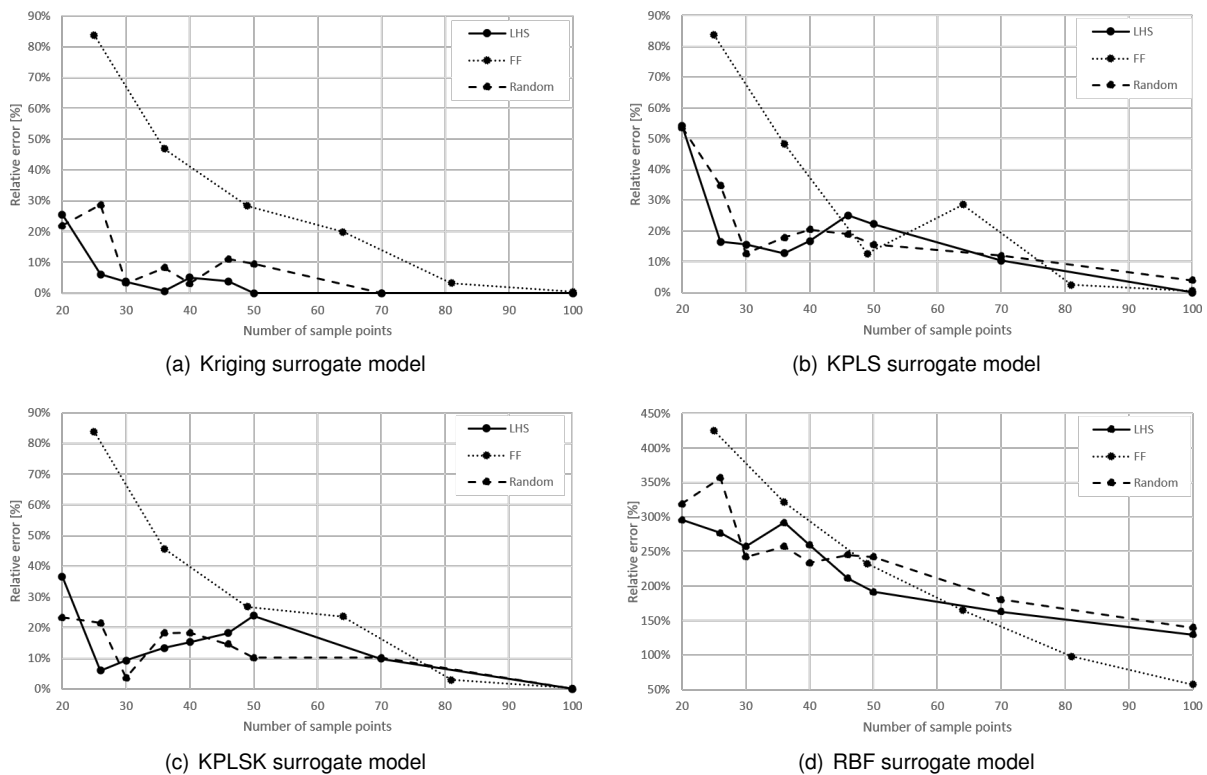
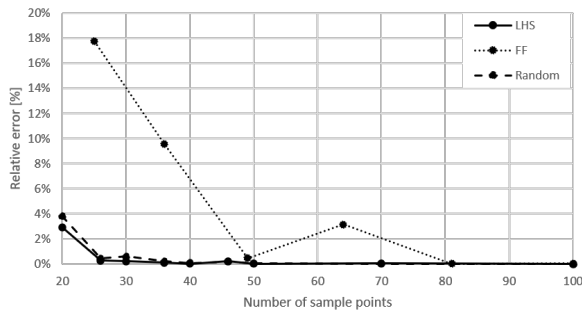
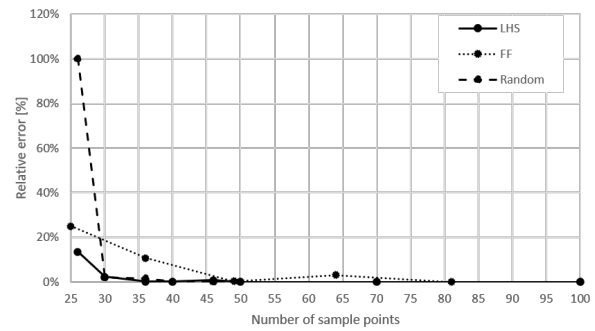


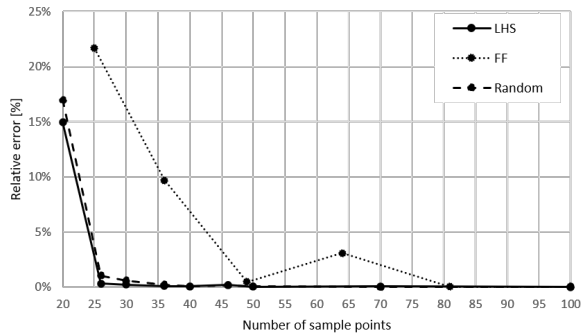
Figure B.1: Average relative error with the different sampling plans to represent the Branin function



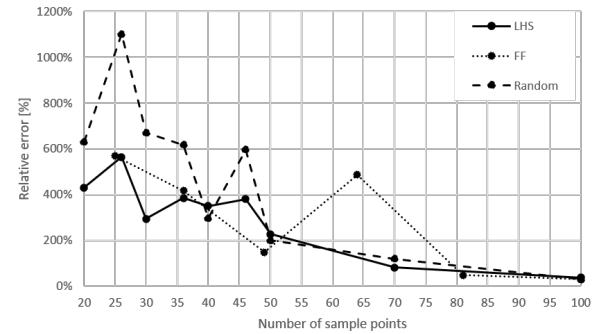
(a) Kriging surrogate model



(b) KPLS surrogate model



(c) KPLSK surrogate model



(d) RBF surrogate model

Figure B.2: Average relative error with the different sampling plans to represent the Rosenbrock function with 2 design variables

As said in section 3.4.1, the from the first study, the LHS was the chosen technique to implement the DOE. Using this sampling plan, different surrogate models techniques were then studied. The results of the study when using the Rosenbrock function with two and four design variables are presented in Tables B.1 and B.2, respectively.

Table B.1: Average relative error obtained with the different surrogate models representing the Rosenbrock function with two design variables, when using LHS plan

# Training points	Kriging	KPLS	KPLSK	RBF
20	2.92 %	145.09 %	14.93 %	430.10 %
26	0.29 %	13.51 %	0.32 %	564.59 %
30	0.23 %	2.34 %	0.22 %	293.52 %
36	0.12 %	0.21 %	0.11 %	384.74 %
40	0.04 %	0.15 %	0.06 %	349.47 %
46	0.21 %	0.76 %	0.19 %	380.63 %
50	0.02 %	0.07 %	0.02 %	226.35 %
70	0.07 %	0.06 %	0.06 %	80.24 %
100	0.01 %	0.01 %	0.01 %	37.17 %

Table B.2: Average relative error obtained with the different surrogate models representing the Rosenbrock function with four design variables

# Training points	Kriging	KPLS	KPLSK	RBF
40	54.63 %	68.93 %	54.75 %	125.82 %
50	45.11 %	65.50 %	50.41 %	115.21 %
60	26.52 %	49.18 %	33.76 %	89.73 %
70	12.32 %	56.94 %	21.72 %	89.58 %
80	12.32 %	56.94 %	21.72 %	89.58 %
90	2.05 %	32.35 %	8.18 %	77.18 %
100	1.05 %	21.76 %	5.77 %	69.64 %
120	0.69 %	2.98 %	0.81 %	60.82 %
140	0.33 %	11.05 %	0.99 %	51.83 %
150	0.21 %	0.56 %	0.19 %	47.03 %

B.2 Optimization using the real functions

In this section, some complementary results of the optimization history when using the real functions are presented.

First, in Figure B.3, the results of the first case study, 2.1, are shown. The, the results of case study 2.2 are presented in Figure B.4. The results for the last of the two design variables case studies, case 2.3, are presented in Figure B.5. Finally, the results of the last two cases, case 4 and case 8, can be observed in Figures B.6 and B.7. In every case, the results presented here show the evolution of both the design variables and the active constraints in each optimization iteration.

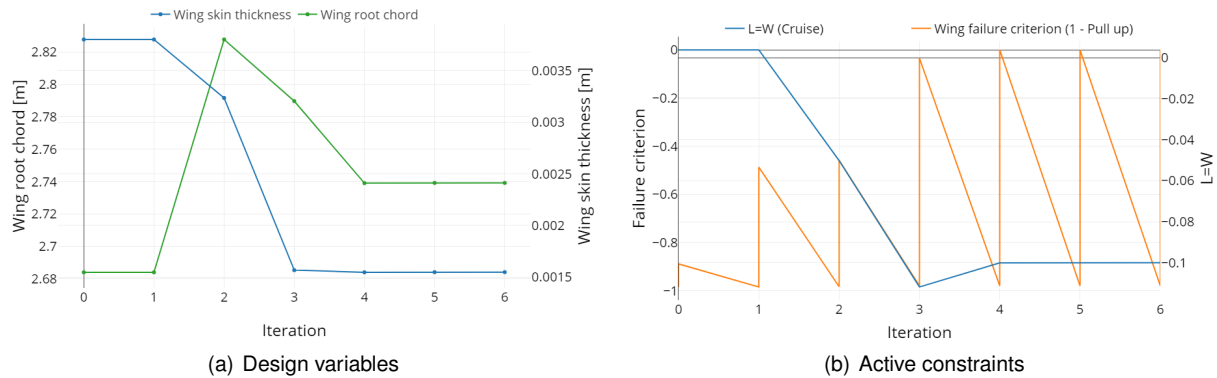


Figure B.3: Optimization history in Case 2.1 (when using the real functions)

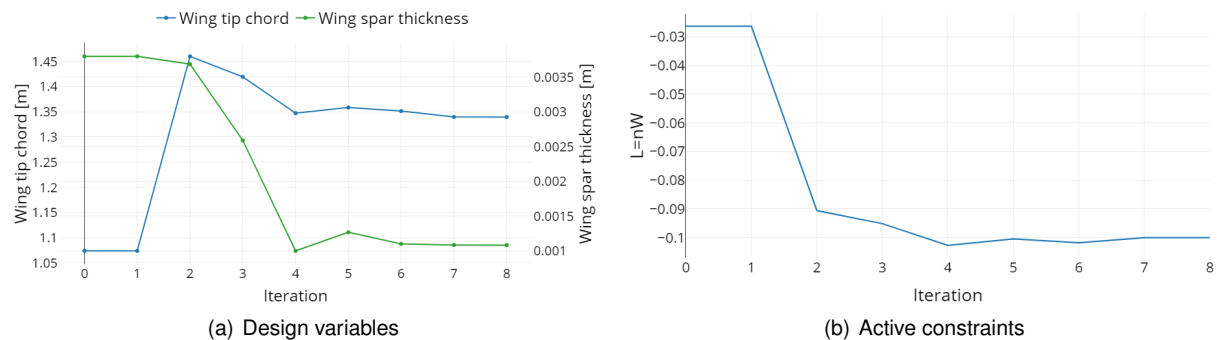
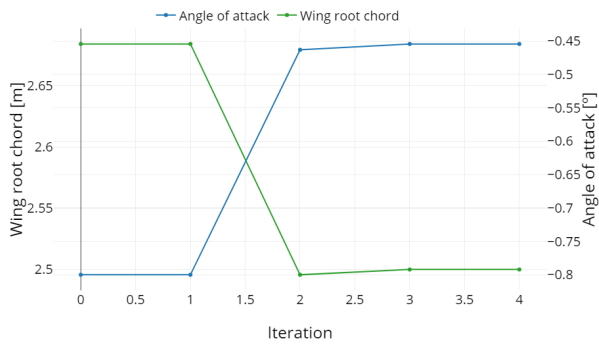
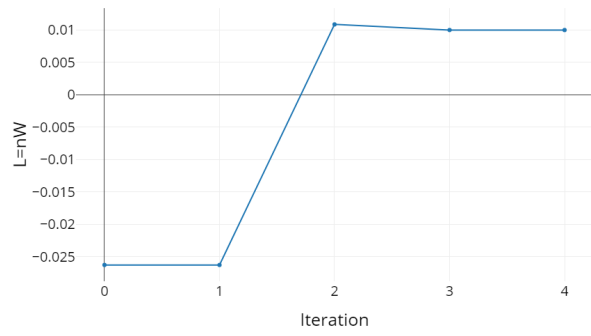


Figure B.4: Optimization history in Case 2.2 (when using the real functions)

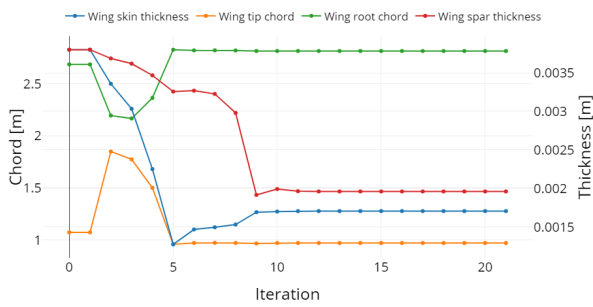


(a) Design variables

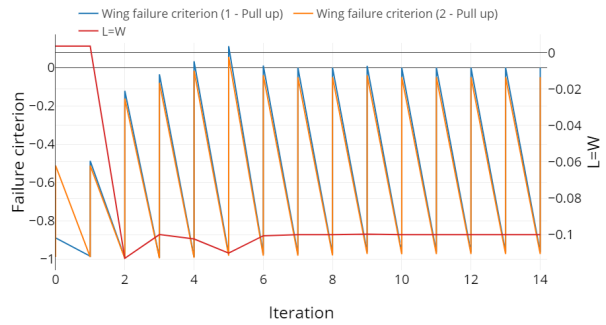


(b) Active constraint

Figure B.5: Optimization history of Case 2.3 (when using the real function)

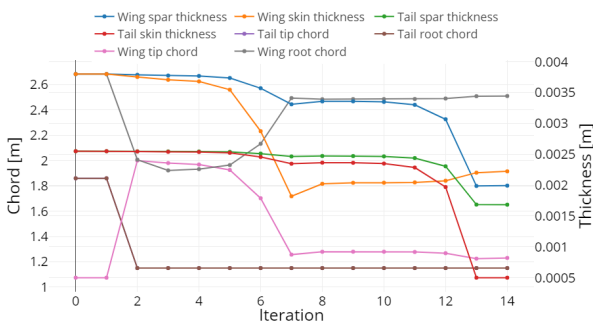


(a) Design variables

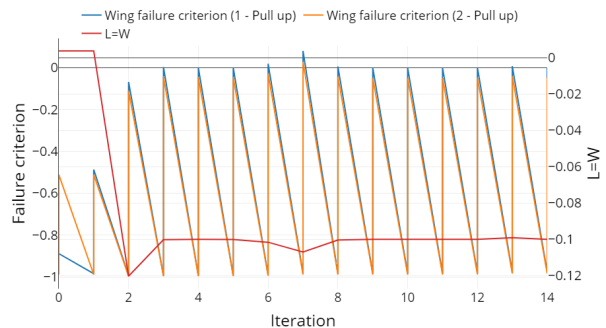


(b) Active constraint

Figure B.6: Optimization history of Case 4 (when using the real function)



(a) Design variables



(b) Active constraint

Figure B.7: Optimization history of Case 8 (when using the real function)

Appendix C

Conceptual design

C.1 Analytical Hierarchy Process

In this section the pairwise comparison matrices for each of the criterion chosen, to evaluate the different concepts, are presented.

Table C.1: Aerodynamics comparison of all the concepts

	I	II	III	IV	V	Priority Vector
I	1	1/3	7	5	1	0.2184
II	3	1	9	7	3	0.4802
III	1/7	1/9	1	1/3	1/5	0.0348
IV	1/5	1/7	3	1	1/5	0.0615
V	1	1/3	5	5	1	0.2050

Table C.2: Structures and Weight comparison of all the concepts

	I	II	III	IV	V	Priority Vector
I	1	3	5	7	3	0.4590
II	1/3	1	3	5	1/2	0.2083
III	1/5	1/3	1	1/3	1/2	0.0575
IV	1/7	1/5	3	1	2	0.1213
V	1/3	2	2	1/2	1	0.1539

Table C.3: Propulsion comparison of all the concepts

	I	II	III	IV	V	Priority Vector
I	1	1/2	7	5	5	0.3115
II	2	1	9	7	7	0.4959
III	1/7	1/9	1	1/3	1/3	0.0368
IV	1/5	1/7	3	1	1	0.0779
V	1/5	1/7	3	1	1	0.0779

Table C.4: Manufacturing and Maintenance comparison of all the concepts

	I	II	III	IV	V	Priority Vector
I	1	1/3	3	1/5	3	0.1169
II	3	1	7	1/3	5	0.2659
III	1/3	1/7	1	1/9	1	0.0451
IV	5	3	9	1	7	0.5207
V	1/3	1/5	1	1/7	1	0.0513

Table C.5: Stability and Control comparison of all the concepts

	I	II	III	IV	V	Priority Vector
I	1	1/2	3	3	3	0.4474
II	2	1	1/5	1/5	1/5	0.0408
III	1/3	5	1	1	1	0.1706
IV	1/3	5	1	1	1	0.1706
V	1/3	5	1	1	1	0.1706

Table C.6: Take-off and Landing comparison of all the concepts

	I	II	III	IV	V	Priority Vector
I	1	1/3	1/5	1/5	1/5	0.0505
II	3	1	1/3	1/3	1/3	0.107
III	5	3	1	1	1	0.2808
IV	5	3	1	1	1	0.2808
V	5	3	1	1	1	0.2808

Table C.7: Noise comparison of all the concepts

	I	II	III	IV	V	Priority Vector
I	1	2	7	5	5	0.4715
II	1/2	1	5	3	3	0.2704
III	1/7	1/5	1	1/3	1/3	0.0470
IV	1/5	1/3	3	1	1	0.1055
V	1/5	1/3	3	1	1	0.1055

C.2 Weight and position Estimations

In this section, the estimates done for the weight of each aircraft's component and its position are presented. The components are divided into functional groups such as: structural components, whose estimates are presented in Table C.8; propulsion system components, and their estimates are shown in Table C.9; equipment components, whose estimations of weight and position are shown in Table C.10; and other components shown in Table C.11. The sources of the estimations are indicated in the column "Source", and it should be noted that when its said to be "Flexcraft" it is a value that was used from the Flexcraft project, "Raymer" is a value calculated with some equation or ratio presented in [81] and "NASA" is from [20].

Table C.8: Structural components' weight estimation and position

Component	Weight Estimation [kg]	Source	Position		
			x [m]	y [m]	z [m]
Wing	585.56	Raymer - eq. (15.46)	1.967	0.0	2.441
Horizontal Tail	53.94	Raymer - eq. (15.47)	6.500	0.0	4.492
Vertical Tail 1	18.49	Raymer - eq. (15.48)	5.727	2.0	3.381
Vertical Tail 2	18.49	Raymer - eq. (15.48)	5.727	-2.0	3.381
Fuselage	284.95	NASA - eq. (56)	2.027	0.0	1.018
Main Landing Gear 1	86.02	NASA - eq. (63)	1.600	2.0	1.090
Main Landing Gear 2	86.02	NASA - eq. (63)	1.600	-2.0	1.090
Tail Landing Gear 1	24.81	NASA - eq. (64)	4.500	2.0	1.879
Tail Landing Gear 2	24.81	NASA - eq. (64)	4.500	-2.0	1.879
Paint	11.57	NASA - eq. (68)	2.027	0.0	2.741
Nacelles & Air Introduction	36.75	NASA - eq. (69)	1.000	0.0	2.741
Tilt System 3	55.50	Ratio	1.279	3.0	2.419
Tilt System 2	55.50	Ratio	1.279	-3.0	2.419
Tilt System 4	55.50	Ratio	3.267	7.5	2.566
Tilt System 1	55.50	Ratio	3.267	-7.5	2.566
Boom 1	60.00	Flexcraft	3.350	2.0	2.292
Boom 2	60.00	Flexcraft	3.350	-2.0	2.292
Wing Pylon	150.00	Flexcraft	2.586	0.0	2.179
Total	1723.41				

Table C.9: Propulsion components' weight estimation and position

Component	Weight Estimation [kg]	Source	Position		
			x [m]	y [m]	z [m]
Engine	160.60	Ratio	1.000	0.0	2.741
Generator	76.95	Ratio	2.250	0.0	2.741
Fuel System/tanks on wing	24.65	NASA - eq. (94)	1.455	0.0	2.376
Fuel System/tanks on fuselage	10.56	NASA - eq. (94)	-1.000	0.0	0.618
Electric motor 3	27.82	Ratio	0.292	3.0	2.419
Propeller and Hub 3	11.13	Ratio	-0.108	3.0	2.419
Electric motor 2	27.82	Ratio	0.292	-3.0	2.419
Propeller and Hub 2	11.13	Ratio	-0.108	-3.0	2.419
Electric motor 4	27.82	Ratio	2.230	7.5	2.566
Propeller and Hub 4	11.13	Ratio	1.830	7.5	2.566
Electric motor 1	27.82	Ratio	2.230	-7.5	2.566
Propeller and Hub 1	11.13	Ratio	1.830	-7.5	2.566
Total	428.56				

Table C.10: Equipment components' weight estimation and position

Component	Weight Estimation [kg]	Source	Position		
			x [m]	y [m]	z [m]
Avionics	97.97	NASA - eq. (108)	1.574	0.0	2.409
Hydraulics	49.17	NASA - eq. (104)	2.249	0.0	2.409
Electrical	99.14	Raymer - eq. (15.56)	2.027	0.0	2.409
Anti-icing	29.59	NASA - eq. (115)	1.000	0.0	2.409
Total	275.87				

Table C.11: Other components. (Note: * are estimated with design point expressions and transition study)

Component	Weight Estimation [kg]	Source	Position		
			x [m]	y [m]	z [m]
Fuel	410	Flexcraft	1.455	0.0	2.441
Reserve fuel	35	Flexcraft	2.050	0.0	0.618
Batteries	76.04	*	1.240	0.0	2.024
Oil	6.68	Raymer	1.900	0.0	2.38
Payload	575	Chosen	2.050	0.0	1.02
Total	1102.72				